

Surface Velocity Variations of the Lower Part of Columbia Glacier, Alaska, 1977–1981

By L.A. RASMUSSEN

STUDIES OF COLUMBIA GLACIER, ALASKA

U. S. GEOLOGICAL SURVEY PROFESSIONAL PAPER 1258-H

An internally consistent, two-dimensional data set of surface topography, surface velocity, bed topography, and mass balance distribution—obtained entirely from vertical aerial photography and photogrammetry.



DEPARTMENT OF THE INTERIOR

MANUEL LUJAN, Jr., *Secretary*

U.S. GEOLOGICAL SURVEY

Dallas L. Peck, *Director*

Any use of trade, product, or firm names in this publication is for descriptive purposes only and does not imply endorsement by the U.S. Government

Library of Congress Cataloging in Publication Data

Rasmussen, L.A.

Surface velocity variations of the lower part of Columbia Glacier, Alaska, 1977-1981.

(U.S. Geological Survey professional paper ; 1258-H)

Bibliography: p.

Supt. of Docs. no.: I 19.16:1258-H

1. Columbia Glacier (Alaska) I. Title. II. Series: Geological Survey professional paper ; 1258.

GB2427.C64R379 1989 551.3'12'09798 88-600063

For sale by the Books and Open-File Reports Section, U.S. Geological Survey,
Federal Center, Box 25425, Denver, CO 80225

CONTENTS

	Page		Page
Symbols and abbreviations	IV	Methods of data interpolation—Continued	
Abstract	H1	The linear algorithm for adjusting a single velocity field	H17
Introduction	1	Use of multiple velocity fields to estimate bed topography and mass-balance distribution	18
Background	1	Resulting data set	18
Purpose and scope	4	Adjusted velocity fields (1977–1981)	20
Methods of data acquisition	5	Inferred bed topography	20
Vertical aerial photography and photogrammetry	5	Inferred mass-balance distribution (1977–1981)	22
Radio-echo soundings and stake measurements	9	Discussion	24
The data consistency condition	9	References cited	28
Parameterization of the vertical variation of velocity	10	Appendixes:	
Application of the continuity equation	11	A: Velocity fields	30
Initial estimation of velocities	12	B: Terminus position as a function of time	52
Methods of data interpolation	15		

ILLUSTRATIONS

	Page
FIGURE 1. Index map of Columbia Glacier, Alaska	H2
2. Low-level oblique aerial photograph showing roughness of the glacier surface, October 8, 1975	4
3. Map showing surface topography of lower part of the glacier on September 1, 1981	6
4. Mosaic of five vertical aerial photographs of lower part of the glacier on September 1, 1981	7
5–20. Diagrams showing:	
5. Rate of change of surface altitude	8
6. Assumed vertical profile of velocity	10
7. Solution region grid nodes	12
8. Spatial distribution of average adjusted velocity from June 2, 1977, through September 1, 1981	13
9. Temporal variation of velocity from June 2, 1977, through September 1, 1981, at selected points	14
10. Data-density weighting factor used in estimating error in initial estimates of velocity	15
11. Dependence of error estimate on velocity gradient and local density of data points	15
12. Spatial distribution of estimated velocity errors averaged from June 2, 1977, through September 1, 1981	16
13. Temporal distribution of estimated velocity error and of the magnitude of the velocity adjustment, both averaged over the entire horizontal region	19
14. Spatial distribution of the velocity adjustment, averaged from June 2, 1977, through September 1, 1981	20
15. Inferred bed topography	21
16. Sensitivity of velocity adjustment to bed altitudes	23
17. Inferred mass balance as a function of altitude and of time	25
18. Temperature and precipitation at Valdez and Cordova	25
19. Sensitivity of the velocity adjustment to the mass-balance parameters	26
20. Measured and calculated mass-balance values	27

TABLES

	Page
TABLE 1. Dates of aerial photography-----	H5
2. Dependence of γ on n and ϕ -----	11
3. Inferred bed altitudes-----	22
4. Inferred mass-balance rates-----	24

SYMBOLS AND ABBREVIATIONS

Symbol	Name	Unit (where applicable)	Symbol	Name	Unit (where applicable)
a	Year.	-----	M	Number of photogrammetric points for a particular inter-flight interval-----	Dimensionless
B	Bed altitude-----	m	m	Meter.	-----
b	Subscript denoting sliding motion.	-----	mm	Millimeter.	-----
\hat{b}	Mass-balance rate, in ice equivalent----	m/a	N	Norm in linear algorithm for V-adjustment-----	Dimensionless
c	Coefficient in linear algorithm for V-adjustment-----	a^{-2}	n	Flow-law exponent-----	Dimensionless
D	Average of δV_{ijL} over 120 (i,j) , over $L=9,10,\dots,29$ -----	Dimensionless	ϕ	Ratio of deformational motion to minimum motion observed-----	Dimensionless
$(D_w)_{ij}$	Average of δu_{ijL} over $L=9,10,\dots,29$ ----	Dimensionless	ψ	Stream function in linear algorithm for V-adjustment-----	m^3/a
$(D_v)_{ij}$	Average of δv_{ijL} over $L=9,10,\dots,29$ ----	Dimensionless	r	Distance of a photogrammetric point from a grid node-----	m
D_L	Average of δV_{ijL} over 120 (i,j) -----	Dimensionless	S	Speed, the magnitude of the surface velocity vector V -----	m/a
d	Subscript denoting deformation motion.	-----	t	Time coordinate-----	a
$(E_w)_{ij}$	Average of $(\epsilon_w)_{ijL}$ over $L=9,10,\dots,29$ ----	m/a	UTM	Universal Transverse Mercator.	-----
$(E_w)_L$	Average of $(\epsilon_w)_{ijL}$ over 114 (i,j) where u defined-----	m/a	u	x -component of surface velocity-----	m/a
$(E_v)_{ij}$	Average of $(\epsilon_v)_{ijL}$ over $L=9,10,\dots,29$ ----	m/a	δu	Relative adjustment, $(u-u_0)/\epsilon_u$ -----	Dimensionless
$(E_v)_L$	Average of $(\epsilon_v)_{ijL}$ over 91 (i,j) where v defined-----	m/a	ϵ_u	Estimated error in u_0 , the initial estimate of u -----	m/a
E_L	Magnitude of vector with components $(E_w)_L$ and $(E_v)_L$ -----	m/a	V	Surface velocity vector, (u,v) -----	m/a
F	Scaled flux divergence, equal to $2\Delta x(b-h)$ -----	m^2/a	δV	Relative adjustment of velocity vector, $(\delta u, \delta v)$ -----	Dimensionless
f	Data-density weighting factor, used to compute ϵ_u, ϵ_v -----	Dimensionless	v	y -component of surface velocity-----	m/a
γ	Ratio of average velocity (through h) to surface velocity-----	Dimensionless	δv	Relative adjustment, $(v-v_0)/\epsilon_v$ -----	Dimensionless
h	Glacier thickness, measured vertically--	m	ϵ_v	Estimated error in v_0 , the initial estimate of v -----	m/a
\bar{h}	Characteristic thickness, equal to γh ----	m	x	Horizontal coordinate, positive to the east-----	m
\dot{h}	Time rate of change of h -----	m/a	Δx	Grid spacing (762.5 meters)-----	m
i	Subscript denoting row of finite-difference grid.	-----	y	Horizontal coordinate, positive to the north-----	m
j	Subscript denoting column of finite-difference grid.	-----	Z	Surface altitude-----	m
km	Kilometer.	-----	\dot{Z}	Time rate of change of Z -----	m/a
L	Subscript denoting flight number or inter-flight interval.	-----	z	Vertical coordinate, positive upward----	m
λ	Weight in linear algorithm for V-adjustment-----	a^2/m^2			

Sea level: In this report "sea level" refers to the National Geodetic Vertical Datum of 1929 (NGVD of 1929)—a geodetic datum derived from a general adjustment of the first-order level nets of both the United States and Canada, formerly called "Mean Sea Level of 1929."

STUDIES OF COLUMBIA GLACIER, ALASKA

SURFACE VELOCITY VARIATIONS OF THE LOWER PART OF COLUMBIA GLACIER, ALASKA, 1977-1981

By L. A. RASMUSSEN

ABSTRACT

A two-dimensional, internally consistent data set of geometry and flow variables is compiled for the lowest 15-kilometer-long reach of Columbia Glacier, a large, grounded, iceberg-calving glacier near Valdez, Alaska. This reach has surface velocities of the order of kilometers per year and ends at the calving terminus, which has been receding for the past several years.

The data set includes four variables: topography of the glacier surface, topography of the glacier bed, fields of surface velocity, and mass-balance distributions. The two topographies and the velocity fields are tabulated on 120 nodes of a 762.5-meter square grid. The mass balance, which measures the addition or subtraction of mass to or from the glacier, principally by snowfall or melting, is approximated as a linear function of altitude.

The surface topography had been obtained earlier by applying the method of optimum interpolation to altitudes of irregularly positioned points determined photogrammetrically from vertical aerial photographs taken 22 times between June 2, 1977, and September 1, 1981. The mass-balance functions and the velocity fields are given here as average values over the 21 intervening intervals. The bed topography inferred here is assumed to be unchanging over the 4.25-year period.

Most photogrammetric points could be tracked over the intervals between flights, and the resulting displacements were converted to average velocities by dividing by the lengths of the intervals. The two components of these irregularly positioned vectors were manually contoured, and initial estimates of the velocity fields were made by interpolating values at the grid nodes. Errors in the initial estimates were estimated by using an assumed function that takes into account both the contour gradient and the density of original vectors near each node.

Internal consistency in the surface velocity fields is achieved with respect to the principle of conservation of mass. The interpolated velocity fields obey a centered finite-difference approximation of the continuity equation. Of all possible consistent fields, they are the ones that are closest, as measured by the estimated errors, to the initial estimates. The adjustment of the velocity fields is cast as a minimization problem in which the bed altitudes at the 120 nodes and the two

coefficients of each of the 21 mass-balance functions are treated as being 162 model parameters. The 205 component values for each of the 21 intervals, both components being used only in the interior of the 120-node grid, constitute 4,305 data values. As a result, the problem is well constrained, and the data set—the surface topography and the surface velocity directly, the bed topography and the mass balance indirectly—can be derived entirely from the aerial photography.

The continuity equation is applied to the total ice flux, not just to the surface velocity, so a factor is introduced to relate the average velocity in a vertical column to the surface velocity. The ratio of the average velocity to the surface velocity was calculated by assuming that (1) the minimum velocity over the entire period was half deformation and half sliding, (2) all the velocity increase above the minimum was due to increased sliding, and (3) the deformation followed Glen's flow law, with the value of its exponent being 3. Because the maximum seasonal velocity was about twice the minimum, the consequence of these assumptions was that the ratio ranged from about 0.90 to 0.95, with an average value of 0.936. Furthermore, the properties of the data set are only slightly sensitive to the assumed partitioning between the two types of motion.

The data set was created for use in studying the mechanisms of glacier flow and calving. Therefore, apart from the assumptions in calculating the velocity ratio, no other assumptions were made about the flow mechanism. No such set of geometry and flow data has appeared before in the glaciological literature.

INTRODUCTION

BACKGROUND

Columbia Glacier is a large, calving glacier near Valdez, Alaska (fig. 1). Although much of its bed is below sea level, the glacier is not floating because the thickness of the ice overcomes the buoyancy force. Nearly all the ice discharge from this large (1,100-km²) glacier occurs at the 5-km-wide calving terminus, with a slight amount of ice flowing into the freshwater lakes along the lateral

STUDIES OF COLUMBIA GLACIER, ALASKA

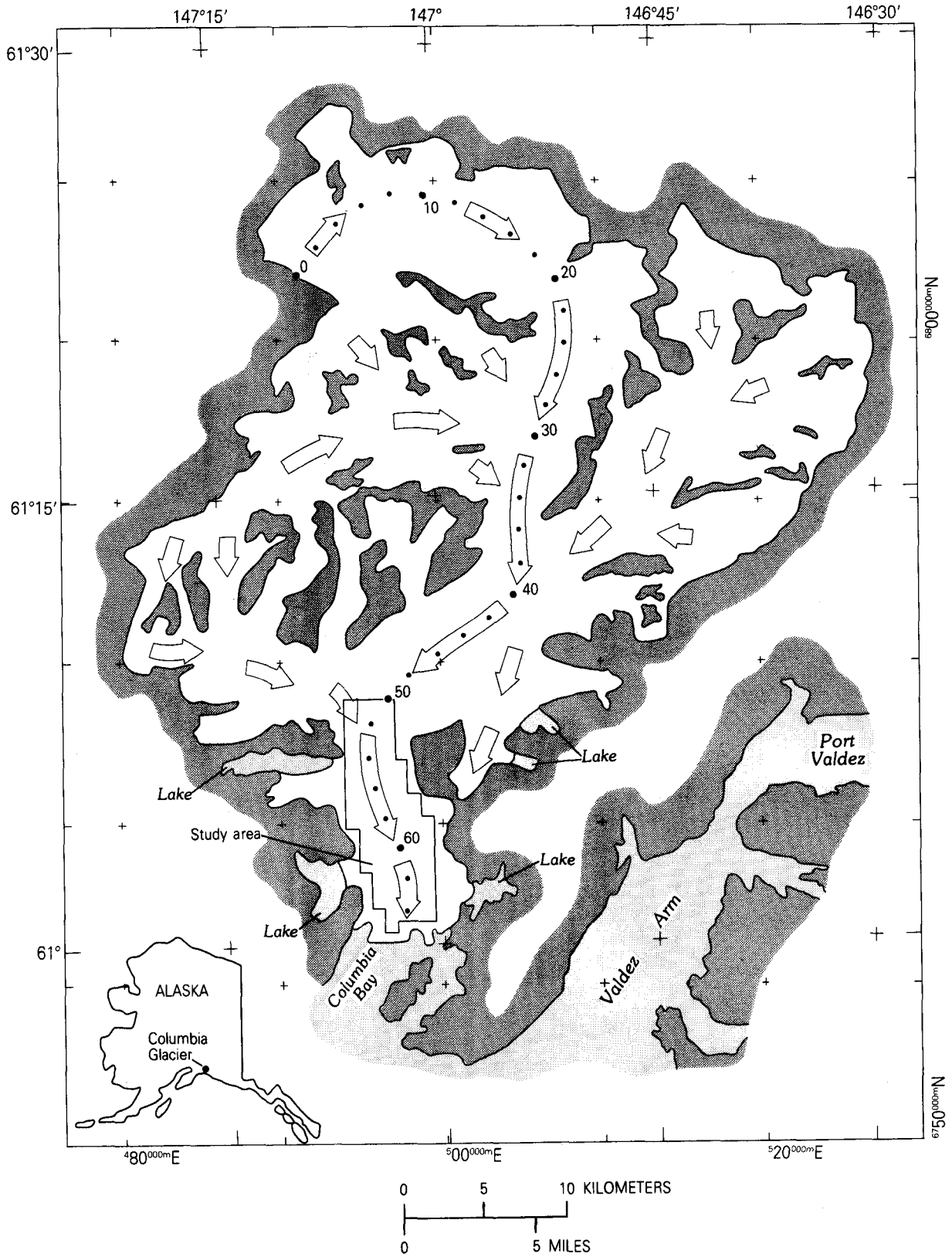


FIGURE 1.—Index map of Columbia Glacier, Alaska. Arrows show direction of flow, the main ice stream being indicated by the longer arrows and by dots at 2-kilometer intervals from the head of the glacier. The September 1, 1981, terminus position is shown. U.S. National Weather Service stations are at Valdez (61°08' N., 146°21' W.) and at Cordova (60°30' N., 145°30' W.).

margins of the lower reach of the glacier. From the time of its first recorded observation in 1794 (Vancouver, 1798) until 1978, its terminus pushed against a moraine shoal, the top of which is about 20 m below local mean sea level.

Austin Post in 1974 conjectured that if a tidewater glacier retreats from its shoal, the retreat will become rapid and irreversible (Post, 1975). The U.S. Geological Survey began an intensive research program in 1977 to determine whether Columbia Glacier would retreat. Ground-based and boat-based fieldwork (Meier and others, 1978; Mayo and others, 1979; Sikonia and Post, 1980) was supplemented by vertical aerial photography (Meier and others, 1985a) and by airborne radio-echo sounding (Brown and others, 1986). A preliminary prediction of retreat was issued in June 1980 (Meier and others, 1980). The results of a continuity-equation model (Rasmussen and Meier, 1982), of a finite-element model (Sikonia, 1982), and of a finite-difference model (Bindschadler and Rasmussen, 1983) all supported the preliminary prediction of rapid retreat and predicted a sharp increase in iceberg production. The finite-element model related calving to the buoyancy force and to subglacial runoff (Sikonia, 1982), and the other two models related calving to water depth (Brown and others, 1982).

By the end of 1987 the terminus had retreated 3 km behind the shoal, so that the length of the main stream of the glacier was 64 km; however, the rate of retreat has been much lower than predicted by any of the three models. As the terminus retreated into the deeper water behind the shoal, both the ice velocity and the iceberg flux from the terminus increased by a factor of about four, to as much as 4 km/a and 5 km³/a, respectively (Meier and others, 1985b; Krimmel and Vaughn, 1987).

Although recent attention was originally motivated by concern for icebergs entering the channel to the oilport at Valdez, it was recognized that the collected data would be valuable in answering several questions in glaciological research in general: (1) What flow law best represents the motion, which is believed to be due mainly to sliding? (2) How should the boundary condition at the calving terminus be represented? (3) What numerical values for the parameters in the flow law give the best match to observed velocities? (4) How does the calving rate depend on glacier geometry and on the ice velocity field? Because calving velocity is defined as the difference between ice velocity and rate of advance or retreat of the terminus, accurate measurement of ice velocity is necessary to determine accurate calving velocity and, thus, is important to further investigation of the calving mechanism. The models may have overestimated the retreat rate because the calving rate was overestimated by the calving laws they used, or because the models did not

properly account for the sharp increase in ice velocity that occurred in the early 1980's. These data could also be useful in studying the influence of the subglacial water regime.

Especially valuable is the vertical aerial photography. It has been obtained from about five flights per year from mid-1976 through 1986, usually over only the 18-km-long lower part of the glacier, which includes the region of greatest speed and the calving terminus. The extreme roughness of the glacier surface (fig. 2) makes foot travel and even helicopter landings nearly impossible over most of the region, but the rough surface is highly suitable for photogrammetric analysis (Meier and others, 1985a). Because individual surface features of the glacier are generally identifiable for many months, their displacement vectors also can be determined. When the displacements are divided by the elapsed time between the two flights from which they were determined, they become average velocities over that period.

The effort to extract as much information as possible from the vertical aerial photography began with publication of the photogrammetrically determined coordinates (Fountain, 1982) for flights through September 1, 1981. All the earlier modeling had parameterized transverse variations of the glacier geometry and flow into one dimension along the glacier's longitudinal axis. The goal for future modeling was to treat those variations explicitly. It was recognized that specifying velocity along with the bed and surface altitudes on the nodes of a square grid would facilitate such modeling work, especially finite-difference formulations. A 762.5-m square grid was established for this. Because both the original point coordinates and the midpoints of their displacements are irregularly positioned spatially, accurate interpolation was needed. The method of optimum interpolation was used to interpolate among the point coordinates to get surface altitudes on the grid nodes (Rasmussen and Meier, 1985).

Mass balance measures the addition or subtraction of mass to or from the glacier; changes are due principally to snowfall and melting, which in glaciological research are termed "accumulation" and "ablation." When mass-balance values, along with bed and surface altitudes and velocities, are specified at the grid nodes, the data are singly redundant. This is because the data must obey the equation of continuity, which expresses the principle of conservation of mass and is the basis for time-dependent models of glacier flow. If the data are not internally consistent in this respect, a model would begin by artificially redistributing the glacier mass to reconcile the inconsistencies. Model results may be very sensitive to slight inconsistencies in the initial conditions they use (Hodge, 1985).



FIGURE 2.—Low-level oblique aerial photograph showing roughness of the glacier surface. The major crevasse valleys are about 20 meters deep and 50 meters apart. Glacier flow is from left to right. U.S. Geological Survey photograph No. 75M5-56 by L.R. Mayo, October 8, 1975.

PURPOSE AND SCOPE

The purpose of this report is to describe the interpolation of the velocities to the grid nodes so that the data do obey the continuity equation. The data obtained from the vertical aerial photography are described in the section "Methods of Data Acquisition," which also includes a description of some independent data on bed topography and mass balance. The application of the

continuity equation to the data at the grid nodes is detailed in the section "The Data Consistency Condition," which also discusses the relation assumed between surface velocity and average horizontal velocity in the vertical column through a grid node. The section "Initial Estimation of Velocities" describes the transformation of the photogrammetrically determined displacement vectors to velocity vectors and the preliminary interpolation

of them to the grid nodes; it also describes how the error in that interpolation was estimated. The section "Methods of Data Interpolation Methods" relates how a linear algorithm for adjusting one velocity field (Rasmussen, 1985) was applied to the Columbia Glacier data; it also relates how that algorithm was used with the velocity fields for 21 flight intervals to estimate the bed topography and the mass-balance distribution.

The sensitivity of the solution, to the values adopted for the bed topography and to the parameters defining the linear balance-versus-altitude functions, is described in the section "Resulting Data Set." Shortcomings of the derived data set are the main subject of the section "Discussion." The internally consistent velocity vectors for the lower part of Columbia Glacier (fig. 3) are tabulated in appendix A for 120 nodes of the square grid, for each of 21 flight intervals spanning the period June 2, 1977, through September 1, 1981. Although the terminus position is not used explicitly in the creation of the internally consistent set of glacier geometry and flow data, it is the variable to be used along with the data set in investigating the calving mechanism; therefore, terminus position, which is taken directly from the aerial photography, is included for convenience in appendix B in terms of the same grid, for the same period. As a result, this report, together with Rasmussen and Meier (1985) of the same U.S. Geological Survey Professional Paper series, contains values at each grid node, for each flight interval, for every variable in the internally consistent set of geometry and velocity data for the lower part of Columbia Glacier for a 4.25-year period.

METHODS OF DATA ACQUISITION

Data for all the variables needed to create an internally consistent set of glacier flow data were obtained from vertical aerial photography and photogrammetry. These variables are surface topography, surface velocity, bed topography, and mass-balance distribution. Data for the first two variables were directly obtained photogrammetrically. Because fields of the first two exist for many time periods, it was possible to obtain data for the last two variables indirectly.

Existing independent determinations of bed topography and mass balance are not adequate for creating a data set. Soundings of the bed are too sparse spatially, and, in the case of the airborne soundings, inferred bed altitudes are subject to large error. The mass-balance measurements are too sparse temporally.

Owing to the lack of adequate independent information on bed topography and mass balance, the internally consistent data set was derived entirely from the photogrammetric data. A redundancy implicit in the large volume of surface velocity and surface topography data

was exploited to obtain the bed topography and the mass-balance indirectly, in a best fit sense. The bed soundings and mass-balance measurements that do exist were used only as a basis of comparison for the bed and mass balance estimated from the aerial photography.

VERTICAL AERIAL PHOTOGRAPHY AND PHOTOGRAMMETRY

The data set is derived from vertical aerial photographs taken during 22 flights (flights 9-30) over the period June 2, 1977, through September 1, 1981 (table 1). Information on flights 1-8 and 31-45 is given by Meier and others (1985a). Flights 3-8 covered only the lowest 4 km of the glacier. Flights 9-30 are the ones for which surface altitudes were carefully interpolated to the grid nodes (Rasmussen and Meier, 1985). Because surface topography is one of the elements of the data set, the interpolation of the velocity vectors is confined to the same period.

TABLE 1.—*Dates of aerial photography*

[Decimal year indicates time of flight; $t=1978.000$ at 0000 hours on January 1, 1978, and increases by 1/365.2422 each day thereafter]

Flight number	Date	Decimal year
1977		
9.....	June 2	1977.418
10.....	July 7	.514
11.....	Aug. 29	.659
12.....	Nov. 8	.854
1978		
13.....	Feb. 28	1978.160
14.....	Apr. 19	.297
15.....	June 11	.442
16.....	July 30	.576
17.....	Aug. 26	.650
18.....	Nov. 8	.853
1979		
19.....	Jan. 6	1979.014
20.....	Apr. 12	.277
21.....	Aug. 18	.628
22.....	Oct. 20	.800
1980		
23.....	Feb. 29	1980.162
24.....	May 12	.361
25.....	July 22	.556
26.....	Sept. 2	.671
27.....	Oct. 30	.830
1981		
28.....	Mar. 7	1981.180
29.....	June 16	.457
30.....	Sept. 1	.667

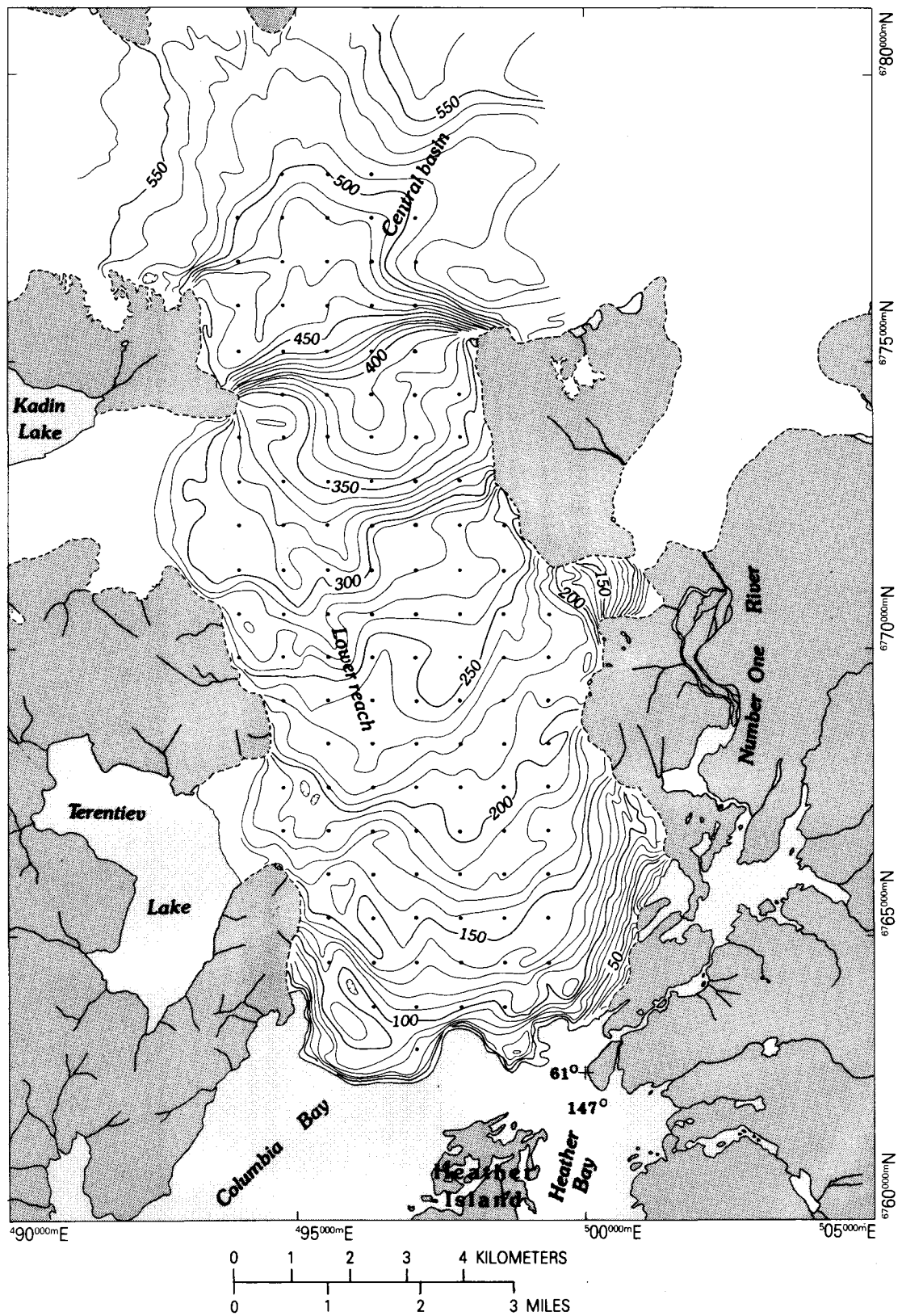


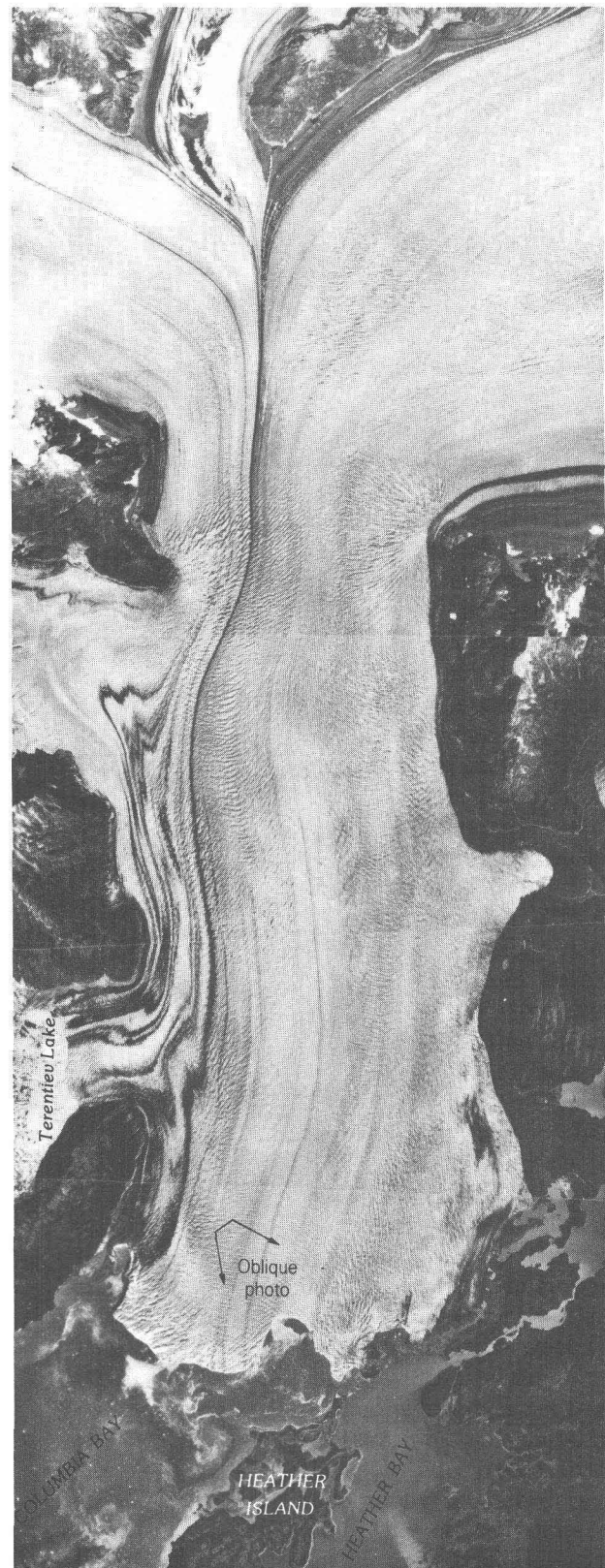
FIGURE 3.—Surface topography of lower part of the glacier on September 1, 1981, from 1:50,000-scale topographic map prepared at 10-meter contour interval by Air Photo Tech, Inc., of Anchorage, Alaska, and smoothed by the author (Rasmussen and Meier, 1985). Part of the vertical aerial photography from which this map was prepared is shown in figure 4. Also shown (dots) are the 120 nodes of the square grid at which data are tabulated.

FIGURE 4.—Mosaic of five vertical aerial photographs of lower part of the glacier taken from about 7,000 meters on September 1, 1981. North is to the top, and ice flow is toward the bottom. The field of view of the low-level oblique photograph (fig. 2), which was taken 6 years earlier, is indicated by the arrows. Photograph by Air Photo Tech, Inc., of Anchorage, Alaska. Approximate scale is 1:100,000.

The photogrammetric analysis of the photography from flights 9-30 was done by the U.S. Geological Survey Western Mapping Center at Menlo Park, Calif. The intricate crevasse pattern of the lower part of the glacier (fig. 4) provides many identifiable features throughout the region. The pattern is so pronounced that winter snowcover does not obliterate it. Because these natural features are irregularly positioned, interpolation was necessary to get surface altitudes at the grid nodes. The method of optimum interpolation was applied to the photogrammetrically determined coordinates of these features, which were subject to an error of about 3.5 m in the vertical, and resulted in surface altitudes at the grid nodes that were accurate to between 2 and 4 m (Rasmussen and Meier, 1985). The reduction of error results from the low spatial correlation of the altitude errors in the photogrammetric points and from the high spatial correlation of the altitude changes themselves.

Surface topography is an explicit element of the data set. Its changes over time are also important, for the condition of internal consistency is expressed in terms of these changes. Although the error in the altitudes themselves ranges from 2 to 4 m, the error in the altitude changes is probably much smaller, and the altitude changes are taken here to be correct to 0.1 m, as published. There are several reasons for this.

One reason is that the errors in successive altitudes at any grid node are believed to be strongly, positively correlated. The error in the altitude change thus tends toward the difference between the errors in the two altitudes from which the change was calculated, as can readily be seen upon considering the statistics of a linear combination of correlated variables. If the errors in successive altitudes were perfectly correlated, the errors in the altitude change would be exactly the difference between the errors in those altitudes. The strong positive correlation between the altitude errors is a result of the way the optimum interpolation algorithm was applied, which was not to the altitudes themselves of the photogrammetric points, but rather to the departures of those altitudes from a first approximation of the surface topography for the date of the flight from which the photogrammetric points were obtained. Interpolating among the altitude departures permitted use of photogrammetric points both from the flight on a particular date and from other flights near that date. In interpolating the surface altitude at a grid node for a particular



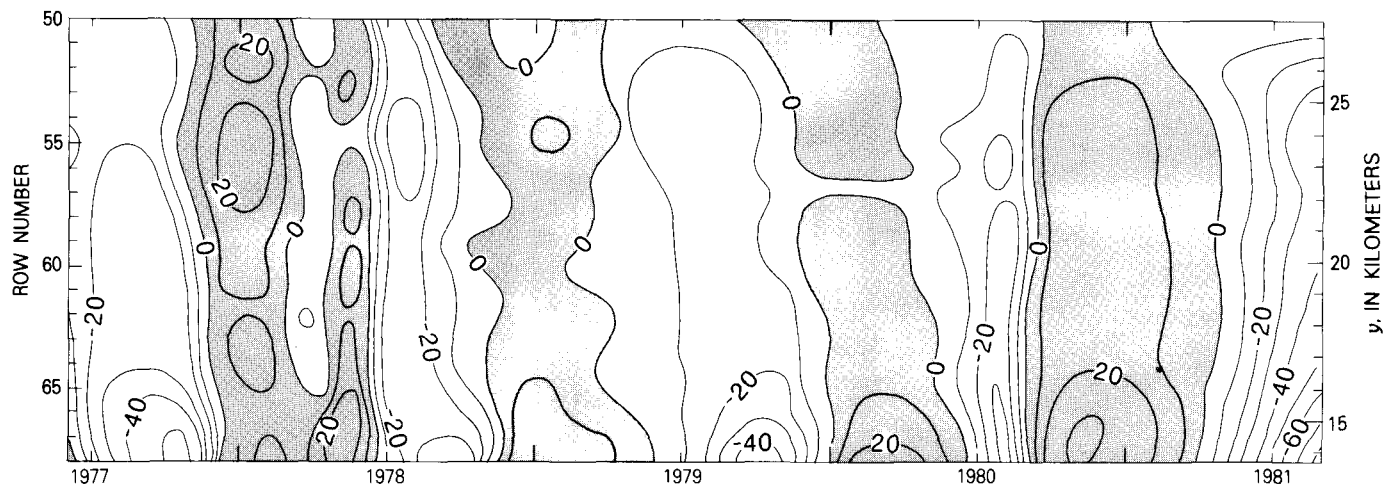


FIGURE 5.—Rate of change of surface altitude as a function of distance downglacier and of time. For each grid row (fig. 7) the rate is averaged across the width of the glacier. What is measured photogrammetrically is the average rate between successive dates of aerial

photography; the hand-drawn contour field is a smooth field that has the same average values over these periods. The contour interval is 10 meters per year, and a positive value (stippled) indicates a rising surface.

date, one-third of the photogrammetric points used were from the flight on that date and the others were from other flights (Rasmussen and Meier, 1985, fig. 16); for a photogrammetric point to be used, it had to be within 1 km of the grid node and within 0.4 a of the date. These ranges are large compared with the average interval between flights (0.2 a) and the grid spacing (762.5 m).

As a consequence, the altitudes interpolated to a grid node on two successive dates were based on many of the same photogrammetric points. The error in the vertical coordinate of such a point would influence the errors in the two interpolated altitudes in similar ways. The two influences are not identical because of changes over time in the composition of the set of photogrammetric points used to interpolate for a particular grid node, and because of changes in the differences between the time coordinates of the points and the date for which the altitude is being interpolated.

There is believed to be little node-to-node variation in the error in the altitude changes. This is suggested by the regularity of the spatial variation of the altitude change between any pair of successive flights (Rasmussen and Meier, 1985, app. B). Systematic error—in which all photogrammetric points on a particular date are in error by an amount that is constant or is weakly varying in space—would not be revealed by plotting the altitude changes. In an internally consistent data set derived entirely from photogrammetry, a systematic error would be incorporated as a distortion of the inferred mass balance. At least one such systematic error is, indeed, believed to exist, as will be mentioned later. The spatial regularity of the altitude changes probably is due to the sharing of photogrammetric points from node to node.

The altitude change over the lower part of the glacier is shown in figure 5 as a function of time and, by averaging across the glacier width, as a function of distance downglacier. The most prominent feature of the change is its synchronism, for no waves are discernible. The change has an annual oscillation—generally rising in winter, falling in summer—with an amplitude about the same size as the annual amount of the long-term rate of surface lowering during 1977–81. The long-term lowering over this period was about 10 m at the top of the region and about 20 m at the bottom, resulting in a slight steepening of the surface slope.

Another reason why the altitude changes are taken to be correct is that, when the condition of internal consistency is imposed, errors in altitude change have a much smaller relative effect on velocity than the relative effect errors in velocity have on altitude change. For example, if the grid spacing in a centered finite-difference approximation of the continuity equation were equal to half the ice thickness, then a 1-m/a error in the rate of thickness change would correspond to a 1-m/a error in velocity; this is significant because the velocity is of the order of 1,000 m/a and the thickness change is of the order of 10 m/a. Moreover, adjustment of altitude changes would have to be done implicitly within a process of explicitly adjusting the altitudes themselves, and it is not obvious how this should be done.

A third reason why the altitude changes are taken to be correct is that they are just as numerous as the velocity vectors: there is a separate value for every flight interval, for every grid node. If the condition of internal consistency were achieved by adjusting the altitudes as well as the velocities, there would be no variance left over from which to estimate the bed topography or

mass-balance distributions. The decision was made to adjust the velocities rather than the altitudes because the altitudes had already been subjected to the method of optimum interpolation, whereas the velocities were still in the form of raw data.

The displacement of a point from the date of one flight to the date of the next was converted to a velocity vector by dividing displacement length by the elapsed time between the flights, the velocity being an average value over that interval. For each of the 21 flight intervals, both horizontal components of velocity were hand contoured at a scale of 1:50,000 to get initial estimates of the velocity fields. The number of displacement vectors declined from about 180 for flights early in the period to about 110 for those late in the period. For all flights, the photogrammetric points were distributed quasi-uniformly over the region (Rasmussen and Meier, 1985, tables 1 and 3, fig. 7). There were slightly fewer displacement vectors than points because, for the displacement during the intervening interval to be determined, the same point had to be located on the dates of both flights.

RADIO-ECHO SOUNDINGS AND STAKE MEASUREMENTS

Radio-echo soundings of the bed were taken in 1978, a few from the glacier surface and many from an airplane flying about 850 m above the surface. Seven north-south and 12 east-west lines were flown over the lower half of the region. The airborne soundings were much more numerous than the surface soundings, but several difficulties—in recording echo arrival times, in correlating them with the airplane's horizontal position, and in determining airplane altitude—added to the deleterious effect of the great airplane altitude and led to an estimated 30-m error in the inferred bed altitudes (Brown and others, 1986). The 10 surface soundings (Mayo and others, 1979) were taken mainly along the lateral margins of the lower half of the region.

Measurements were made at 11 ablation stakes in the region from August 21, 1977, to September 3, 1978 (Mayo and others, 1979). They covered the region well, but they spanned less than a quarter of the 4.25-year period of the data set. The dates of initial and final measurements corresponded fairly well with dates of aerial photography (flights 11 and 17), but only five of the stakes were read an additional time during the year, and only one of these was read more than once during the year.

THE DATA CONSISTENCY CONDITION

The only condition of internal consistency that is imposed on the data is the principle of conservation of

mass, which is expressed by the continuity equation. As little as possible is assumed about the relation between the velocity field and the glacier geometry. This is done because the flow law—of ice masses generally and of Columbia Glacier particularly—is poorly known (Hooke, 1981), because the abundance of photogrammetric data permits avoiding most assumptions, and because an independently obtained internally consistent data set may be a valuable tool for studying the flow law. Two things, nevertheless, did have to be assumed about the flow: the first was that the minimum velocity observed during the 4.25-year period of record was divided equally between sliding and deformational motion; the second was that the vertical profile of the deformational motion followed a power law with the commonly used value $n=3$ for the exponent.

Earlier modeling work (Bindschadler and Rasmussen, 1983), which did not benefit from the present abundance of data and which explicitly treated only the longitudinal component of the flow, used a set of initial conditions that was internally consistent with respect both to the continuity equation and to a flow law; it was assumed that both the functional form of the flow law and the numerical values of its parameters were known. Internally consistent initial conditions are important to models so that the changes they compute in surface altitudes will represent realistic estimates of the glacier's dynamics. If inconsistencies exist in the initial conditions, a model will produce an artificial redistribution of mass to reconcile them.

There are many uncertainties concerning the flow law. One is in knowing the correct functional form for the dependence of velocity on geometry, both for the deformational component and for the sliding component of motion. Another is in knowing the numerical values of the parameters appearing in any particular functional form. These uncertainties are compounded by the well-known fact that flow is not a function of just geometry; it also depends on temperature and other properties of the ice and, in the case of temperate glaciers, on the properties of the subglacial water regime, which often vary in time, principally seasonally.

It was not possible, however, to remain absolutely independent of the flow law while creating the internally consistent data set. Two assumptions about the flow had to be made; however, as will be shown, they have only a minor combined effect on the resulting data set. These assumptions were necessary because the continuity equation pertains to the flow through the entire thickness of the glacier, not just to the velocity at the surface. Therefore, a means was needed of using the surface velocity to estimate the average velocity throughout the thickness. One assumption concerned the numerical value of the exponent in a power-law formulation of the

flow law, and the other concerned the amount of the motion that was due to sliding.

Although some assumptions were made about the vertical variation of the flow, no assumptions were made about its transverse variation. Instead, the continuity equation was referred to two independent horizontal coordinates so that the full two-dimensional variation of a two-dimensional velocity vector could be represented explicitly. All rates—both surface velocities and mass-balance rates—are average values over the intervals between successive flight dates.

PARAMETERIZATION OF THE VERTICAL VARIATION OF VELOCITY

The average velocity throughout the thickness of the glacier is some fraction $\gamma \leq 1$ of the surface velocity; the two are equal and $\gamma = 1$ only in the special case when the motion is due entirely to sliding. Although γ is in reality a property of the velocity profile, the following mathematical development can be expressed more concisely if it is associated with thickness instead. Because the surface velocity is the variable that is obtained explicitly from the photogrammetric points, it is more convenient to think of γ as scaling the thickness instead of the velocity. Where h is the thickness, $\bar{h} = \gamma h$ is termed the "characteristic thickness." The product of \bar{h} and the surface velocity is the same as the product of h and the average velocity. Both of these products are simplified representations of the flux, which is actually the integral of the vertical profile of velocity from the bed to the surface (fig. 6). This representation of the flux in terms of the surface velocity is based on the assumption that the direction of flow is constant with depth.

Where S is the magnitude of the velocity vector V at the glacier surface, the product $\bar{h}S$ is the flux. The factor γ depends on the numerical value of the exponent n used in the flow law assumed for the deformational component S_d of the ice motion, and it depends on the relative contributions of the deformational component and the sliding component S_b to the total motion $S = S_d + S_b$. Thus (Rasmussen, 1985, eq. 5),

$$\gamma = \frac{n+1}{n+2} \cdot \frac{S_d + S_b}{S} \quad (1)$$

from which $\gamma = 1$ only for pure sliding motion, $S = S_b$.

It is generally believed that the deformational component depends on the gross geometry of the glacier (Nye, 1952), whereas the sliding component depends on the geometry and also on the subglacial, liquid phase water (Bindschadler, 1983; Kamb and others, 1985). The gross geometry is defined by the glacier's surface topography and its bed topography. Changes during the period 1977–81 in the bed topography are unknown, but they are

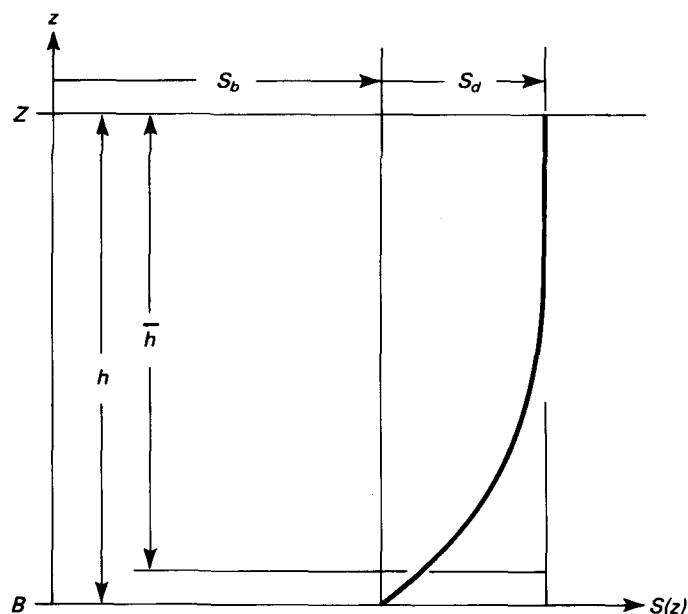


FIGURE 6.—Assumed vertical profile of velocity in the direction of flow. In this direction the magnitude of the flow vector is the speed S . The sliding component S_b is constant with depth, and the deformational component S_d follows a power law governed by the exponent in the flow law. The characteristic thickness \bar{h} is a fraction of the total glacier thickness h between the surface altitude Z and the bed altitude B . Its product $\bar{h}S$ with the surface speed $S = S_b + S_d$ is equal to the integral of the vertical profile $S(z)$ through the actual glacier thickness.

assumed to be negligible. Changes in the surface topography during this period (Rasmussen and Meier, 1985) also are small, especially compared with later changes (Meier and others, 1985b), and would produce a change of only about 2 percent in S_d (Meier and others, 1985a, p. 34).

Thus, at any point on the glacier, the variation in the total velocity—with high speeds the order of twice the low speeds—must have been due almost entirely to variation in the sliding component, which is believed to be due to large but unmeasured changes in the state of the subglacial water. In addition, the sliding component may well account for more than the variation above the lowest speed, because part of the lowest speed itself may be due to sliding. The extreme case—in which the lowest speed is taken to be due entirely to deformation, as assumed by Bindschadler and Rasmussen (1983, p. 5), and the sliding component is taken to vary from zero up to a value roughly equal to the deformational component—is rejected here. Instead, the deformational component is assumed here to be some fraction of the lowest speed, that is, $S_d = \phi S_{min}$, in which S_{min} is the minimum speed over the 1977–81 period. If this is substituted into equation 1, along with the relation $S = S_d + S_b$, there occurs

$$\gamma(x, y, t) = 1 - \frac{\phi}{n+2} \cdot \frac{S_{min}(x, y, t)}{S(x, y, t)} \quad (2)$$

to get the value of γ corresponding to the value of S at any particular time.

This formulation for γ is based on two assumptions. The first is that the changes in thickness and surface slope (fig. 5) are so slight over the period that changes induced by them in the deformational component of the motion are negligible compared with other uncertainties involved in using equation 2; thus, the deformational component of the motion is taken to be unchanging over the period. The second assumption is that the small change of bed slope in the transverse direction permits use of vertical profiles of velocity having the same shape (Nye, 1965) throughout the solution region.

Because the product term in equation 2 is small compared with unity, any errors in either n or ϕ are transformed into a much smaller error in γ itself. This effect is illustrated, for representative values of n and ϕ , in table 2. The smaller of these sources of error is n ,

TABLE 2.—Dependence of γ on n and ϕ

[The value $S_{min}/S=2/3$ is used in equation 2. This is very near the value of the ratio as averaged over all 120 grid nodes, over all 21 flight intervals. The number in parentheses shows the ratio of the indicated value of γ to the value for $n=3, \phi=0.5$]

ϕ	n		
	2	3	4
0.3	0.950 (1.02)	0.960 (1.03)	0.967 (1.04)
0.5	0.917 (0.98)	0.933 (1.00)	0.944 (1.01)
0.7	0.883 (0.95)	0.907 (0.97)	0.922 (0.99)

which embodies the only assumption about the flow law entering into the data adjustment calculations. Moreover, γ enters the equations only in the form of the product $\gamma h = \bar{h}$, in which relative error in h is believed (Brown and others, 1986) to exceed relative error in γ .

The values of the ratio γ that were used in the creation of the data set were calculated from the initial estimates of the velocity fields. Calculating them from the adjusted velocities would introduce substantial additional nonlinearity into the problem. As will be shown, only a small adjustment was needed to make the velocity fields obey the continuity condition. It is believed, therefore, that this discrepancy has a slight effect compared with the effects of other sources of uncertainty in specifying γ .

In creating the data set, the commonly used value $n=3$ was used for the flow-law exponent, and $\phi=0.5$ was used to express the assumption that the minimum velocity was due in equal parts to deformation and sliding. This

was chosen as a value intermediate between two unrealistic extremes: (1) that all the minimum velocity was due to sliding ($\phi=0$), rejected on the basis that the existing surface slope imparts shear stresses, which drive the deformational flow; and (2) that all the minimum velocity was due to deformation ($\phi=1$), rejected because the minimum velocity is much greater than deformation could produce by itself. From equation 2, then, $0.9=\gamma\leq 1$, so that $\gamma=0.90$ when $S=S_{min}$ and $\gamma=0.95$ when $S=2S_{min}$. The average value of γ was 0.936, when averaged over all 120 grid nodes, over all 21 flight intervals.

APPLICATION OF THE CONTINUITY EQUATION

A mathematical framework must be established for expressing the continuity equation. This requires a continuous coordinate system, to which the velocity vectors can be referred, and a square grid for use in approximating their spatial derivatives. The continuity equation is expressed in exact form in the continuous coordinate system and in finite-difference form on the grid.

Coordinate systems are chosen following conventional usage. Just as north is conventionally toward the top of the page and east is to the right, the x -axis is chosen to be positive to the right and the y -axis positive to the top. The origin of the x, y coordinate system is positioned so that (fig. 7)

$$\begin{pmatrix} x \\ y \end{pmatrix} = \frac{1}{0.9996} \begin{pmatrix} \text{UTM Easting} - 490,000 \text{ m} \\ \text{UTM Northing} - 6,750,000 \text{ m} \end{pmatrix} \quad (3)$$

Here the factor accounts for the fact that the Universal Transverse Mercator (UTM) surface is, at the latitude of Columbia Glacier, beneath the surface of the Earth. The vertical coordinate z is positive above local mean sea level.

In this coordinate system, the continuity equation may be written as

$$\dot{b} - \dot{h} = \nabla \cdot (h\gamma V) = \nabla \cdot (\bar{h}V) = [\partial(\bar{h}u)/\partial x + \partial(\bar{h}v)/\partial y] \quad (4)$$

in which all variables are functions of x, y , and t . The horizontal velocity vector V has components u and v in, respectively, the x and y directions. The balance rate \dot{b} is in ice equivalent. The time rate of change of thickness \dot{h} is taken to be equal to the time rate of change of the surface altitude \dot{Z} , which is equivalent to setting the time rate of change of the bed altitude \dot{B} to zero. This is done on the assumption that both glacio-isostatic adjustment since the 1964 Alaska earthquake (Plafker, 1969, p. 33) and glacial erosion were negligible over the 4.25-year period of the data set. When the equation is referred to

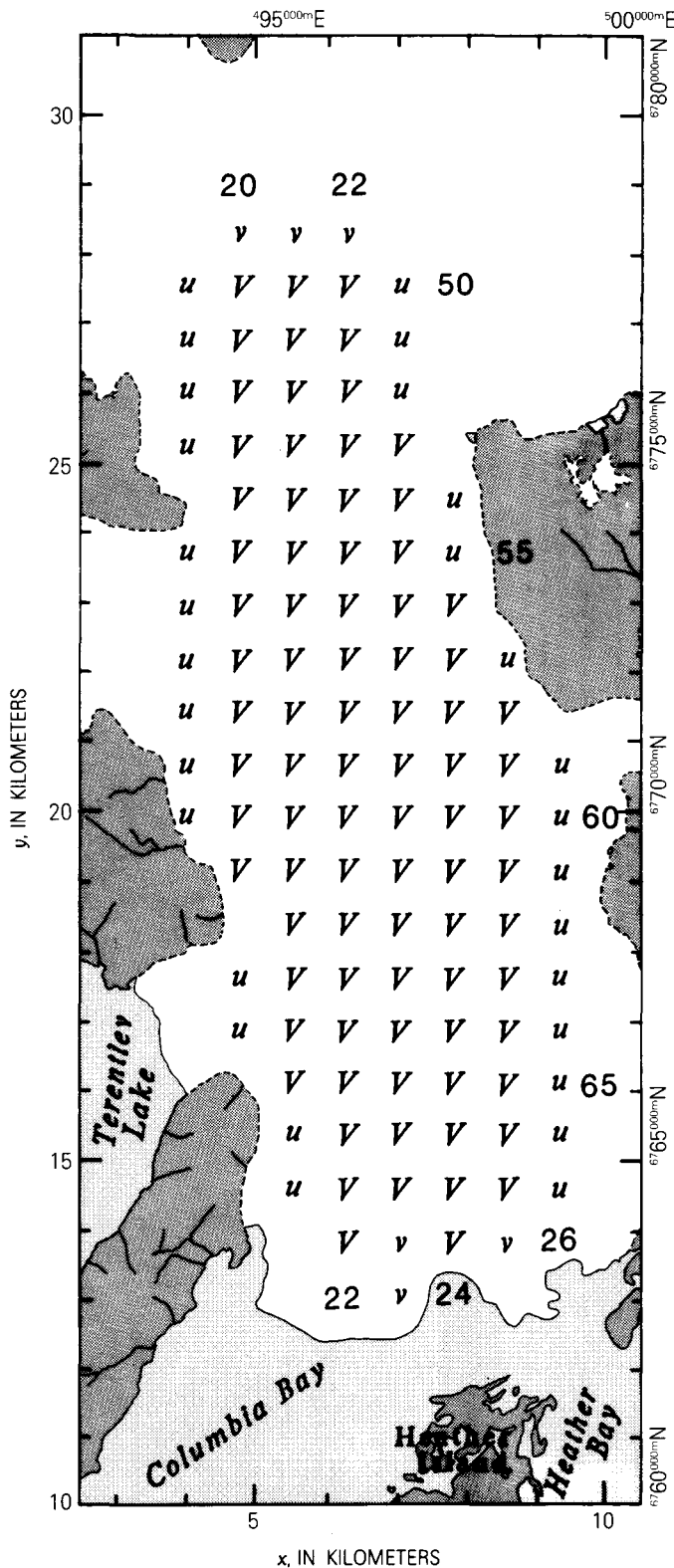


FIGURE 7.—Solution region grid nodes. The symbols *u*, *v*, and *V* indicate for each of the 120 nodes whether one, the other, or both velocity components are adjusted there. Row indices and column indices refer to the 762.5-meter, 71-by-63, square grid that covers the entire glacier.

the Columbia Glacier data, all variables are averages over the interval between successive photography flights.

Density does not appear explicitly in this version of the continuity equation. If the glacier density is assumed to be known, then the balance rate is also in those units. Rather than specifying this to be the density of ice, it is taken to be the bulk density of the glacier—a combination of ice, air, liquid phase water, and rock—and it is assumed to be constant in space and time. The most significant exception to this assumption of spatial constancy is probably the region very near the terminus, which the grid nodes barely reach. This assumption of constant density does not apply to winter accumulation of snow, which is at a much lower density. Thus, a special interpretation must be made of observed altitude changes and inferred mass-balance values during winter; this is discussed in the section “Resulting Data Set.”

Conventional matrix notation—with the row index *i* increasing down the page and the column index *j* increasing to the right—is used for denoting the nodes of the square 71-by-63 finite-difference grid, which is chosen to cover the whole glacier so that

$$\begin{pmatrix} i \\ j \end{pmatrix} = \frac{1}{762.5} \begin{pmatrix} 65,648 - y \\ 10,458 + x \end{pmatrix} \quad (5)$$

The 762.5-m spacing resulted, in the early days of the Columbia Glacier research program, from the combination of a particular graph paper and map scale. The irregularity of equations 5—with *j* related to *x* and *i* related (negatively) to *y*—is a consequence of following conventional notation for the coordinate systems themselves. The relations could have been regularized only by adopting unconventional notation, either for the grid indices or for the *x, y* system.

A centered finite-difference approximation of equation 4 is

$$(\bar{h}u)_{ij+1} - (\bar{h}u)_{ij-1} + (\bar{h}v)_{i-1j} - (\bar{h}v)_{i+1j} = 2\Delta x(\dot{b} - \dot{h}) \equiv F_{ij} \quad (6)$$

Because the right side of equation 4 is the flux divergence, F_{ij} is the flux divergence scaled by $2\Delta x$. Equation 6 is applied at the 77 interior nodes of the solution region (fig. 7): at rows $i=50-53, 55-60$ for column $j=20$; at $i=50-61, 63, 64$ for $j=21$; at $i=50-67$ for $j=22$; at $i=54-68$ for $j=23$; at $i=57-67$ for $j=24$; and at $i=59-67$ for $j=25$. The full vector *V* is defined at 85 nodes, only the *u*-component at 29 nodes, and only the *v*-component at 6 nodes. The tangential component at a boundary node does not enter equation 6, and therefore is undefined there.

INITIAL ESTIMATION OF VELOCITIES

The first step in obtaining internally consistent velocity data is to transform the photogrammetrically deter-

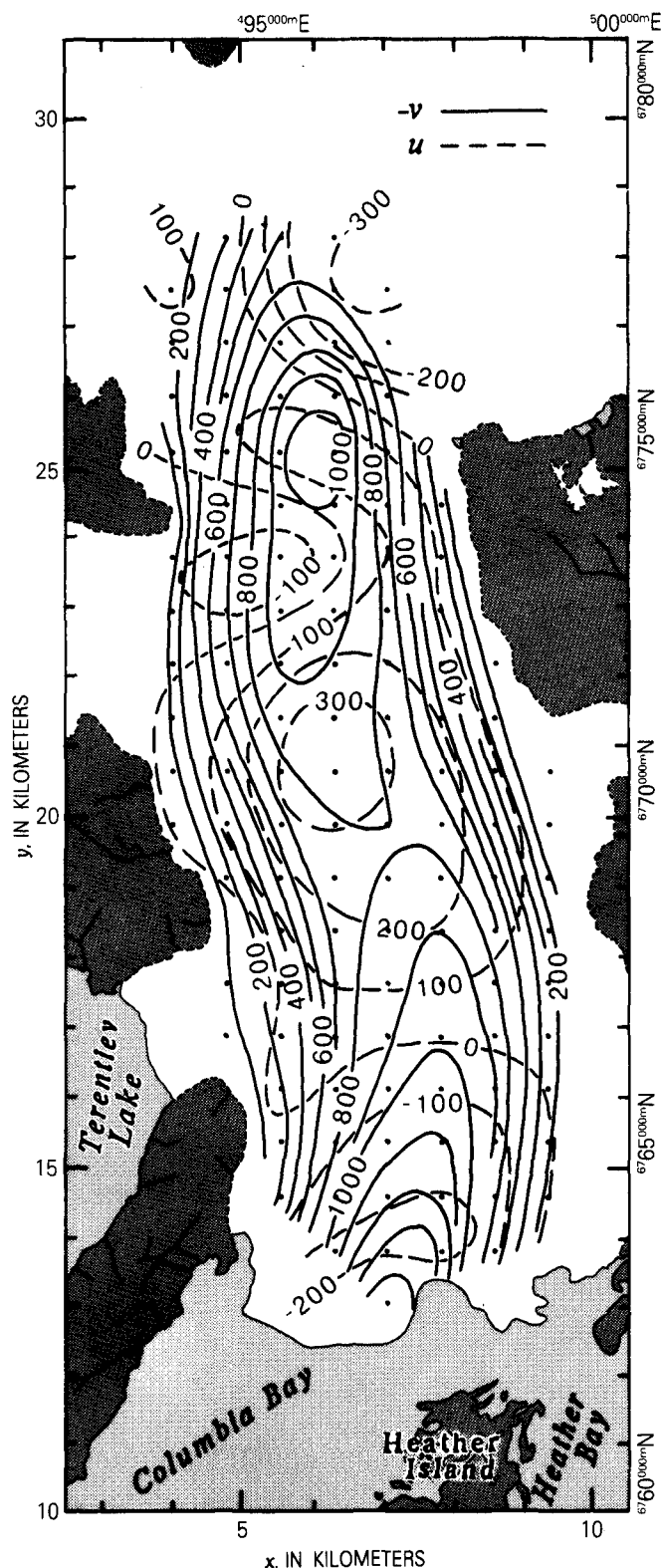
FIGURE 8.—Adjusted velocity, averaged from June 2, 1977, through September 1, 1981. Both the v -field (solid) and the u -field (dashed) are hand contoured from the adjusted values at the grid nodes, following the u - v pattern of figure 7; the contour interval is 100 meters per year.

mined displacements into velocity vectors. For each of 21 flight intervals $L=9,10,\dots,29$, each velocity component was contoured separately as a function of x and y . The displacement components were converted to velocity components by dividing by the length Δt of the interval, and they were plotted at the midpoint of the photogrammetric point's trajectory (Fountain, 1982). Because the strain rates in this region of the glacier are so low, and because the time intervals between flights were so short, the error in doing this is negligible (Rasmussen, 1983).

The contouring was done by hand at a scale of 1:50,000, at a contour interval of 50 m/a. Of 2,909 photogrammetric displacements available for contouring the 21 pairs of u -fields and v -fields, 39 were disregarded as being aberrant. These disregarded displacements originated, presumably, because occasionally one point on the glacier surface was mistaken for another during the photogrammetry, so that the line segment joining the position of one point on one date to the position of some other point on the next date was mistakenly interpreted as being the true displacement of the first point. Apart from disregarding the 39 aberrant displacements, the contouring was done as if the original data were exact; that is, no intentional smoothing or revision was attempted during the contouring.

Values for each component were then interpolated visually at each of the 120 grid nodes. Because the number of nodes is comparable to the number of displacement vectors, interpolating to the nodes did not alter the scale of definition of the data. The u -field and v -field averaged over the 4.25-year period of the data set—as weighted by the lengths of the individual flight intervals—are shown in figure 8. Fields for individual intervals would roughly resemble the long-term average fields if all contour labels were to be multiplied by a factor that ranges, from interval to interval, from about 0.7 to about 1.4. The variation in time for three of the nodes is shown in figure 9. (Although the adjusted velocity vectors are the subject of later sections of this report, they are the ones that are shown in figs. 8 and 9. The adjusted vectors are more significant than the initial estimates and differ little from them.)

The initial estimates of the velocity components are tabulated in appendix A for all 120 nodes, for all 21 flight intervals. Although the tangential components at the boundaries are not adjusted, they are indirectly part of the data set. They are used in equation 2 in forming the velocity ratio γ .



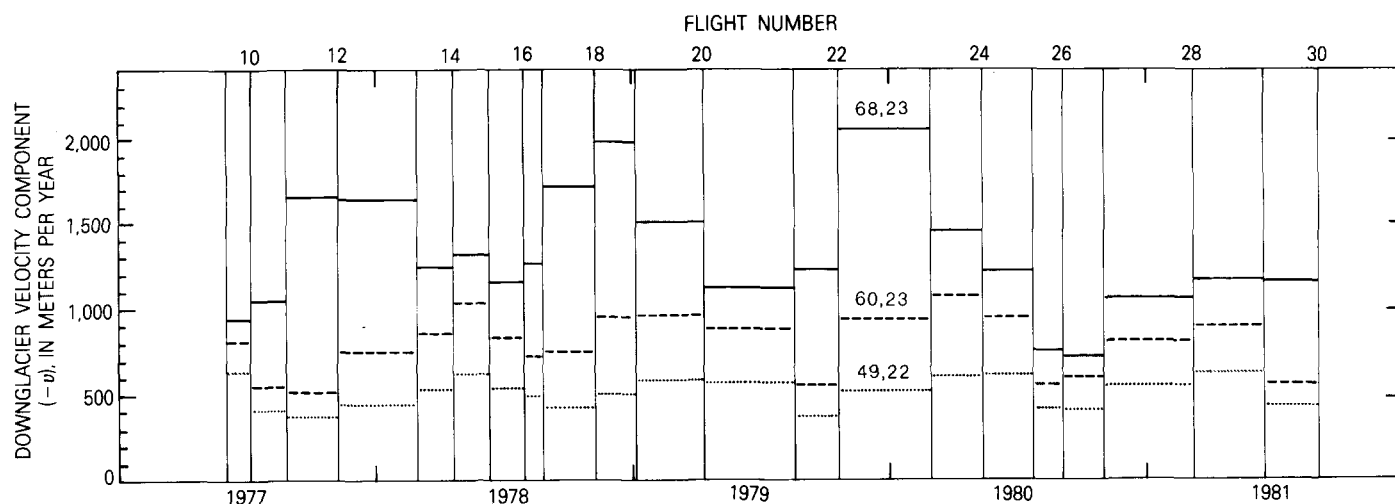


FIGURE 9.—Adjusted velocity as a function of time at three selected grid nodes (fig. 7), June 2, 1977, through September 1, 1981. The downglacier component $-v$ is shown as average values over the periods between successive dates of vertical aerial photography.

The errors ϵ_u and ϵ_v in the values of the components interpolated to a grid node are assumed to be proportional to the values of the gradients $|\nabla u|$ and $|\nabla v|$. The gradients are estimated from the initial contouring of the u and v fields and are averaged over a horizontal distance of about 1 km in the vicinity of the node. Several effects are believed to contribute to the errors.

A reference value of 1 mm was taken as a measure of the combined effects of the human error, both in the placing of the contours and in interpolating between them to get the initial estimate of a value at a grid node. Because the scale of the contour fields was 1:50,000, the 1-mm error corresponds, for example, to a 5-m/a error in the velocity if the average gradient was 100 m/a per kilometer in the vicinity of the node. The component error corresponding to the 1-mm error was adopted if the contouring was supported by a particular high density of photogrammetric displacement points in the vicinity of the node: three points, each 100 m from the node.

The accuracy of the contours is assumed to be proportional to the spatial density of the photogrammetric displacement vectors in the vicinity of the node. To represent this, the error corresponding to a 1-mm contouring error is scaled by

$$f = 15 \left[1 + 700 \sum_{k=1}^3 (50 + r_k)^{-1} \right]^{-1} \quad (7)$$

The distances from the grid node to the M displacement points from which the contouring was done are denoted $r_1 \leq r_2 \leq r_3 \leq \dots \leq r_M$. In accord with the definition that the 1-mm error applies to the reference case when $r_1 = r_2 = r_3 = 100$ m, the coefficients of equation 7 give $f = 1$

when that occurs. The coefficients were also chosen, subjectively, to give $f = 5$ when the typical low density $r_1 = r_2 = r_3 = 1,000$ m occurs. The dependence of f on r_k is illustrated in figure 10.

Another contribution to ϵ_u and ϵ_v is the standard 4-m error (Meier and others, 1985a) in determining the displacements of the photogrammetric points. This 4-m error is a combination of the errors in determining a point's positions at the beginning and at the end of the flight interval. These two errors are assumed to be uncorrelated with each other, so that their resultant is assumed to be independent of the direction of flow. The 4-m error is transformed into a velocity error by dividing by the length Δt of the interval. The position error is here arbitrarily assigned the same direction as the error obtained by scaling the gradients by f , to which it is added according to

$$\begin{pmatrix} \epsilon_u \\ \epsilon_v \end{pmatrix} = [f^2 + (4/\Delta t)^2 / (|\nabla u|^2 + |\nabla v|^2)]^{1/2} \begin{pmatrix} |\nabla u| \\ |\nabla v| \end{pmatrix} \quad (8)$$

Whereas the values of ϵ_u and ϵ_v are intended to be physically realistic, only their relative sizes from node to node have any effect on the creation of the data set. This is because they are used as weights in a least squares minimization and could all be scaled arbitrarily without affecting its result. The intent was that they be standard errors, which the 4-m displacement errors are. The ϵ_v at several nodes are shown in figure 11 for the initial estimation of the v -component for flight interval 25.

The spatial and temporal distributions of the errors are summarized by the following average values

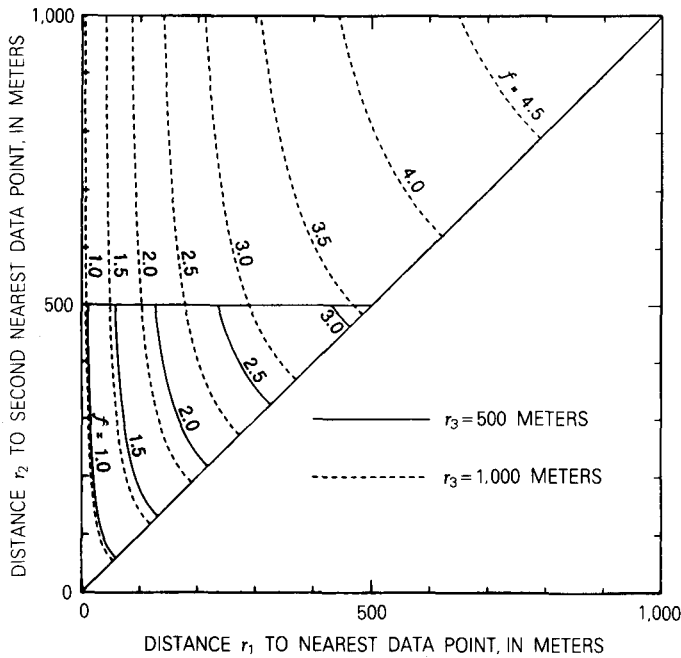


FIGURE 10. — Data-density weighting factor used in estimating error in the initial estimate of the ice velocity at a grid node. The factor f (eq. 7) is contoured, at an interval of 0.5, as a function of the distances r_1 and r_2 of the two data points nearest the grid node. Two cases are shown: where the distance r_3 of the third nearest data point is 500 meters (solid) and where it is 1,000 meters (dashed). At $r_1 = r_2 = 0$, the value of f is 0.495 when $r_3 = 500$ meters and is 0.506 when $r_3 = 1,000$ meters.

$$(E_u)_{ij} = \left[\frac{1}{21} \sum_{L=9}^{29} (\epsilon_u)_{ijL}^2 \right]^{1/2} \quad (9)$$

$$(E_v)_{ij} = \left[\frac{1}{21} \sum_{L=9}^{29} (\epsilon_v)_{ijL}^2 \right]^{1/2} \quad (10)$$

$$E_L = \left[\frac{1}{205} \sum_{ij} (\epsilon_u)_{ijL}^2 + (\epsilon_v)_{ijL}^2 \right]^{1/2} \quad (11)$$

For the average for flight interval L , the i, j summation in equation 11 runs over all 120 grid nodes, but ϵ_u is defined on only the 114 nodes where u is adjusted and ϵ_v on only the 91 nodes where v is adjusted.

The 114 $(E_u)_{ij}$ and 91 $(E_v)_{ij}$ are contoured in figure 12. The former, whose root-mean-square (rms) average is 27 m/a, are roughly uniformly distributed over the region. The latter, whose rms average is 67 m/a, have a more pronounced spatial variation, with values on the high-gradient margin of the region (fig. 8) being two or three times greater than in the low-gradient interior.

The E_L , which range from 36 to 60 m/a over the 21 flight intervals, are shown in figure 13. The rms average of the 21 values is 49 m/a. Apart from the effect of space

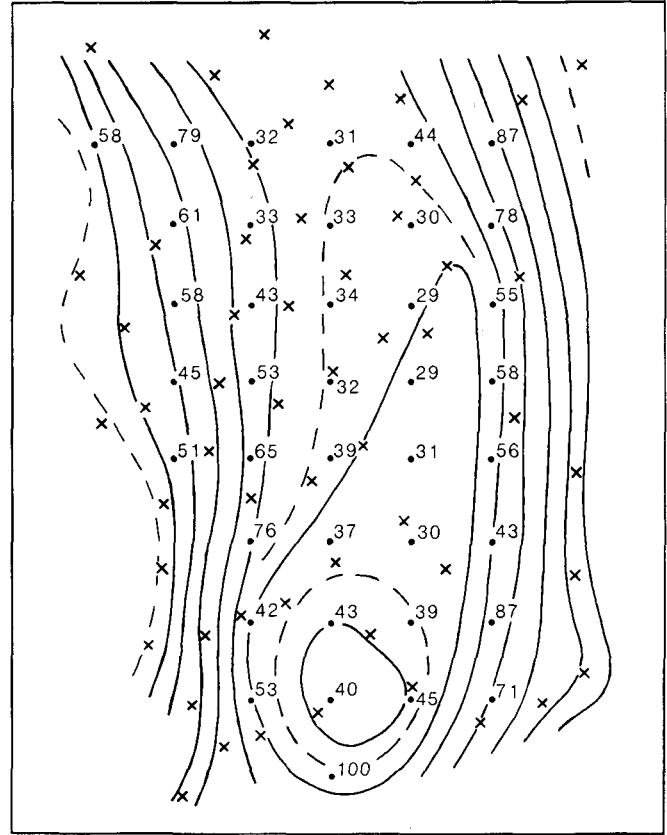


FIGURE 11. — Dependence of error estimate on velocity gradient and local density of data points. The contour field, drawn manually from values at the data points (x's), is the v -component for flight interval 25 (July 22 to September 2, 1980); the contour interval is 100 meters per year, and four intermediate contours (dashed curves) are shown. The values at the grid nodes (solid circles) are the estimated errors, in meters per year, in the estimates of the v -components at those nodes. The nine lowest rows of the grid are shown. The relation between error and gradient is readily apparent. That between error and data density is less so, because the density is more nearly homogeneous than the gradient is. The errors at the first and last nodes of the third row from the bottom, however, do illustrate the effect of data density; the much greater data density at the 42 overrides the fact that the gradient is about half again as strong there as it is at the 87.

and time variations in the data-density factor f (eq. 7), the estimated errors are nearly proportional to the components of the velocity gradient (eq. 8). Because there is so little change over time in the shapes of the u and v fields, changes in the velocity gradient at any point are nearly proportional to changes in the velocity there. As a consequence, the time variation of the E_L roughly follows the variation of velocity (fig. 9).

METHODS OF DATA INTERPOLATION

If only one field of velocity vectors is available, there are numerous ways an internally consistent data set

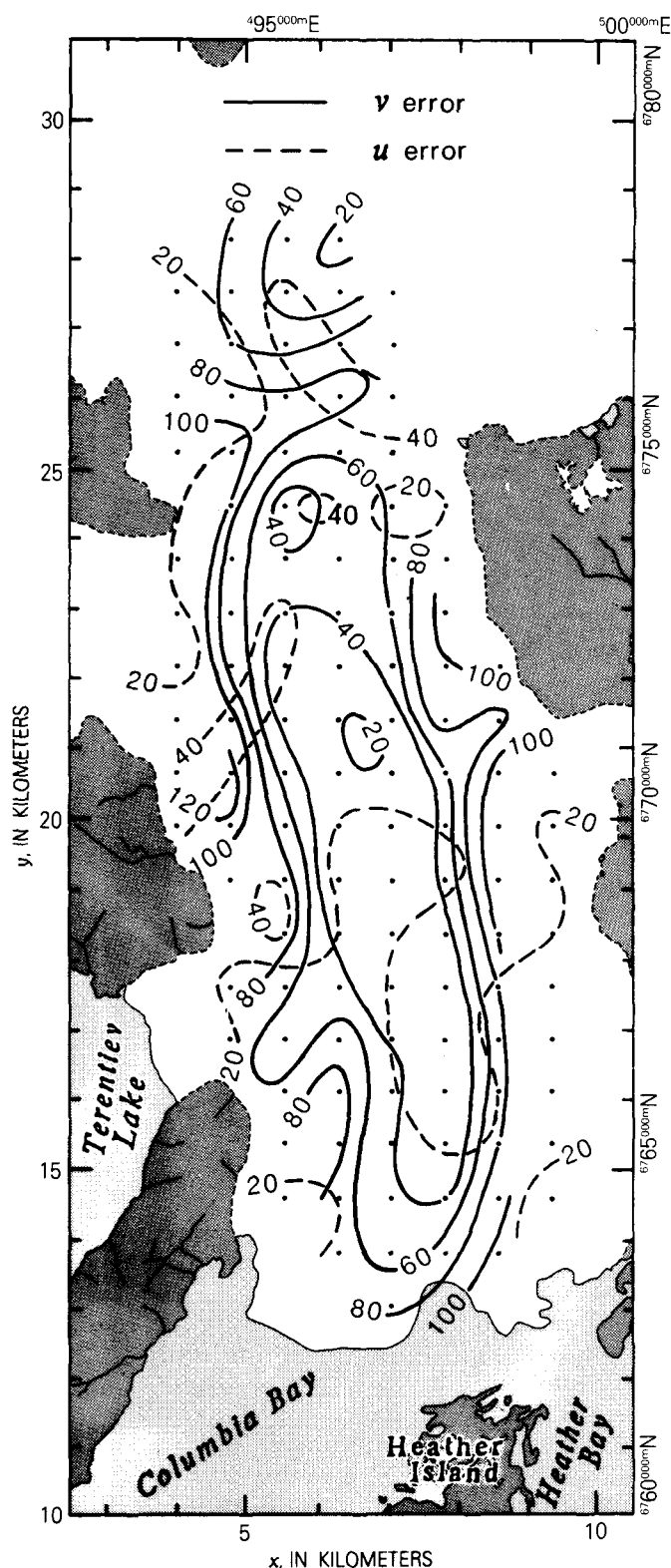
FIGURE 12.—Spatial distribution of estimated velocity errors averaged from June 2, 1977, through September 1, 1981. Both the E_u field (dashed) and the E_v field (solid) are hand contoured from the values at the grid nodes, following the u - v pattern of figure 7; the contour interval is 20 meters per year. The values are unweighted averages over the 21 flight intervals.

could be created. If the vector components—along with the surface altitudes Z_{ij} , their rates of change \dot{Z}_{ij} , the bed altitudes B_{ij} , and the velocity ratios γ_{ij} —are taken to be exact, then equation 6, with $(Z-B)\gamma$ substituted for \bar{h} , could be used to solve for the balance rate \dot{b}_{ij} at each node where the equation is applied. This would produce internally consistent values, but, if typical unadjusted velocity vectors are used, the \dot{b}_{ij} would be wildly erratic. A variation of this would be to specify the \dot{b}_{ij} , and to use the equation to solve for the \dot{Z}_{ij} , which would also be wildly erratic. This variation is what is done, essentially, when a numerical model operates on initial conditions that are inconsistent: the erratic \dot{Z}_{ij} cause the extraneous redistribution of glacier mass.

Another variation, in the case of having only one field of velocity vectors, would be to take both the \dot{b}_{ij} and \dot{Z}_{ij} to be exact and to choose the B_{ij} so that the data set is internally consistent. This would lead, however, to an underdetermined system of simultaneous linear equations. Because equation 6 is linear in the \bar{h}_{ij} , it is also linear in the B_{ij} . The system is underdetermined because the equation involves a larger number of B_{ij} than the number of nodes at which it is applied. In the case of the Columbia Glacier data, the equation is applied at 77 nodes in terms of the B_{ij} at 120 nodes.

Yet another variation, if only one velocity field is available, also leads to an underdetermined system at first, but it leads next to a well-behaved unique solution. It leads eventually, in the case of multiple velocity fields, to a solution in which both the B_{ij} and the \dot{b}_{ij} are estimated. It begins by assuming that values are known for all variables except the velocity vectors, for which only initial estimates exist. It is underdetermined because equation 6 is applied at only 77 nodes in terms of 205 velocity components; both the u -component and the v -component are used at each of 85 interior nodes, and only the component normal to the boundary is used at each of 35 boundary nodes. A unique solution occurs upon imposing the requirement that the velocity components not only must satisfy the 77 applications of equation 6 but also must minimize a weighted least-squares measure of their differences from the initial estimates of them. A noniterative, linear algorithm exists (Rasmussen, 1985) for adjusting the velocity vectors to obtain this solution.

When multiple velocity fields are available, the linear algorithm can be used as a component of a broader procedure for estimating the bed topography and mass-



balance distribution. Where D_L is the magnitude of the adjustment of the velocity field for flight interval L , the objective of the procedure is to choose the B_{ij} and the \hat{b}_{ijL} to minimize the sum of the squares of the D_L for the 21 intervals. In doing this, the \hat{b}_{ijL} are assumed to follow a separate linear function of altitude for each flight interval; because a linear function can be specified with two coefficients, only $21 \times 2 = 42$ balance parameters are introduced account for the \hat{b}_{ijL} . The result is that the data—that is, the photogrammetrically observed surface altitudes and velocity vectors—are the sole determinants of the bed topography and mass-balance distributions in a way that is constrained only by the condition of internal consistency.

Because the Columbia Glacier data set spans 21 flight intervals, there are $21 \times 205 = 4,305$ data values. When the 42 balance parameters are taken together with the 120 bed altitude parameters, which are assumed to be unchanging over the period of the data set, there are a total of 162 model parameters. The gross data-to-parameter ratio, thus, is a robust $4,305/162 = 26.6$. The initial estimates of the velocity vectors are regarded as data contaminated by error, rather than as model parameters.

THE LINEAR ALGORITHM FOR ADJUSTING A SINGLE VELOCITY FIELD

Once fields of the characteristic thickness \bar{h} and the flux divergence F are set, the method of Rasmussen (1985) is used to make the minimum adjustment of the velocity field V_{ij} that is required for satisfying continuity, but the adjustment weights λ_{ij} are chosen here to reflect the errors in the initial estimates of the velocity vectors $(u_0, v_0)_{ij}$. Rather than scaling the adjustments by the magnitude of the initial estimate, so that the sum of the squares of the relative adjustments is minimized, the weights are taken instead from independent estimates of the error, $(\epsilon_u)_{ij}$ and $(\epsilon_v)_{ij}$, in each component of each vector in the initial estimate of the velocity field. The quantity to be minimized then, for any particular flight interval L , is the norm:

$$N = \sum_{ij} \left[\frac{(\bar{u} - u_0)_{ij} + (\psi_{i+1j} - \psi_{i-1j}) / (2\bar{h}_{ij}\Delta x)}{(\epsilon_u)_{ij}} \right]^2 + \left[\frac{(\bar{v} - v_0)_{ij} + (\psi_{ij+1} - \psi_{ij-1}) / (2\bar{h}_{ij}\Delta x)}{(\epsilon_v)_{ij}} \right]^2 \quad (12)$$

Here $(\bar{u}, \bar{v})_{ij}$ is the easily formed parallel flow field with the $\bar{v}_{ij} = 0$ and the \bar{u}_{ij} formed by simply integrating equation 6 in the x -direction, and ψ_{ij} is a stream function.

Setting $\partial N / \partial \psi_{ij}$ to zero for all ψ_{ij} leads to the system of simultaneous linear equations for getting the ψ_{ij} :

$$\begin{aligned} & [(c_u)_{i+1j} + (c_u)_{i-1j} + (c_v)_{ij+1} + (c_v)_{ij-1}] \psi_{ij} \\ & - (c_u)_{i+1j} \psi_{i+2j} - (c_u)_{i-1j} \psi_{i-2j} - (c_v)_{ij+1} \psi_{ij+2} - (c_v)_{ij-1} \psi_{ij-2} \\ & = 2\Delta x \{ [(\bar{u} - u_0)\bar{c}_u]_{i+1j} - [(\bar{u} - u_0)\bar{c}_u]_{i-1j} + [(\bar{v} - v_0)\bar{c}_v]_{ij+1} \\ & \quad - [(\bar{v} - v_0)\bar{c}_v]_{ij-1} \} \quad (13) \end{aligned}$$

in which $c_u = \bar{c}_u / \bar{h}$ and $c_v = \bar{c}_v / \bar{h}$, with $\bar{c}_u = (\epsilon_u)^2 / \bar{h}$ and $\bar{c}_v = (\epsilon_v)^2 / \bar{h}$. Thus, equations 12 and 13 of Rasmussen (1985) are applied to incorporate individual, independent estimates of the errors $(\epsilon_u)_{ij}$ and $(\epsilon_v)_{ij}$ as the weights λ_{ij} .

The vector field that satisfies the continuity equation, and that resembles the original field as closely as possible, as defined by the weights, is obtained directly from the stream function that minimizes N :

$$\begin{pmatrix} u \\ v \end{pmatrix}_{ij} = \begin{pmatrix} \bar{u} \\ \bar{v} \end{pmatrix}_{ij} + \frac{1}{2\bar{h}_{ij}\Delta x} \begin{pmatrix} \psi_{i+1j} - \psi_{i-1j} \\ \psi_{ij+1} - \psi_{ij-1} \end{pmatrix} \quad (14)$$

The linear algorithm must be applied four times to adjust one velocity field. Because the increments of the subscripts to ψ in equation 13 are all ± 2 , all the row subscripts have the same even-odd parity, and all the column subscripts have the same even-odd parity. Four interlacing positionings of the ψ pattern are needed to cover the solution region: (row, column) = (even, even), (even, odd), (odd, even), and (odd, odd). The ψ on the (even, even) nodes, for example, produce u only on the (odd, even) and v only on the (even, odd) nodes, as given by equation 14. For a more complete description of these patterns, see Rasmussen (1985). The magnitude of the adjustment of an entire velocity field is, thus, the sum of the N -values for the four ψ positionings.

In terms of the Columbia Glacier data, the rms adjustment D_L for flight interval L is given by

$$D_L = \left(\frac{1}{205} \sum_{ij} \delta u_{ijL}^2 + \delta v_{ijL}^2 \right)^{1/2} \quad (15)$$

in which $\delta u = (u - u_0) / \epsilon_u$ and $\delta v = (v - v_0) / \epsilon_v$. This is the quantity that is minimized when the four N values are minimized. The subscript 0 denotes the initial estimate of the component, and the unsubscripted component is the adjusted value. The summation convention is that i, j run over all 120 nodes, but $\delta u = 0$ on those 6 boundary nodes where only v is adjusted and $\delta v = 0$ on those 29 nodes where only u is adjusted. The total adjustment over all 21 flight intervals is

$$D = \left(\frac{1}{21} \sum_{L=9}^{29} D_L^2 \right)^{1/2} \quad (16)$$

It may also be decomposed node-by-node as

$$D = \left(\frac{1}{114} \sum_{ij} (D_u)_{ij}^2 + \frac{1}{91} \sum_{ij} (D_v)_{ij}^2 \right)^{1/2} \quad (17)$$

in which the summations run over the 114 nodes where u is adjusted and the 91 where v is adjusted, with

$$(D_u)_{ij} = \left(\frac{1}{21} \sum_{L=9}^{29} \delta u_{ijL}^2 \right)^{1/2} \quad (18)$$

and

$$(D_v)_{ij} = \left(\frac{1}{21} \sum_{L=9}^{29} \delta v_{ijL}^2 \right)^{1/2} \quad (19)$$

USE OF MULTIPLE VELOCITY FIELDS TO ESTIMATE BED TOPOGRAPHY AND MASS-BALANCE DISTRIBUTION

A parameter-by-parameter method was used to find the bed altitudes and mass-balance values that minimize D . The bed topography is specified by the altitudes at the grid nodes. The linear $\hat{b}(z)$ functions were specified, for convenience, by their values \hat{b}_{100} and \hat{b}_{500} at $z=100$ and 500 m. When such a function is applied to the surface topography $Z(x,y)$, the spatial distribution of the mass balance is $\hat{b}[Z(x,y)]$.

In the beginning, rough estimates were made of the bed topography and the flux divergence. The bed inferred from the airborne radio-echo sounding was used in the lower part of the solution region, and it was continued at about the same depth and shape into the upper part. The flux divergence F was assumed to be zero, which is equivalent to assuming that all changes in surface altitude were due entirely to the mass-balance process.

In phase 1 of the method, the linear algorithm was applied—using these estimates of flux divergence and bed—to the velocity fields for all 21 flight intervals. The bed altitude at a grid node was revised according to whether the linear algorithm generally increased or generally decreased the velocities at that node. Increasing the velocities increased the fluxes, which could also have been accomplished by associating a greater thickness with the unadjusted velocities, and therefore the estimate of the bed altitude at such a node was revised downward to increase the thickness. Conversely, if the algorithm generally decreased the velocities at a grid node, the bed altitude there was raised. The amount by which to change a bed altitude is analyzed in the last section of Rasmussen (1985).

In phase 2, the revised bed topography was used in conducting a set of 21 two-parameter minimizations to estimate the linear $\hat{b}(z)$ functions for each of the 21 flight intervals. For each flight interval, every time this was done, D_L appeared to be a convex function of the two parameters \hat{b}_{100} and \hat{b}_{500} , which made finding the inter-

val's minimum very easy. The function $D_L(\hat{b}_{100}, \hat{b}_{500})$ is absolutely independent of the values of \hat{b}_{100} and \hat{b}_{500} used for any other flight interval.

About six cycles were made through phase 1 and phase 2. In subsequent cycles through phase 1, the revision of the B_{ij} was done by working from the inner, high-velocity nodes to the outer, low-velocity nodes. That is, the high fluxes were considered before the low fluxes. As the B_{ij} approached the minimizing values, the adjustment for a particular B_{ij} was generally done by taking it to be the minimum of the parabola through the three points $D(B_{ij}-10\text{ m})$, $D(B_{ij})$, $D(B_{ij}+10\text{ m})$. This procedure was facilitated by the small effect adjusting the bed altitude at one node had on the apparent minimizing bed altitude at nodes more than two rows or columns away from it. Adjusting the bed altitude at a low-velocity node had almost no effect on the minimizing bed altitude at any high-velocity node.

About 300 evaluations of D were needed to perform one cycle through phase 1 and phase 2. Two evaluations, at $B_{ij}-10\text{ m}$ and at $B_{ij}+10\text{ m}$, were used at each of the 120 grid nodes in phase 1. About 50 evaluations, each articulated into the 21 components $D_9, D_{10}, \dots, D_{29}$, were used in phase 2 to estimate the minimizing balance parameters.

A systematic method—which would estimate all 162 parameters simultaneously—would require vastly more evaluations of D . The Hessian matrix, which is usually employed, is a symmetric, real matrix that would be of order 162. It has 13,203 distinct elements, each being the mixed second derivative of D with respect to a particular pair of the parameters. Only those 840 second derivatives with respect to two balance parameters from two different flight intervals would be identically zero. As the finite-difference approximation of a mixed second derivative requires four evaluations of the variable, D would have to be computed about 50,000 times to form the matrix. Once the matrix is formed, it is used to solve a system of simultaneous linear equations to get the estimated adjustments to the 162 parameters. The method does not produce the minimizing values of the parameters in one such step, but rather must be applied iteratively.

There is no guarantee that any systematic method will converge or that, if it does, it will converge to a global minimum of D . Nor is there a guarantee that the parameter-by-parameter method has these properties. In the case of the Columbia Glacier data, however, the parameter-by-parameter method did converge toward an apparent global minimum.

RESULTING DATA SET

The result of the minimization procedure was an internally consistent, two-dimensional data set describ-

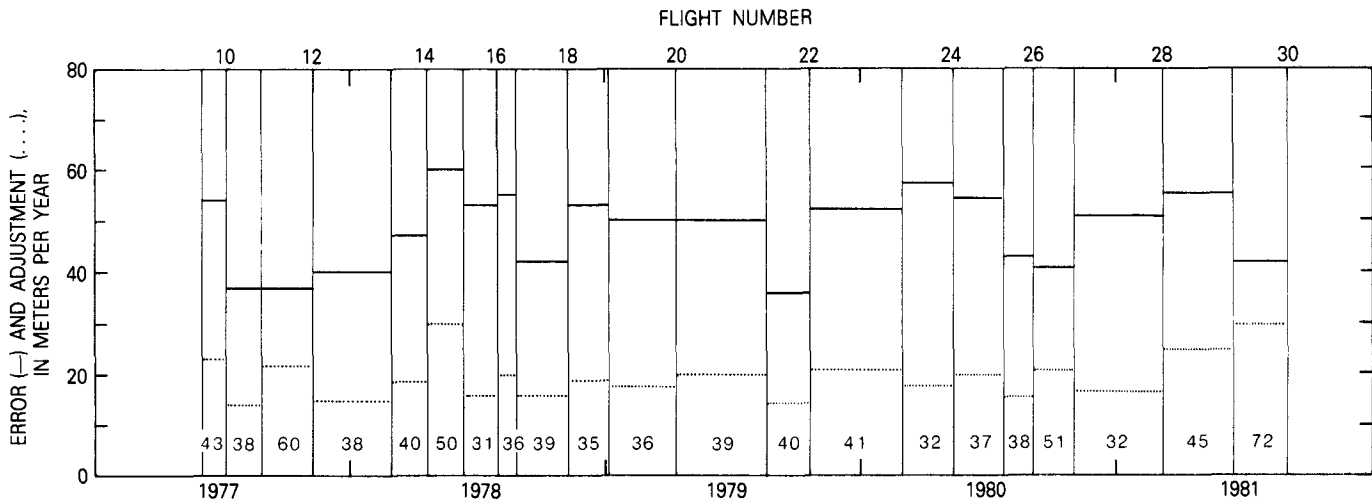


FIGURE 13.—Temporal distribution of estimated velocity error and of the magnitude of the velocity adjustment. Both the error E_L and the adjustment D_L are averaged over the 120 grid nodes of the solution region, and they are shown as average values over each of the 21 flight intervals. The number shown is $100D_L$, which is dimensionless, and the dotted line is the product $D_L E_L$, in meters per year.

ing the flow and geometry of the lower part of Columbia Glacier for the 4.25-year period ending September 1, 1981. The procedure adjusted initial estimates of the surface velocities, and it indirectly inferred both the bed topography and the spatial and temporal variations of mass balance. These quantities, together with the variations in surface topography given by Rasmussen and Meier (1985), obey a centered finite-difference approximation of the continuity equation (eq. 6).

The parameter-by-parameter version of the minimization procedure was terminated when the total adjustment D (eq. 16) reached 0.427. Although this is not the absolute minimum, it is probably very nearly so. The partial derivatives of D were very nearly zero for all 42 balance parameters and for all 120 bed parameters except those at low-velocity nodes at or near the margins. No interpretation of the value 0.427 is offered except to note that it may indicate simply that the data errors were overestimated.

The temporal distribution of D is shown in figure 13 in the form of the D_L (eq. 15) and of the product $D_L E_L$. The spatial distribution is shown in figure 14 in the form of the $(D_u)_{ij}$ and $(D_v)_{ij}$. Each of these distributions is roughly uniform, which indicates that the solution is not unduly controlled by conditions localized in either time or space. The most prominent exceptions to this rough uniformity exist in the cases of the last flight interval and in the region very near the terminus.

The calculations were stopped short of finding the absolute minimum because the painstaking parameter-by-parameter method was so time-consuming and because the main objectives of the work had been achieved. A data set had been created that was internally consistent and that was faithful to the photogrammetric

data. It had been demonstrated that the bed topography and mass-balance distribution of an ice mass could be estimated solely from aerial photography and photogrammetry.

For the same reasons, the sensitivity of the results to the numerical value $n=3$ assumed for the flow-law exponent was not investigated experimentally, nor was the sensitivity to the part of the velocity during any particular flight interval that was assumed to be due to deformation, an amount equal to half ($\phi=0.5$) of the minimum velocity over the entire 4.25-year period. A partial analysis of the sensitivity can be accomplished, though, by considering the governing equations and typical numerical values for the quantities involved.

If the characteristic thickness \bar{h} at any node were unvarying, the minimization could be performed by using the \bar{h}_{ij} as the geometry parameters, for the continuity equation constraint (eq. 6) is expressed in terms of them. However, variation does exist, though it is small compared with the average value of \bar{h} at any node. It is caused by the variation in Z as the surface topography varies and by the variation in γ as the speed S of the ice flow varies. It is small because the variation of Z is small compared with the total thickness and because γ varies over such a narrow range. If \bar{h} did not vary, n and ϕ would be used only for recovering the bed altitude B from \bar{h} and Z ; as it is, given a provisional value of B , they are used to impart small changes to \bar{h} as Z and S vary.

To the degree that the \bar{h}_{ij} could be used as the geometry parameters, the balance parameters are independent of the values assumed for n and ϕ . The balance is determined by the sum of the flux divergence and the change of the surface altitude. The continuity equation is

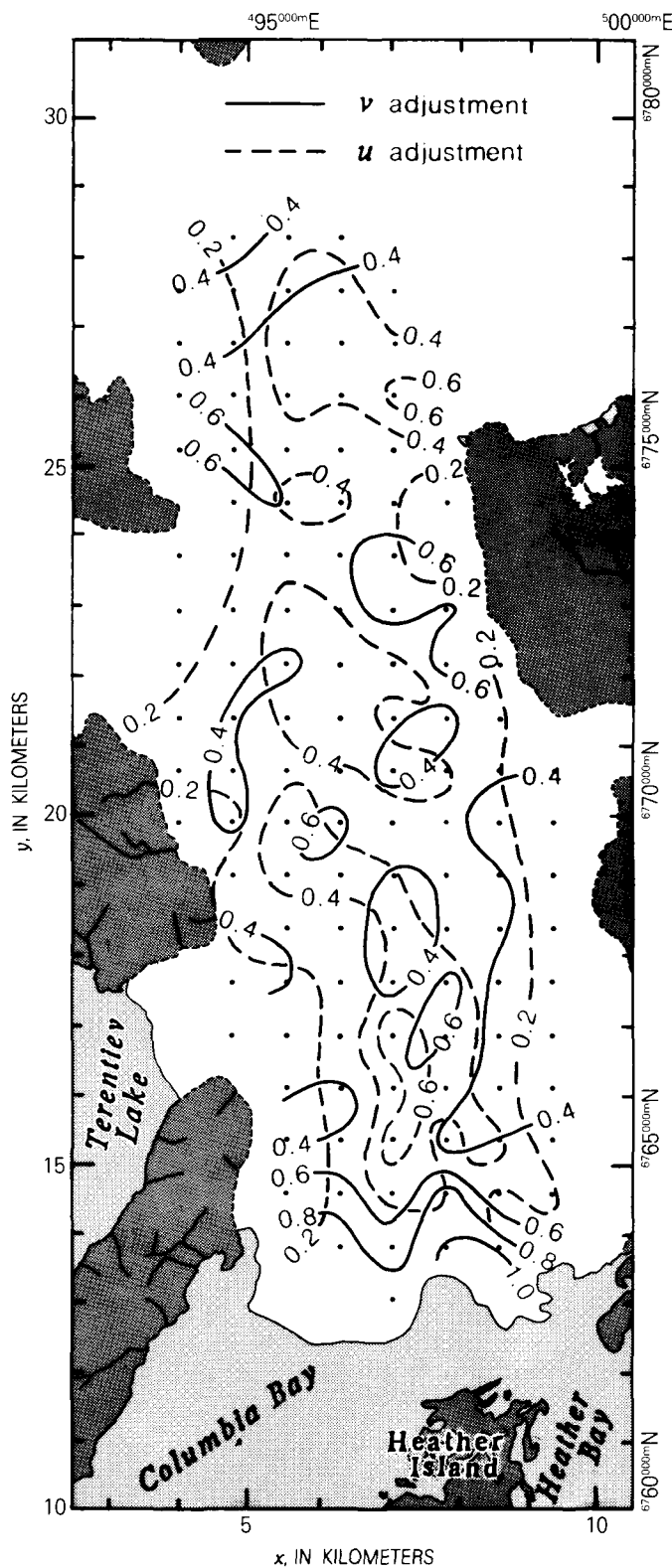


FIGURE 14.—Spatial distribution of the average velocity adjustment. The fields are hand contoured from the $(D_u)_{ij}$ and $(D_v)_{ij}$ values (eqs. 18, 19). The contour interval is 0.1.

concerned only with the flux itself, not with the partitioning of the flux into its three factors h , γ , and V .

The effect on the bed topography inference can be estimated from equation 2 if different values are considered for either n or ϕ . By differentiating it, $\partial\gamma/\partial n = \phi S_{min}/[S(n+2)^2]$ and $\partial\gamma/\partial\phi = -S_{min}/[S(n+2)]$. The two definitions $\bar{h} = \gamma h$ and $h = Z - B$ yield $\partial h/\partial\gamma = -\bar{h}/\gamma^2$ and $\partial B/\partial h = -1$. From the product rule, $\partial B/\partial n = \bar{h}\phi S_{min}/[S\gamma^2(n+2)^2] > 0$ and $\partial B/\partial\phi = -\bar{h}S_{min}/[S\gamma^2(n+2)] < 0$. For typical numerical values $\bar{h} = 500$ m, $S_{min}/S = 2/3$, and $\gamma = 0.95$, along with the assumed values $n = 3$ and $\phi = 0.5$, a change of $\Delta B = +1$ m will result either from the change $\Delta n/n = +0.05$ or the change $\Delta\phi/\phi = -0.03$.

ADJUSTED VELOCITY FIELDS (1977-1981)

The velocity fields are tabulated in appendix A. For each node, for each flight interval, both the initial estimate and the adjusted value, along with the estimated errors in the initial estimates, are shown for each component. The spatial distribution of their 4.25-year average is shown in figure 8. The temporal variation of the velocity at three selected grid nodes is shown in figure 9.

The minimization approach is susceptible to biases that may exist in the initial estimates of the velocity fields; it cannot detect them, and it will react to them by inducing compensating features into the inferred bed topography. For example, if a local maximum in the velocity field were consistently overemphasized in the contouring of the fields for the 21 flight intervals, the bed altitude in that region would be inferred to be too high. Raising the bed altitude reduces the thickness, and the product of the too-great speed and the too-small thickness would tend to yield a flux that is consistent with nearby fluxes.

The initial estimates were made by hand contouring the component fields, a partially subjective process. Features may be missed that are only faintly expressed by the data, and others not expressed may be falsely perceived. Having a sequence of many fields probably lessens the amount of bias introduced. Having a greater data density would certainly lessen it.

Two places where bias is suspected in the initial contouring are at the bottom of the solution region, where the u -fields were hard to draw, and at the top, where both the u -field and the v -field were hard to draw. Owing to the relatively lower density of photogrammetric displacements and the possibly greater complexity of the flow there, the contouring was difficult to do. Bias may also exist in places where contouring was easy to do.

INFERRED BED TOPOGRAPHY

The inferred bed topography is shown in figure 15, and the altitudes at the grid nodes are tabulated in table 3.

FIGURE 15. — Inferred bed topography. Solid contours (50-meter interval) are hand drawn from the altitudes (table 3) at the grid nodes. Dashed contours (20-meter interval) show the amount by which this bed differs from that inferred from airborne radio-echo sounding (Brown and others, 1986), a negative value indicating that the inferred bed is lower than the radio-echo bed.

The contour field is not continued to the margins of the region because of the unreliability of the bed inference at the low-velocity nodes (fig. 8). The reliability at a grid node is roughly proportional to the average velocity there. As the velocity goes to zero, so does the flux; when the flux goes to zero, the thickness and, hence, the bed altitude are no longer subject to the continuity equation (eq. 4). This effect is compounded at the lateral margins, because only the generally weaker normal component u is used there. The bed altitudes along the margins, all of which are rounded to the nearest 10 m, were estimated on the basis of continuity with the topography in the interior of the region and on the exposed rock along the glacier margins. As noted earlier, the inferred bed topography will be distorted from the true bed topography in response to any bias in the initial estimates of the velocity fields.

Also shown in figure 15 is a comparison of the inferred bed with that inferred in the lower half of the region from airborne radio-echo sounding (Brown and others, 1986). The principal difference is at the margins, where the radio-echo bed is much higher. The east-west sounding lines ended inside the glacier margins; as a consequence, the envelope of their reflection lobes rose at each end of the sounding line and led to an artificially high indication of the altitude. The north-south sounding lines were well confined to the interior of the region, and the agreement between the two beds is much better there, although the series of closed depressions along the bottom of the valley shown in the radio-echo bed is not reproduced here; as each closed depression corresponds to the intersection of an east-west line and a north-south line, the depressions are suspected (Brown and others, 1986) of being spurious features of the sounding record.

The sensitivity of the solution to the bed parameters is shown in figure 16. The sharpest responses to experimentally varying a bed altitude are at the high-velocity nodes in the interior of the region. Along the low-velocity margins the magnitude of the velocity adjustment required to satisfy continuity is almost independent of the value assumed for the bed altitude. Evidence of the incompleteness of the solution is present at a few nodes, near the margins in all cases, where the response curve does possess significant curvature but the adopted altitude is not at its minimum. The curve for node (62,21) suggests, for example, that the minimizing bed altitude is about 5 m higher than the adopted value; the curve at node (61,21) suggests that the minimizing altitude is

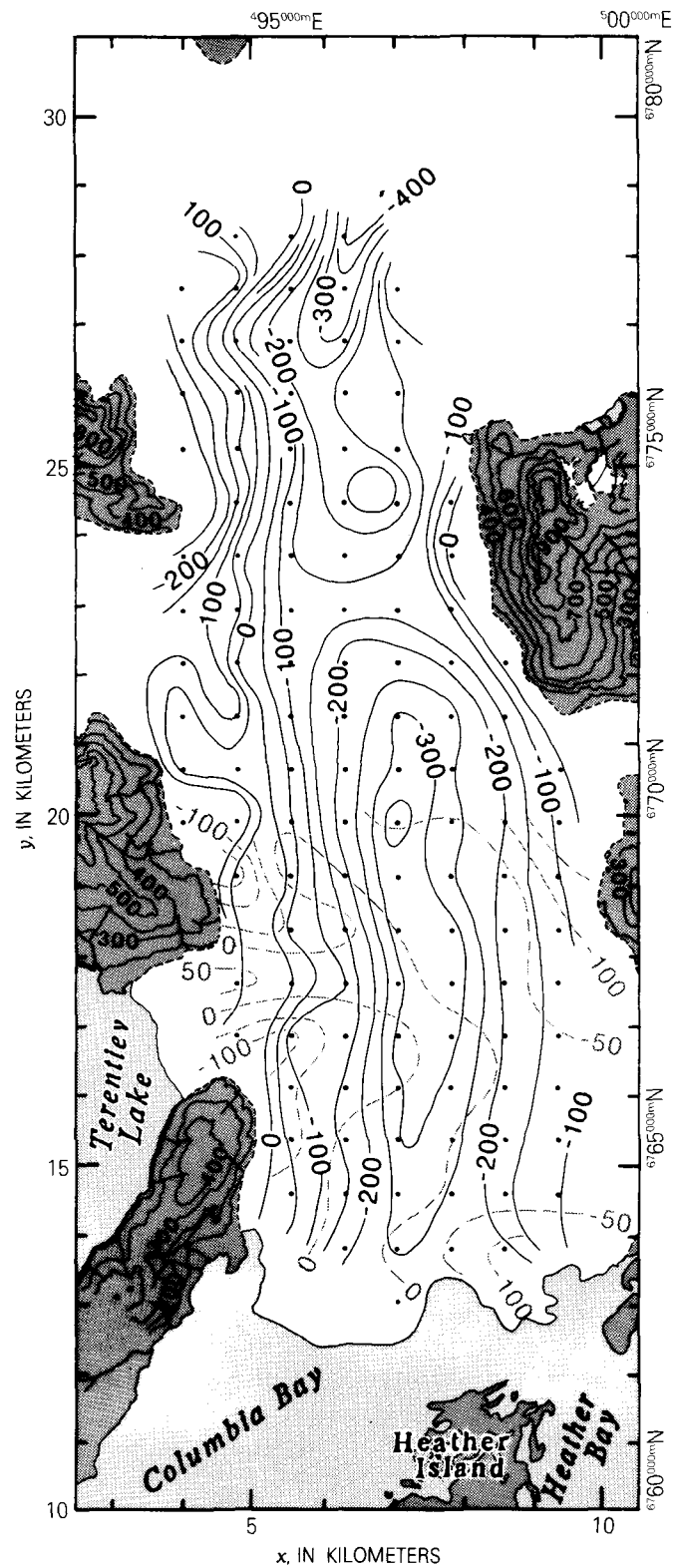


TABLE 3.—*Inferred bed altitudes at indicated grid nodes (rows 49–69, columns 19–26; see figs. 7, 15)*
 [In meters above or below mean sea level. Values are given only on the grid nodes (shown in figs. 3, 7, 8, 12, 14–16)
 where the solution is computed]

Row	Column							
	19	20	21	22	23	24	25	26
49		53	17	-403				
50	180	159	-171	-325	-34			
51	190	-104	-241	-292	-141			
52	250	126	-197	-171	-160			
53	290	114	-72	-220	-154			
54		194	-130	-242	-246	-40		
55	240	24	-142	-184	-155	50		
56	130	69	-127	-138	-128	-167		
57	90	0	-111	-214	-227	-191	-50	
58	20	99	-96	-215	-303	-273	-150	
59	40	42	-55	-219	-310	-251	-191	-60
60	180	166	-55	-230	-375	-277	-200	-90
61		19	-2	-193	-316	-260	-183	-100
62			-58	-144	-328	-306	-190	-130
63		70	7	-99	-288	-317	-191	-140
64		20	-109	-124	-323	-309	-195	-120
65			-84	-160	-282	-274	-172	-120
66			-70	-169	-301	-272	-171	-130
67			-40	-145	-254	-241	-166	-100
68				-196	-259	-231	-218	
69					-225			

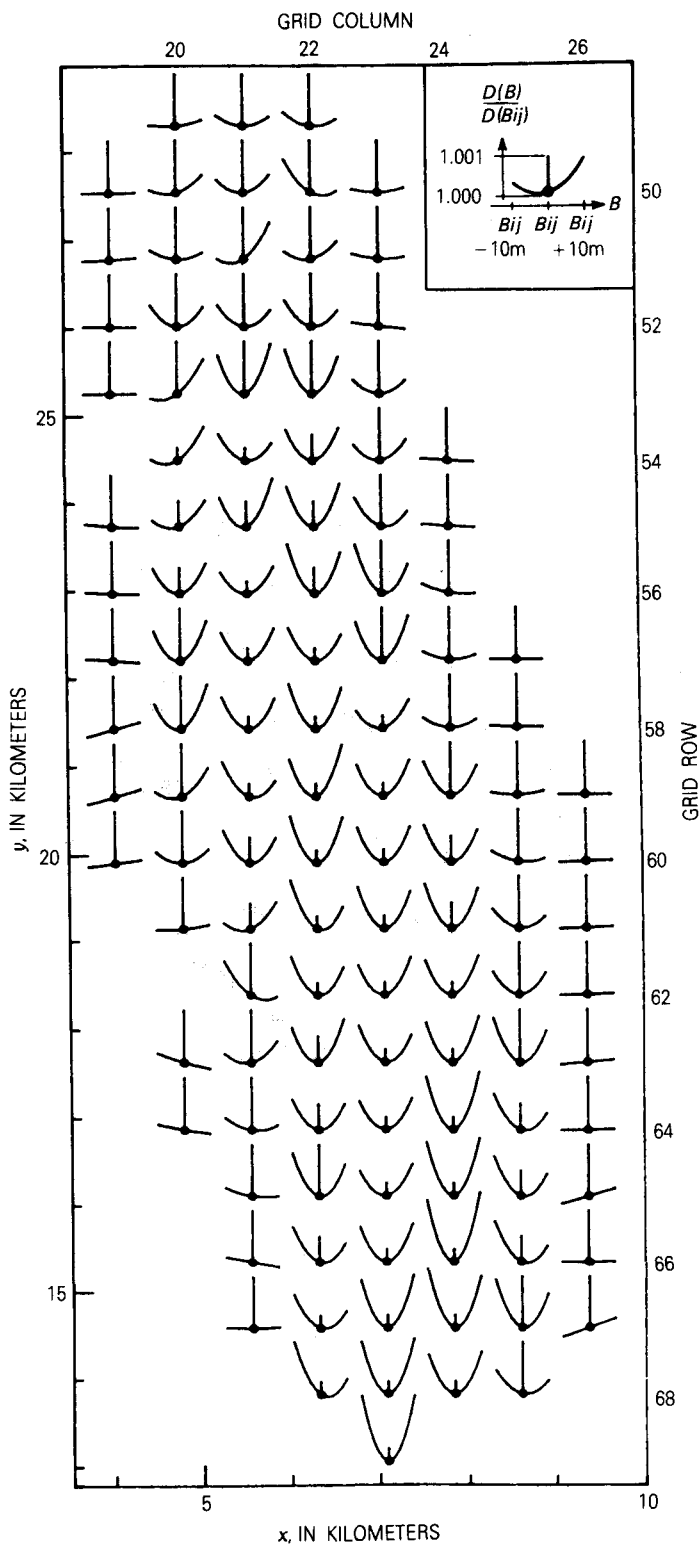
about 3 m lower than the adopted value. Because the confidence in the bed altitudes at the margins is so low, it is not possible to predict from them whether Terentiev Lake (fig. 3) will remain a freshwater lake after the terminus retreats past it or whether it will become an arm of the fiord.

INFERRED MASS-BALANCE DISTRIBUTION (1977–1981)

The inferred mass-balance rates are shown in figure 17 and tabulated in table 4. For convenience, the linear $b(z)$ functions are specified by their values at $z=100$ and 500 m, rather than by $\dot{b}(0)$ and $d\dot{b}/dz$. The $\dot{b}(t)$ functions have reasonable accumulation rates of the order of 30 mm per day in winter and reasonable ablation rates of the order of 100 mm per day in summer. They have a regular seasonal progression except for the reversals in early 1978 and, for \dot{b}_{500} only, during the winter of 1980–81. For 15 of the 21 intervals they indicate a positive balance gradient $d\dot{b}/dz$; the negative balance gradients, three of which occur in winter, are only mildly negative. The four most strongly positive gradients occur in spring—the season when the low-albedo ice is exposed in the lower part of the region and is still covered by the high-albedo snowpack in the upper part—of each of the 4 years.

A special interpretation must be accorded mass-balance parameters inferred for winter periods, when the ice is overlain by lower density snow. This must be done because photogrammetry measures only the geometric surface altitude, not the altitude of the (lower) ice-equivalent surface. The initially inferred positive balance rates therefore should be discounted, say by half, and the subsequent negative balance rates should be also, up to the time when the cumulative negative rate becomes equal to the total winter cumulation of positive rates. Recovering the exact ice-equivalent balance change over some flight interval would require knowing both the thickness and the average density of the snowpack, at both the beginning and the end of the interval.

Systematic altitude error δZ in the photogrammetric analysis will be absorbed in the inferred model parameters in two ways. To a first approximation, the mean of δZ over the 22 flights will affect the bed altitudes by that same amount, which is small compared with the amount the balance parameters are affected; the difference $\Delta(\delta Z)$ between the errors for successive flights, when divided by the length Δt of the intervening flight interval, will affect the balance parameters \dot{b} for the interval by that ratio. The rate of change of the surface \dot{Z} will absorb that ratio directly, and \dot{b} will absorb it with but slight modification.



If $\Delta(\delta Z) = 1$ m and if $\Delta t = 0.2$ a, for example, then $\delta \dot{Z} = 5$ m/a. From the continuity equation (eq. 4), \dot{b} is the difference between \dot{Z} and the emergence velocity, $-\nabla \cdot (h\gamma V)$, in which the thickness value used is the height above the bed of the average surface altitude

during the interval. The thickness error δh will then be the average of the δZ for the two flights, less the 21-interval average of δZ . Even with a small thickness of 400 m and a strong emergence velocity of 40 m/a, the error in the emergence velocity will be only 0.1 m/a for each meter of δh . Because this is so small compared with $\delta \dot{Z}$, it can but slightly modify the absorption of $\delta \dot{Z}$ by \dot{b} .

A likely instance of systematic error is the photogrammetry for flight 14. If its error was 2 m more negative than for flights 13 or 15, \dot{b} errors of -14.6 m/a in the interval between flights 13 and 14 (0.137 a) and of $+13.8$ m/a in the interval between flights 14 and 15 (0.145 a) would be produced. Subtracting these amounts would remove the reversal from the $\dot{b}(t)$ curves in figure 17 as well as from the $\dot{Z}(y,t)$ contours in figure 5 over the period $1978.160 \leq t \leq 1978.442$ between flights 13 and 15. No such reversal appears in any of the other years; nor is a reversal supported by the meteorological record (fig. 18), which shows nearly constant precipitation and continuous warming, interval by interval, through the first half of 1978 (flights 13-16).

The foregoing would apply to a systematic error that was either constant or weakly varying spatially. Of the six cases of negative inferred balance gradient db/dz (fig. 17), three could have been caused by a gradient in $\Delta(\delta Z)$ as weak as 1 m over the 15-km stretch from the lower part of the region ($z \approx 100$ m) to the upper part ($z \approx 500$ m); the three larger negative gradients correspond to a difference in $\Delta(\delta Z)$ of 1.5, 2.0, and 2.8 m over the stretch. If any systematic error is plausible, a spatially varying error is plausible as well, for a separate three-dimensional triangulation model is used (Meier and others, 1985a, p. 7) for the overlap of each pair of photographs in the sequence obtained on an individual flight. The flights followed a north-south line, so any model-to-model variation in the errors would be in the direction of the gradient mentioned. A sample of 58 points surveyed from the ground near the dates of three of the flights (Mayo and others, 1979) was insufficient to detect either spatial gradients or flight-to-flight variations in

FIGURE 16. — Sensitivity of the velocity adjustment to bed topography parameters. The graph at each grid node shows the effect of changing the bed altitude at only that node, while the adopted bed altitudes are used at all other nodes, and while the adopted values of the mass-balance parameters are used. The curve is a parabola through the values $D(B_{ij}-10$ meters), $D(B_{ij})$, $D(B_{ij}+10$ meters) and is scaled by dividing by $D(B_{ij})$. The adopted value of the bed parameter is B_{ij} , and D is the magnitude of the velocity adjustment averaged over all 120 grid nodes, over all 21 flight intervals. The height of the vertical line through each grid node corresponds to an increase of D by a ratio of 1.001. The line occurs in the diagram in three different lengths, in the proportions 1:2:4. Because the solution is not absolutely optimum, the minimum value of the adjustment does not occur exactly at the adopted value of the parameter.

TABLE 4.—*Inferred mass-balance rates at 100 (\dot{b}_{100}) and 500 meters (\dot{b}_{500}) above mean sea level*
[In meters per year of ice equivalent]

Flight number	\dot{b}_{100}	\dot{b}_{500}
9	-40.0	-14.4
10	-31.6	-19.0
11	-7.9	-22.2
12	12.8	16.5
13	-16.2	2.4
14	-8.0	16.0
15	-32.0	-26.6
16	-20.7	-29.2
17	-0.2	-3.5
18	17.8	5.6
19	-4.3	11.6
20	-23.8	-3.2
21	-11.2	-16.0
22	10.2	12.2
23	-13.2	13.8
24	-22.6	-7.2
25	-30.7	-22.6
26	7.9	8.7
27	11.5	7.3
28	-23.7	8.9
29	-32.2	-26.6
30		

δZ , although it did suggest an average systematic error of +1.5 m (Rasmussen and Meier, 1985).

The sensitivity of the solution to the mass-balance parameters is shown in figure 19. For each flight interval the range shown for each parameter is ± 5 m/a. Because the average length of the intervals is 0.2 a, this corresponds to the order of ± 1 m in the cumulative balance change over the interval. For every interval, the most sensitivity is roughly in the direction of increasing or decreasing both \dot{b}_{100} and \dot{b}_{500} together, and the least sensitivity is in the direction of increasing one and decreasing the other. Thus, the solution is more sensitive to the total amount of balance change over the region than it is to its spatial distribution. This is to be expected from the continuity equation (eq. 4) when integrated over the region: the integral of \dot{h} is determined by the photogrammetry, and the integral of the flux divergence is approximately the difference between the flow into the region at the top and the flow out of the region at the bottom, so that the integral of \dot{b} is tightly constrained.

Comparison of inferred balances with stake measurements (Mayo and others, 1979) is sketchy (fig. 20). The calculated $b(z)$ function for each of the three depicted

periods—each consisting of two or more flight intervals—is a straight line, just as it is for any individual interval, because a linear combination of linear functions is itself a linear function. The variable b is the time integral of \dot{b} over the indicated period. As all the stake measurements occurred within 8 days of the date of one flight or another, it is unlikely this discrepancy contributes much to the scatter of the points about the line.

In the August–June period the slope of the calculated line is consistent with the five measured values, but the balance is about 3 m more positive. In the subsequent June–August period the line has no gradient, whereas the six measurements faintly suggest a negative one, and it is about 1.5 m more negative. In the combined August–August period, for which more stake measurements exist, over a greater altitude range, the gradient of the line is comparable with that implied by the measurements, and it is about 1 m more positive. The most serious discrepancy between the lines and the measurements is that the measurements do not closely fit a linear function, or any simple function; this is perhaps because each stake is subject to highly localized conditions. Braithwaite (1986) estimated a standard error of 0.23 m water equivalent for stake measurements of the annual balance at a site in Greenland.

DISCUSSION

No glaciological analysis of the interpolated velocities is contained in this report. Several conclusions can be drawn about the value of the data set for use in glacier flow models, however. The potential application of the velocity interpolation method to other ice masses is also considered.

It is implicit in the way the velocities were interpolated—being made to satisfy the continuity equation—that they are relatively free of noise. They should not, therefore, give rise to large, spurious redistributions of mass when used in numerical models of glacier flow. By contrast, as measured by equations 4 and 6, the initial estimates of the velocities are highly erratic. The interpolated velocities also closely resemble the initial estimates of them, so it is unlikely any major systematic error was introduced.

The possibly erratic values of mass balance inferred for some flight intervals should not detract unduly from the usefulness of the data set in dynamics calculations, which is its main purpose. In dynamic modeling, the mass balance is used only to modify the redistribution of mass determined by the calculated flow field; investigating how the geometry influences the flow field is the principal challenge. It is fortunate, to this end, that the bed

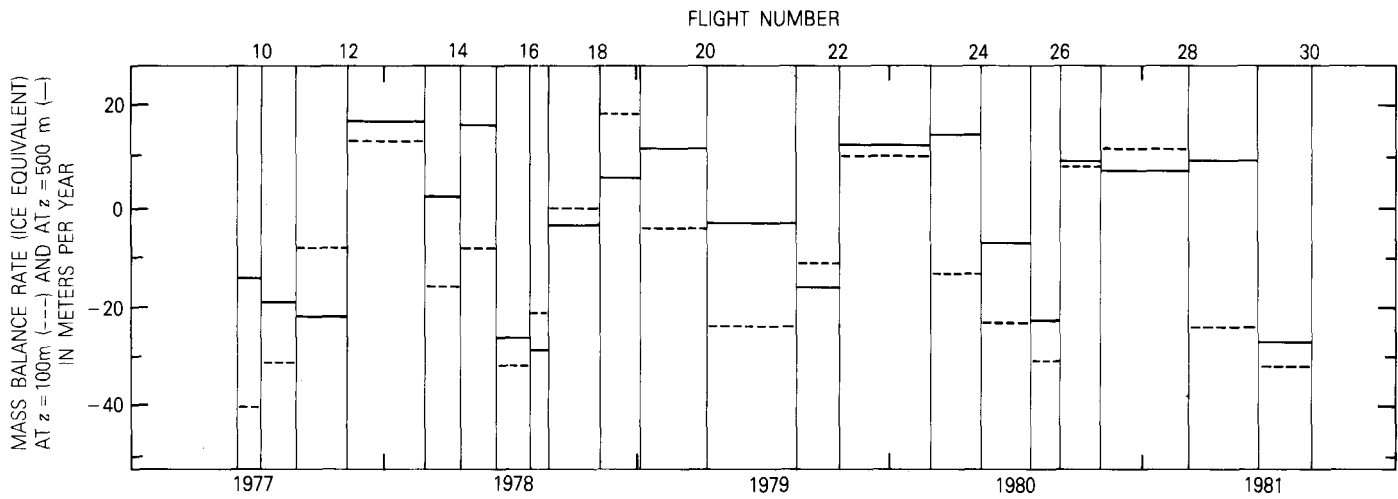


FIGURE 17.—Inferred mass balance as a function of altitude and of time.

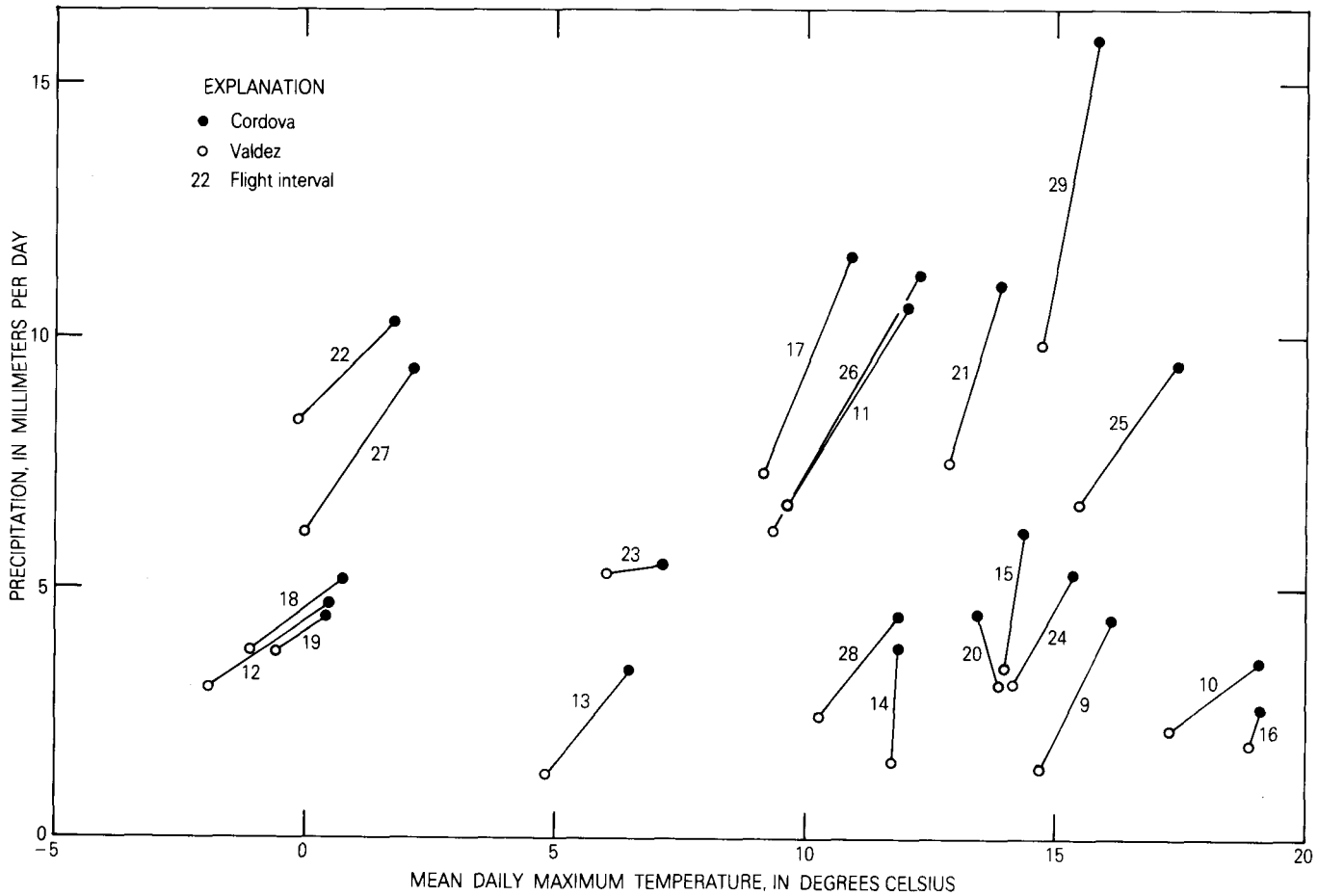


FIGURE 18.—Temperature and precipitation at Valdez and Cordova. The two variables are averaged over the indicated intervals between successive dates of vertical aerial photography (table 1). The circles showing the conditions at the two stations for an individual interval are connected with a straight line to emphasize the relation between the conditions at the two stations.

FIGURE 19.—Sensitivity of the velocity adjustment to the mass-balance parameters. The adopted values of the parameters are $(b_{100})_L$ and $(b_{500})_L$ for each of the flight intervals $L=9,10,\dots,29$ (table 1; flight interval 9 is the interval between flights 9 and 10, and so forth); these values correspond to the center (cross) of each contour field, where the magnitude of the adjustment of the velocity vectors for that flight interval is D_L . The ratio $D(b_{100}, b_{500})/D_L$ is contoured over the region $b_{100}=(b_{100})_L \pm 5$ meters per year increasing to the right, and $b_{500}=(b_{500})_L \pm 5$ meters per year increasing upward. In each contour field the progression of contours is 1.01, 1.05, 1.10, 1.20,.... Because the solution is not absolutely optimum, the minimum value of the adjustment does not occur exactly at the adopted values of the parameters.

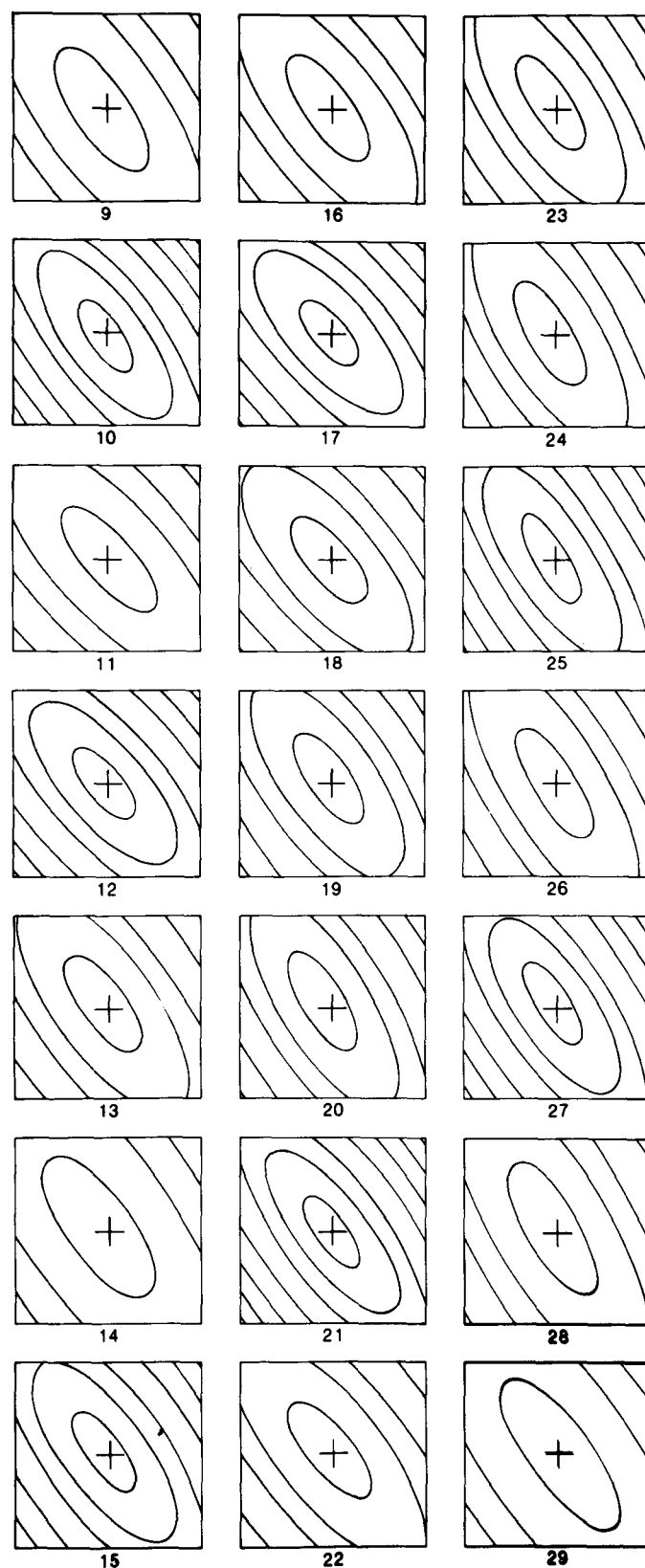
parameters are less strongly contaminated by photogrammetric error than are the mass-balance parameters.

There are two shortcomings of the data set. The first is that particular numerical values were assumed both for the flow-law exponent, $n=3$, and for the part of the motion that is due to deformation, which was taken to be equal to one-half of the minimum velocity observed during the period. Although values were assumed that are believed to be physically reasonable, future modeling work might require the use of different numerical values for these two quantities. If a data set based on different numerical values is required for any purpose, revising the present data set will be a formidable task. The second shortcoming of the data set is that, although there is closure of the variable set with respect to the geometry and flow of the glacier, concurrent data do not exist on the state of the subglacial water regime, which is believed (Bindschadler, 1983; Kamb and others, 1985) to exert a profound influence on the part of the motion that is due to sliding.

The solution is incomplete in two senses. The first is that the altitude changes are taken to be exact as published, which was done for the reasons given in the section "Methods of Data Acquisition." In a complete solution, errors would also be associated with these changes, which would be adjusted simultaneously with the adjustment of the velocity vectors. The second sense of incompleteness is that even for the reduced problem, in which the altitude changes are taken to be exact, the solution is not absolutely minimum. That is, the partial derivatives of D with respect to the 162 parameters are not all exactly zero.

Although the solution is not absolutely minimum, it appears to be a good one. The adjustments of the velocity vectors are small compared with the estimated errors in the initial estimates of the velocity vectors. The inferred bed topography and mass-balance distributions are physically reasonable. This solution would probably be a good first approximation to finding one that is absolutely minimum.

It is unlikely that a minimum solution would be of much more value than the one obtained. Although the



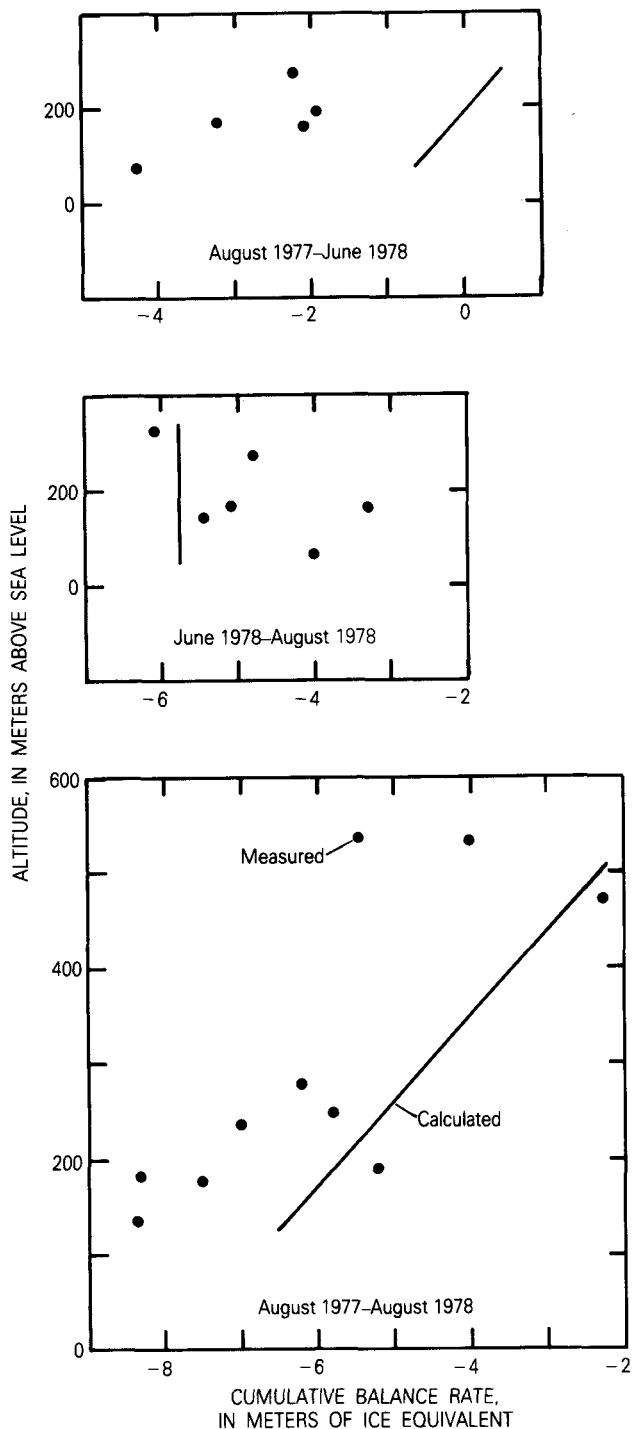


FIGURE 20.—Measured and calculated mass-balance values. The calculated balance functions are for the three periods defined by aerial-photography flights 11, 15, and 17 (table 1). The stake measurements occurred (Mayo and others, 1979) from 2 to 8 days before flight 11, from 2 to 5 days before flight 15, and from 4 to 8 days after flight 17.

assumptions that the flow-law exponent is 3 and that the deformational component equals one-half of the minimum

velocity may be reasonable, the solution nevertheless pertains to only those values; refining the present solution to make it absolutely minimum would yield no information on the sensitivity of the results to those two assumptions. As the solution approached the absolute minimum, it would become no less susceptible to whatever spurious features might exist in the initial estimation of the velocity components and the errors in them, both of which are strongly influenced by the manual contouring of the displacement data. A greater density of photogrammetric points, and thus of the displacement vectors, would lessen this effect; photogrammetric analysis of 1984 photography produced a density twice as great (Krimmel, 1987) as that of the 1977-81 photography, on which the work here is based. The true mass-balance distribution may contain gradients in x and y that are uncorrelated with changes in the glacier altitude in those directions, so that ignoring them by using linear $\hat{b}(z)$ functions would inject artificiality into a minimum solution. The truncation error introduced by the finite-difference approximation of the continuity equation also distorts the solution. The value of a parameter appearing as part of an absolutely minimum solution is not necessarily the correct value physically.

It is not possible here to prove that the data adjustment problem cannot be formulated as a variation of the standard multiple linear regression problem, a variation in which the ordinates are taken to be exact and the errors are associated with the abscissae. The continuity equation is a linear function of the model parameters, the B values and the \hat{b} values. The ordinates would be the \hat{h} values. The abscissae would be the velocity components u and v , with which the errors are associated. On the other hand, it is not possible here to devise such a formulation, either. The difficulty lies in there being some other terms involving neither the \hat{h} values nor the parameters.

The method of estimating the bed topography and the mass-balance distribution from photogrammetry may have application to other ice masses. Once a bed topography is adopted and a distribution of the velocity ratio γ is specified, the balance distribution for subsequent periods could be obtained as the solution to a much simpler minimization problem than that in which the bed altitudes are also estimated. The model could be extended to more than the two parameters making up the linear $\hat{b}(z)$ functions used with the Columbia Glacier data—so that horizontal gradients or nonlinear trends might be estimated—and the minimization problem would still be relatively easy to solve.

Appendix A, along with the report of Rasmussen and Meier (1985), comprehensively tabulates numerical values for all the variables describing the flow and geometry of the lower part of Columbia Glacier. The resulting data

set is internally consistent with respect to the principle of conservation of mass, which is important because inconsistent data can produce anomalous results when used with numerical models of glacier flow. Values are given on a two-dimensional grid, so transverse variations of the flow and geometry can be modeled explicitly, rather than being parameterized in the usual way. Having values on the nodes of a grid also facilitates making finite-difference approximations of spatial derivatives. The data are given for 21 separate time intervals spanning a 4.25-year period. Nothing even approaching the richness of this data set has ever before been published in the glaciological literature.

In addition, the feasibility of estimating bed topography and mass balance solely from aerial photography is established. Until now, aerial photography had been used in glaciology only for mapping the glacier surface and the surface velocity field; other, much more expensive, methods have been used to determine the bed and mass balance. The bed and mass balance not only are necessary in creating an internally consistent set of data for numerical models, but also are important for numerous other reasons. Perhaps the method described here could be applied to satellite imagery as well as to aerial photography. Greenland and Antarctica are such potential applications.

REFERENCES CITED

- Bindschadler, R.A., 1983, The importance of pressurized subglacial water in separation and sliding at the glacier bed: *Journal of Glaciology*, v. 29, no. 101, p. 3-19.
- Bindschadler, R.A., and Rasmussen, L.A., 1983, Finite-difference model predictions of the drastic retreat of Columbia Glacier, Alaska: U.S. Geological Survey Professional Paper 1258-D, 17 p.
- Braithwaite, R.J., 1986, Assessment of mass-balance variations within a sparse stake network, Qamanarssup Sermia, West Greenland: *Journal of Glaciology*, v. 32, no. 110, p. 50-53.
- Brown, C.S., Meier, M.F., and Post, Austin, 1982, Calving speed of Alaska tidewater glaciers, with application to Columbia Glacier: U.S. Geological Survey Professional Paper 1258-C, 13 p.
- Brown, C.S., Rasmussen, L.A., and Meier, M.F., 1986, Bed topography inferred from airborne radio-echo sounding of Columbia Glacier, Alaska: U.S. Geological Survey Professional Paper 1258-G, 26 p.
- Fountain, A.G., 1982, Columbia Glacier photogrammetric altitude and velocity: Data set (1957-1981): U.S. Geological Survey Open-File Report 82-756, 225 p.
- Hodge, S.M., 1985, Two-dimensional, time-dependent modeling of an arbitrarily shaped ice mass with the finite-element technique: *Journal of Glaciology*, v. 31, no. 109, p. 350-359.
- Hooke, R.L., 1981, Flow law for polycrystalline ice in glaciers: Comparison of theoretical predictions, laboratory data, and field measurements: *Reviews of Geophysics and Space Physics*, v. 19, no. 4, p. 664-672.
- Kamb, Barclay, Raymond, C.F., Harrison, W.D., Engelhardt, Hermann, Echelmeyer, K.A., Humphrey, Neil, Brugman, M.M., and Pfeffer, Thaddeus, 1985, Glacier surge mechanism: 1982-1983 surge of Variegated Glacier, Alaska: *Science*, v. 227, no. 4686, p. 469-479.
- Krimmel, R.M., 1987, Columbia Glacier, Alaska, photogrammetry data set, 1981-1982 and 1984-1985: U.S. Geological Survey Open-File Report 87-219, 104 p.
- Krimmel, R.M., and Vaughn, B.H., 1987, Columbia Glacier, Alaska: Changes in velocity 1977-1986: *Journal of Geophysical Research*, v. 92, no. B9, p. 8961-8968.
- Mayo, L.R., Trabant, D.C., March, Rod, and Haeberli, Wilfried, 1979, Columbia Glacier stake location, mass balance, glacier surface altitude, and ice radar data, 1978 measurement year: U.S. Geological Survey Open-File Report 79-1168, 72 p.
- Meier, M.F., Post, Austin, Brown, C.S., Frank, David, Hodge, S.M., Mayo, L.R., Rasmussen, L.A., Seneor, E.A., Sikonia, W.G., Trabant, D.C., and Watts, R.D., 1978, Columbia Glacier progress report—December 1977: U.S. Geological Survey Open-File Report 78-264, 56 p.
- Meier, M.F., Rasmussen, L.A., Krimmel, R.M., Olsen, R.W., and Frank, David, 1985a, Photogrammetric determination of surface altitude, terminus position, and ice velocity of Columbia Glacier, Alaska: U.S. Geological Survey Professional Paper 1258-F, 41 p.
- Meier, M.F., Rasmussen, L.A., and Miller, D.S., 1985b, Columbia Glacier in 1984: Disintegration underway: U.S. Geological Survey Open-File Report 85-81, 16 p.
- Meier, M.F., Rasmussen, L.A., Post, Austin, Brown, C.S., Sikonia, W.G., Bindschadler, R.A., Mayo, L.R., and Trabant, D.C., 1980, Predicted timing of the disintegration of the lower reach of Columbia Glacier, Alaska: U.S. Geological Survey Open-File Report 80-582, 47 p.
- Nye, J.F., 1952, The mechanics of glacier flow: *Journal of Glaciology*, v. 2, no. 12, p. 82-93.
- 1965, The flow of a glacier in a channel of rectangular, elliptic, or parabolic cross-section: *Journal of Glaciology*, v. 5, no. 41, p. 661-690.
- Plafker, George, 1969, Tectonics of the March 27, 1964, Alaska earthquake: U.S. Geological Survey Professional Paper 543-I, 74 p.
- Post, Austin, 1975, Preliminary hydrography and historic terminal changes of Columbia Glacier, Alaska: U.S. Geological Survey Hydrologic Investigations Atlas 559, 3 sheets [1976].
- Rasmussen, L.A., 1983, Calculation of a velocity distribution from particle trajectory end-points: *Journal of Glaciology*, v. 29, no. 102, p. 203-215.
- 1985, Adjusting two-dimensional velocity data to obey continuity: *Journal of Glaciology*, v. 31, no. 108, p. 115-119.
- Rasmussen, L.A., and Meier, M.F., 1982, Continuity equation model of the predicted drastic retreat of Columbia Glacier, Alaska: U.S. Geological Survey Professional Paper 1258-A, 23 p.
- 1985, Surface topography of the lower part of Columbia Glacier, Alaska, 1974-1981: U.S. Geological Survey Professional Paper 1258-E, 63 p.
- Sikonia, W.G., 1982, Finite element glacier dynamics model applied to Columbia Glacier, Alaska: U.S. Geological Survey Professional Paper 1258-B, 74 p.
- Sikonia, W.G., and Post, Austin, 1980, Columbia Glacier, Alaska: Recent ice loss and its relationship to seasonal terminal embayments, thinning, and glacier flow: U.S. Geological Survey Hydrologic Investigations Atlas 619, 3 sheets.
- Vancouver, George, 1798, A voyage of discovery to the North Pacific Ocean and round the world in the years 1790-1795: London, printed for G.G. and J. Robinson, Paternoster Row, and J. Edwards, Pall Mall, v. 3.

APPENDIXES A, B

APPENDIX A: VELOCITY FIELDS

Given in the following tables are values for both horizontal components of velocity, for flight intervals 9-29. Grid indices—rows 49-69 and columns 19-26—refer to a section (fig. 7) of the 762.5-m square grid that covers the entire glacier. The three numbers at

each node, all in meters per year, are the initial estimate (top), the estimated error in the initial estimate (middle), and the adjusted value (bottom). The initial estimate is shown for those nodes where only the other component is adjusted, because it is used in computing the ratio γ (eq. 1).

Flight interval 9 (June 2 to July 7, 1977)

	<i>u</i> -component								<i>v</i> -component							
	19	20	21	22	23	24	25	26	19	20	21	22	23	24	25	26
49		40	-220	-320						-360	-640	-630				
										62	33	25				
										-378	-638	-639				
50	110	60	-240	-320	-330				-200	-530	-760	-710	-590			
	19	45	64	49	23					76	43	38				
	111	57	-224	-312	-335					-515	-737	-700				
51	90	70	-70	-210	-240				-190	-620	-810	-860	-660			
	18	21	69	34	38					107	79	61				
	89	65	-71	-193	-232					-604	-830	-809				
52	80	80	100	50	-80				-90	-680	-1030	-1100	-800			
	11	12	31	60	44					76	83	88				
	80	80	94	49	-78					-698	-1016	-1057				
53	40	150	210	250	130				-90	-900	-1150	-1150	-840			
	8	19	22	22	36					97	66	62	82			
	40	147	205	257	142					-873	-1126	-1159	-801			
54		-50	-30	100	200	80				-790	-1060	-1100	-790	-180		
		31	37	42	19	33				94	40	45	85			
		-52	-28	99	200	85				-790	-1069	-1084	-742			
55	-50	-150	-180	-50	80	60			-90	-700	-980	-1070	-830	-240		
	32	28	33	41	20	32				97	54	45	54			
	-50	-153	-197	-50	86	64				-750	-997	-1035	-820			
56	-110	-110	-50	70	90	70			-170	-700	-1060	-1050	-800	-320		
	29	45	46	45	34	44				121	43	53	78	169		
	-107	-109	-96	51	106	87				-760	-1053	-1042	-819	-507		
57	-30	40	150	200	170	110	60		-250	-710	-980	-940	-770	-420	-80	
	15	37	49	46	36	51	41			101	38	37	76	148		
	-29	32	96	216	202	115	48			-773	-976	-948	-782	-534		
58	0	130	270	320	240	160	70		-260	-700	-930	-870	-770	-530	-190	
	24	47	40	40	37	36	26			120	40	25	43	109	91	
	6	127	235	314	263	169	66			-686	-941	-881	-763	-563	-299	
59	30	170	310	330	270	180	120	60	-180	-590	-850	-850	-800	-640	-370	-40
	45	44	34	28	33	29	27	50		133	52	35	33	70	109	
	36	169	305	327	283	195	114	43		-522	-851	-873	-801	-669	-450	
60	10	130	240	270	270	200	140	80	-50	-390	-770	-810	-820	-740	-510	-100
	56	43	29	28	23	31	17	20		143	72	35	39	53	86	
	17	129	240	267	271	214	137	78		-363	-779	-811	-797	-753	-540	
61		50	160	220	220	210	140	90	-200	-610	-720	-810	-820	-640	-210	
		41	37	25	22	19	24	23		114	86	40	36	61	110	
		51	160	210	227	222	134	85		-136	-618	-754	-815	-857	-662	
62			50	150	180	180	150	110			-480	-720	-810	-870	-720	-300
			33	27	24	29	20	22			72	45	39	39	96	
			74	149	171	191	143	107			-523	-723	-823	-852	-725	
63	-160	-30	80	110	110	120	110		-200	-390	-700	-790	-870	-780	-340	
	28	14	18	28	31	16	17			69	65	47	36	72		
	-157	-30	75	110	137	120	107			-464	-683	-778	-856	-759		
64	-130	10	30	30	30	70	80		-70	-300	-620	-790	-880	-800	-350	
	28	11	15	25	31	16	10			56	75	42	31	63		
	-120	12	24	18	42	68	80			-270	-615	-763	-850	-767		
65		30	-40	-70	-70	-20	50			-240	-610	-820	-910	-800	-310	
		9	14	20	30	18	13			60	72	47	34	60		
		30	-43	-81	-44	-13	49			-175	-577	-777	-888	-776		
66		-10	-120	-120	-130	-90	10			-240	-700	-820	-890	-730	-240	
		19	14	20	27	14	13				76	44	35	63		
		-7	-124	-131	-115	-89	11				-630	-815	-885	-731		
67		-110	-160	-160	-180	-110	30			-260	-770	-870	-910	-610	-180	
		11	16	14	18	12	21				58	46	43	71		
		-111	-164	-163	-172	-107	29				-731	-858	-924	-626		
68			-250	-250	-220	-100					-750	-900	-860	-410		
			17		16						60	45	56	63		
			-256		-214						-789	-943	-932	-395		
69					-280								-930			
													41			
													-970			

Flight interval 10 (July 7 to August 29, 1977)

	<i>u</i> -component								<i>v</i> -component							
	19	20	21	22	23	24	25	26	19	20	21	22	23	24	25	26
49		50	-140	-210						-250	-440	-425				
										43	26	17				
										-254	-435	-418				
50	130	70	-100	-240	-320				-110	-330	-480	-480	-410			
	13	31	46	34	13					52	31	26				
	130	65	-143	-225	-318					-345	-455	-486				
51	50	60	-40	-250	-260				-120	-370	-560	-600	-390			
	11	11	48	27	16					57	55	49				
	51	57	-50	-227	-262					-419	-575	-591				
52	35	70	90	-20	-110				-110	-430	-740	-810	-530			
	5	9	24	45	38					54	63	66				
	35	70	66	-9	-81					-457	-748	-833				
53	25	100	120	150	110				-90	-630	-840	-870	-580			
	5	15	15	16	26					74	46	45	59			
	25	97	117	156	103					-569	-827	-861	-533			
54		-30	-70	30	80	40				-620	-800	-830	-490	-170		
		21	25	28	11	17				63	27	30	52			
		-32	-83	28	83	43				-595	-820	-820	-514			
55	-120	-210	-160	-30	120	60			-120	-530	-760	-760	-420	-230		
	21	20	21	29	17	21				68	35	32	45			
	-120	-208	-161	-30	120	58				-540	-777	-776	-517			
56	-150	-140	-70	50	140	100			-160	-550	-770	-710	-550	-270		
	21	31	31	34	22	20				83	29	40	50	78		
	-149	-138	-79	85	143	87				-594	-758	-735	-555	-245		
57	-30	0	90	160	175	130	30		-160	-530	-720	-660	-550	-310	-40	
	13	28	36	29	18	26	21			76	27	23	38	76		
	-29	-4	91	175	168	124	32			-547	-705	-658	-520	-279		
58	30	100	230	270	230	180	80		-120	-470	-640	-630	-530	-350	-100	
	15	34	27	24	23	24	23			86	27	15	26	72	83	
	31	90	219	289	233	172	84			-457	-654	-623	-520	-340	-87	
59	40	130	245	295	245	200	120	30	-40	-400	-560	-610	-570	-420	-200	-20
	31	32	25	19	22	19	17	31		96	38	24	22	47	70	
	46	138	234	289	249	201	122	31		-408	-598	-606	-559	-411	-209	
60	20	100	220	250	230	200	130	45	-20	-270	-500	-560	-570	-510	-320	-50
	40	31	21	19	16	21	12	13		103	53	24	26	36	61	
	23	104	212	241	233	204	131	45		-240	-508	-567	-549	-505	-314	
61		50	150	190	195	170	135	50	-150	-420	-520	-580	-600	-420	-110	
		30	27	17	15	13	16	15		84	62	28	24	42	76	
		59	150	178	193	174	137	51		-117	-382	-538	-577	-594	-443	
62			60	130	150	130	95	55			-340	-510	-580	-620	-500	-190
			24	19	17	20	14	14			53	32	27	27	64	
			63	127	143	137	97	54			-329	-507	-590	-617	-494	
63	-120	-30	60	80	70	70	40		-100	-270	-500	-590	-640	-550	-220	
	16	10	13	19	21	11	11			52	47	31	24	48		
	-119	-30	57	77	75	71	40			-277	-496	-608	-645	-567		
64	-105	-10	25	10	10	30	40		-60	-200	-490	-600	-660	-580	-230	
	20	8	11	18	22	11	7			42	56	30	22	44		
	-104	-10	25	7	14	30	40			-185	-480	-597	-648	-574		
65		10	-20	-60	-65	-30	25			-140	-490	-640	-730	-600	-190	
		7	10	15	19	13	9			47	55	35	22	44		
		10	-21	-66	-62	-26	25			-134	-477	-648	-730	-592		
66		-30	-80	-110	-130	-80	0			-150	-560	-730	-750	-600	-140	
		13	12	15	19	11	9				64	32	25	48		
		-30	-78	-111	-132	-80	-1				-571	-751	-767	-576		
67	-50	-160	-150	-170	-90	20			-230	-720	-870	-820	-540	-120		
	10	14	11	12	10	16					50	34	29	56		
	-50	-160	-150	-173	-90	23					-720	-881	-823	-520		
68			-180	-150	-180	-80					-850	-1050	-900	-360		
			15		13						55	34	48	51		
			-176		-183						-861	-1047	-909	-403		
69					-280								-1200			
													36			
													-1176			

Flight interval 11 (August 29 to November 8, 1977)

	u-component								v-component							
	19	20	21	22	23	24	25	26	19	20	21	22	23	24	25	26
49		20	-150	-220						-215	-360	-380				
										39	27	14				
										-247	-360	-385				
50	70	40	-120	-240	-300				-130	-270	-420	-400	-330			
	10	26	41	29	10					44	27	22				
	72	40	-138	-239	-302					-294	-420	-404				
51	40	30	-50	-190	-270				-130	-320	-500	-520	-330			
	7	8	34	25	14					42	38	45				
	41	30	-73	-190	-271					-342	-498	-525				
52	0	50	50	-20	-60				-100	-360	-610	-710	-450			
	4	7	20	38	28					46	53	55				
	0	50	41	-17	-77					-389	-625	-693				
53	10	70	120	140	110				-80	-520	-710	-720	-500			
	4	12	11	12	24					60	33	34	56			
	10	70	115	139	110					-434	-700	-725	-501			
54		-30	-40	30	90	50				-520	-650	-670	-460	-70		
		16	20	21	8	14				48	22	23	37			
		-31	-32	36	88	50				-491	-654	-674	-454			
55	-50	-110	-120	-30	70	60			-50	-420	-630	-640	-460	-170		
	15	15	15	22	21	16				50	24	24	58			
	-50	-108	-119	-39	67	61				-423	-624	-628	-461			
56	-70	-100	-50	50	70	60			-80	-390	-640	-610	-470	-310		
	13	22	26	26	23	18				59	24	31	53	69		
	-70	-106	-50	65	69	60				-395	-618	-606	-471	-251		
57	-30	-10	70	150	120	80	20		-80	-380	-590	-570	-480	-330	-30	
	9	21	28	20	20	21	15			57	21	16	43	61		
	-30	-18	68	160	114	81	23			-364	-570	-566	-467	-278		
58	-10	50	150	190	160	120	20		-60	-330	-530	-525	-480	-360	-90	
	11	28	27	20	18	18	11			70	27	12	21	53	39	
	-10	24	145	217	160	122	22			-274	-518	-519	-478	-342	-82	
59	10	60	160	180	170	130	80	0	-30	-280	-505	-560	-490	-400	-200	-10
	24	26	22	15	17	16	13	27		77	33	18	17	38	51	
	5	44	155	189	176	131	83	2		-274	-525	-541	-491	-420	-191	
60	0	55	140	165	160	140	100	-10	-10	-200	-430	-515	-510	-470	-300	-40
	35	27	18	15	11	17	11	20		91	45	19	19	29	57	
	-2	47	126	174	171	140	100	-9		-237	-428	-511	-512	-491	-269	
61		30	100	135	140	130	80	0	-130	-370	-480	-530	-530	-390	-90	
		38	23	15	12	11	15	13		105	53	24	19	36	69	
		-4	87	144	148	128	79	2		-174	-437	-509	-546	-584	-424	
62			30	95	105	100	50	10		-270	-490	-585	-620	-520	-190	
			23	17	15	16	12	13		50	28	23	22	57		
			25	103	119	92	45	9		-294	-517	-596	-635	-481		
63		-75	-60	60	70	50	25	5	-50	-210	-500	-620	-670	-580	-310	
		14	10	13	16	17	9	11		51	45	27	20	41		
		-77	-60	66	79	36	23	8		-197	-522	-632	-687	-577		
64		-90	-40	10	-5	-20	-25	-80	-60	-180	-500	-670	-760	-640	-430	
		18	8	11	16	21	11	7		42	53	27	21	46		
		-91	-40	15	16	-42	-33	-80		-219	-501	-698	-768	-622		
65			-5	-25	-105	-120	-120	-120		-130	-550	-790	-900	-740	-400	
			8	12	15	18	15	10		51	63	36	21	48		
			-5	-20	-94	-149	-128	-117		-145	-537	-782	-884	-725		
66			-25	-80	-175	-230	-230	-70		-110	-670	-1000	-1050	-730	-200	
			16	14	16	17	13	10			76	36	23	59		
			-26	-74	-163	-243	-235	-70			-738	-985	-1045	-714		
67			-50	-210	-270	-320	-240	-130		-190	-1020	-1330	-1260	-610	-190	
			39	22	14	19	20	22			80	46	45	116		
			-42	-198	-266	-346	-250	-118			-1037	-1269	-1190	-663		
68				-370	-280	-310	-150				-1460	-1700	-1600	-400		
				26		24					92	42	86	79		
				-366		-314					-1373	-1642	-1383	-603		
69					-450							-2000				
												150				
												-1852				

Flight interval 12 (November 8, 1977, to February 28, 1978)

	<i>u</i> -component								<i>v</i> -component							
	19	20	21	22	23	24	25	26	19	20	21	22	23	24	25	26
49		30	-170	-270						-240	-450	-455				
										37	30	12				
										-234	-443	-453				
50	110	60	-150	-280	-350				-130	-330	-490	-500	-420			
	9	24	41	28	13					41	27	22				
	110	57	-153	-271	-349					-307	-487	-484				
51	60	30	-90	-250	-340				-150	-420	-620	-640	-440			
	6	7	36	30	18					37	41	53				
	60	30	-88	-246	-331					-422	-650	-667				
52	20	40	50	10	-60				-110	-470	-770	-830	-520			
	3	9	24	43	33					57	64	63				
	20	40	53	-1	-59					-507	-790	-869				
53	10	75	140	170	80				-85	-600	-900	-905	-640			
	4	14	15	13	29					72	44	37	65			
	10	75	138	170	92					-615	-890	-922	-677			
54		-40	-40	50	120	50				-600	-840	-870	-640	-120		
		17	20	26	8	16				52	22	28	38			
		-40	-36	57	119	48				-616	-841	-893	-633			
55	-50	-130	-130	-20	100	80			-50	-520	-800	-850	-690	-260		
	14	17	17	23	22	19				59	28	25	61			
	-50	-130	-130	-23	94	81				-518	-802	-842	-698			
56	-40	-80	-30	70	120	110			-80	-540	-830	-850	-720	-380		
	13	23	37	28	22	24				62	35	33	50	94		
	-40	-79	-32	76	121	104				-562	-823	-863	-717	-366		
57	-20	20	120	220	210	130	30		-80	-500	-770	-760	-710	-420	-50	
	6	22	34	19	27	30	18			62	26	15	58	88		
	-20	19	122	220	192	134	31			-513	-771	-766	-701	-402		
58	5	90	220	270	260	165	40		-70	-440	-710	-745	-710	-490	-100	
	10	32	31	23	22	24	13			82	31	15	25	72	46	
	5	92	233	272	247	160	41			-402	-719	-743	-689	-496	-122	
59	20	110	250	310	260	180	100	10	-30	-320	-660	-720	-725	-580	-280	-10
	22	30	30	13	14	23	16	30		91	46	17	14	55	62	
	22	113	252	303	257	203	100	5		-312	-658	-713	-719	-617	-272	
60	10	90	230	260	230	190	120	20	-20	-210	-600	-710	-730	-710	-430	-30
	31	30	22	13	9	21	18	23		101	54	16	16	35	88	
	10	91	228	257	231	198	117	21		-191	-549	-709	-740	-719	-403	
61		40	170	220	220	180	125	40	-100	-480	-700	-780	-870	-570	-90	
		41	24	15	11	13	20	15		114	55	24	18	42	92	
		25	173	223	220	181	123	39		-87	-476	-694	-787	-822	-546	
62			80	170	185	180	125	40		-370	-680	-830	-875	-690	-160	
			28	19	15	16	13	15		61	31	25	21	60		
			72	170	185	178	127	41		-338	-706	-846	-890	-650		
63		-80	-20	110	125	120	80	20	-60	-260	-680	-870	-925	-800	-200	
		12	11	13	17	17	10	12		57	48	28	20	46		
		-81	-18	116	123	111	77	21		-245	-717	-860	-934	-789		
64		-70	0	50	35	10	15	20	-45	-180	-700	-920	-1030	-870	-200	
		15	8	8	17	24	14	8		41	39	29	24	54		
		-71	0	50	34	11	14	20		-216	-677	-907	-1014	-862		
65			20	0	-75	-110	-100	-10	-100	-720	-1030	-1130	-960	-100		
			7	16	18	20	19	9		50	87	43	23	63		
			21	1	-78	-117	-103	-9		-113	-687	-1004	-1132	-942		
66			-5	-80	-175	-215	-190	-20	-100	-820	-1160	-1240	-970	-70		
			14	15	19	16	17	10		85	41	21	74			
			-5	-84	-173	-213	-192	-19		-807	-1164	-1237	-926			
67			-20	-175	-280	-320	-240	0	-170	-1100	-1400	-1380	-800	-30		
			16	27	14	10	16	22		95	46	25	92			
			-19	-171	-282	-323	-241	6		-1093	-1362	-1376	-896			
68				-350	-450	-440	-200				-1400	-1670	-1500	-500		
				30		18					106	73	66	95		
				-378		-429					-1286	-1636	-1487	-643		
69					-550							-1750				
												42				
												-1807				

Flight interval 13 (February 28 to April 19, 1978)

	u-component								v-component							
	19	20	21	22	23	24	25	26	19	20	21	22	23	24	25	26
49		0	-230	-340						-300	-530	-545				
										47	39	18				
										-280	-534	-544				
50	110	40	-210	-340	-380				-190	-410	-660	-640	-480			
	13	31	55	46	18					53	37	36				
	109	42	-179	-350	-379					-379	-642	-596				
51	60	20	-40	-300	-360				-210	-500	-800	-830	-500			
	9	9	62	49	30					45	71	88				
	59	19	-62	-262	-335					-496	-787	-769				
52	25	40	70	30	-100				-160	-560	-940	-1000	-610			
	6	13	27	44	43					83	73	64				
	25	40	74	28	-82					-550	-968	-1039				
53	25	70	140	210	130				-100	-640	-1030	-1050	-720			
	6	19	25	22	33					94	74	64	75			
	25	68	144	214	146					-712	-1063	-1101	-754			
54		0	-30	80	180	50				-680	-990	-1010	-720	-150		
		22	30	44	11	20				67	32	48	52			
		1	-28	77	180	48				-717	-1010	-1033	-713			
55	-40	-140	-130	-20	110	100			-50	-650	-940	-980	-730	-300		
	23	23	26	31	32	29				77	42	34	88			
	-40	-136	-137	-36	116	101				-701	-976	-993	-795			
56	-50	-100	-40	100	140	120			-80	-740	-1000	-1025	-790	-380		
	20	28	53	36	32	34				76	49	43	73	130		
	-48	-88	-44	83	128	105				-731	-1024	-1028	-832	-427		
57	-15	0	150	280	210	140	40		-100	-730	-950	-950	-810	-440	-100	
	10	32	45	38	20	35	25			89	34	30	43	102		
	-15	15	141	255	213	133	38			-703	-962	-940	-815	-499		
58	0	100	300	350	280	190	70		-110	-640	-900	-900	-820	-530	-170	
	17	43	50	37	25	29	17			110	50	23	29	88	61	
	1	132	285	319	284	175	68			-607	-883	-904	-815	-532	-147	
59	20	130	330	350	310	230	110	-10	-55	-510	-830	-890	-860	-660	-310	-20
	34	41	44	22	22	29	21	37		122	66	27	22	71	83	
	17	142	340	344	310	225	109	-6		-468	-767	-883	-847	-684	-267	
60	0	90	260	280	270	240	130	0	-20	-300	-730	-830	-860	-790	-500	-40
	43	35	24	22	18	26	22	15		118	61	27	29	45	112	
	1	95	255	269	278	240	125	1		-315	-695	-837	-847	-792	-437	
61		30	190	240	250	240	140	40	-110	-580	-790	-880	-900	-610	-100	
		32	29	22	17	14	22	19		90	68	34	29	45	102	
		30	195	235	247	240	139	43		-101	-540	-796	-864	-885	-574	
62			90	190	200	180	130	50		-450	-760	-890	-930	-710	-250	
			37	23	21	25	13	18		80	38	33	34	61		
			87	180	203	188	130	53		-422	-783	-884	-933	-708		
63		-90	-20	120	120	100	70	30	-110	-330	-740	-900	-960	-800	-300	
		19	13	12	20	27	16	14		67	44	34	31	72		
		-91	-18	119	109	104	69	32		-357	-767	-899	-968	-781		
64		-100	-20	30	20	20	20	0	-75	-240	-710	-920	-990	-890	-250	
		22	10	14	23	29	15	10		49	71	38	29	61		
		-98	-19	25	17	28	18	1		-251	-713	-916	-1005	-849		
65			10	-20	-90	-105	-70	-20		-170	-700	-960	-1060	-910	-110	
			8	18	20	23	20	13		56	97	47	26	66		
			11	-24	-94	-108	-77	-18		-148	-678	-963	-1044	-911		
66			-10	-110	-150	-180	-160	-30		-120	-770	-1020	-1080	-880	-40	
			15	16	19	22	17	11			91	42	29	75		
			-9	-114	-159	-177	-157	-29			-758	-1041	-1058	-805		
67			-40	-200	-230	-250	-175	-20		-190	-900	-1080	-1110	-660	-30	
			15	19	14	15	14	20			69	46	36	78		
			-38	-202	-236	-257	-174	-11			-862	-1094	-1125	-717		
68				-280	-330	-320	-110				-1030	-1220	-1060	-320		
				21		15					74	59	55	63		
				-284		-318					-926	-1239	-1073	-435		
69					-400							-1220				
												37				
												-1233				

Flight interval 14 (April 19 to June 11, 1978)

	<i>u</i> -component								<i>v</i> -component							
	19	20	21	22	23	24	25	26	19	20	21	22	23	24	25	26
49		50	-200	-350						-400	-630	-630				
										50	41	18				
										-396	-651	-626				
50	180	90	-120	-300	-320				-200	-500	-760	-750	-570			
	15	33	56	45	20					57	37	35				
	180	99	-144	-341	-317					-507	-771	-732				
51	90	50	50	-200	-300				-190	-580	-910	-920	-610			
	11	11	69	56	36					53	79	101				
	90	51	-37	-229	-284					-587	-887	-856				
52	10	80	140	110	-80				-150	-680	-1080	-1180	-750			
	7	16	29	50	48					101	76	74				
	10	82	127	78	-46					-673	-1108	-1198				
53	0	90	200	260	170				-110	-790	-1170	-1230	-890			
	7	21	29	26	35					105	88	73	79			
	0	93	192	252	179					-786	-1197	-1257	-876			
54		0	-10	120	160	80				-800	-1180	-1240	-880	-390		
		27	34	50	12	27				82	37	54	53			
		4	-19	70	161	81				-720	-1165	-1218	-861			
55	-100	-250	-210	-30	150	130			-100	-800	-1150	-1200	-850	-400		
	30	24	27	36	35	32				84	44	40	95			
	-106	-251	-196	-36	167	134				-843	-1143	-1229	-914			
56	-40	-50	-10	100	160	120			-200	-810	-1200	-1150	-850	-450		
	28	35	58	50	46	42				94	54	59	105	160		
	-37	-43	-14	86	143	112				-863	-1174	-1202	-1050	-631		
57	-5	50	120	200	200	140	50		-240	-840	-1210	-1250	-920	-540	-150	
	14	40	45	54	28	42	31			111	34	44	60	121		
	-7	39	161	272	204	118	43			-836	-1197	-1243	-957	-606		
58	15	150	290	360	440	250	130		-160	-780	-1060	-1170	-1050	-680	-240	
	24	61	55	48	21	41	21			156	55	30	24	123	75	
	18	147	280	400	440	223	128			-784	-1083	-1132	-1024	-694	-187	
59	10	180	370	420	370	300	205	30	-50	-600	-970	-1020	-1020	-830	-400	-20
	56	74	57	22	25	37	28	48		221	86	28	25	89	111	
	-21	177	330	409	403	324	199	41		-684	-1028	-1032	-1009	-907	-390	
60	-30	100	330	400	345	310	230	70	-50	-420	-840	-930	-1020	-950	-600	-40
	69	58	26	22	19	31	33	19		194	66	28	31	54	167	
	-19	107	333	395	342	311	216	70		-595	-898	-975	-1022	-970	-568	
61		10	260	320	310	300	235	100	-280	-700	-900	-1050	-1080	-780	-110	
		40	39	23	18	17	37	27		112	89	36	31	54	173	
		24	278	300	307	304	219	104		-209	-662	-900	-1047	-1111	-737	
62			140	190	240	230	230	60		-580	-920	-1050	-1130	-980	-230	
			57	22	21	29	21	24		124	37	33	39	100		
			179	189	242	231	221	61		-543	-911	-1037	-1111	-868		
63	-280	30	165	150	140	115	30		-270	-470	-910	-1040	-1165	-1030	-300	
	25	16	13	23	28	22	18			82	49	38	33	95		
	-277	32	159	144	149	114	35			-474	-901	-1051	-1129	-989		
64	-150	5	35	30	20	30	30		-200	-300	-870	-1060	-1170	-1030	-300	
	32	13	18	24	29	20	14			67	91	41	29	81		
	-150	7	35	17	10	32	31			-256	-867	-1046	-1170	-1069		
65		30	20	-100	-100	-20	20		-230	-860	-1090	-1220	-1020	-260		
		13	22	21	26	28	19			89	116	50	30	92		
		31	6	-104	-83	-21	23			-225	-831	-1116	-1219	-1060		
66		5	-130	-160	-180	-130	10		-240	-930	-1160	-1220	-970	-180		
		16	17	19	22	16	13			96	40	29	74			
		6	-127	-167	-187	-129	10			-927	-1164	-1206	-1038			
67	-160	-230	-220	-255	-160	60			-340	-1080	-1210	-1250	-800	-130		
	37	21	14	16	17	23				77	46	38	94			
	-154	-241	-225	-247	-157	59				-1041	-1219	-1260	-809			
68		-300	-330	-280	-70					-1040	-1220	-1220	-560			
		20		15						72	52	54	80			
		-295		-283						-1001	-1302	-1255	-546			
69				-370								-1400				
												39				
												-1381				

Flight interval 15 (June 11 to July 30, 1978)

	u-component								v-component							
	19	20	21	22	23	24	25	26	19	20	21	22	23	24	25	26
49		40	-170	-300						-330	-540	-550				
										59	41	18				
										-320	-543	-546				
50	160	100	-150	-305	-330				-160	-400	-640	-620	-540			
	15	31	45	37	19					53	30	29				
	160	101	-159	-309	-328					-401	-633	-614				
51	100	40	-70	-250	-310				-170	-490	-780	-780	-600			
	10	11	47	44	37					57	54	80				
	100	39	-86	-231	-302					-506	-755	-741				
52	50	90	100	30	-130				-150	-590	-950	-1020	-680			
	7	16	27	56	42					97	72	83				
	50	89	89	46	-106					-636	-924	-1002				
53	60	130	200	210	110				-110	-700	-1050	-1090	-710			
	7	18	27	24	30					91	82	68	68			
	60	128	189	217	117					-694	-1049	-1106	-697			
54		-10	-45	70	140	40				-710	-1010	-1050	-720	-200		
		28	29	39	13	25				85	31	42	61			
		-11	-52	73	142	41				-693	-1011	-1053	-729			
55	-40	-150	-165	-30	130	110			-80	-750	-965	-1020	-760	-290		
	47	30	25	31	28	26				104	40	34	77			
	-40	-156	-169	-18	135	109				-775	-984	-1043	-795			
56	-40	-90	-30	100	190	150			-130	-800	-1020	-1020	-850	-420		
	37	35	50	41	22	34				95	47	48	50	130		
	-38	-85	-16	92	186	147				-815	-1033	-1042	-846	-471		
57	5	30	150	270	240	180	60		-150	-800	-980	-980	-830	-450	-70	
	14	36	45	41	25	38	29			100	35	33	53	109		
	5	27	150	276	240	180	57			-778	-985	-985	-825	-492		
58	25	120	270	350	340	210	120		-150	-730	-920	-920	-800	-520	-180	
	23	50	39	40	26	36	20			127	39	25	30	109	72	
	25	134	287	331	333	208	118			-711	-928	-928	-808	-580	-173	
59	30	150	310	360	330	265	160	40	-90	-580	-850	-875	-850	-650	-350	-30
	43	48	49	22	26	34	28	47		145	74	28	26	83	110	
	31	154	334	362	324	255	155	42		-585	-851	-877	-850	-695	-291	
60	20	130	270	330	290	275	180	50	-30	-450	-750	-830	-830	-800	-520	-70
	62	52	27	22	18	25	29	19		173	68	28	30	42	145	
	20	138	277	325	288	270	173	51		-442	-741	-827	-822	-797	-479	
61		40	200	245	255	260	170	60	-200	-620	-800	-850	-900	-670	-170	
		36	37	20	19	17	34	26		101	86	33	31	54	161	
		40	209	245	253	259	164	62		-197	-571	-781	-851	-873	-603	
62			100	175	190	200	150	50		-500	-750	-870	-930	-770	-300	
			49	17	20	27	24	23		108	28	32	36	110		
			93	176	193	192	150	53		-484	-757	-854	-930	-780		
63		-140	-30	115	105	90	85	45	-130	-380	-740	-875	-960	-840	-370	
		23	15	15	22	26	20	18		74	54	37	30	88		
		-140	-28	113	96	98	83	46		-392	-752	-860	-926	-839		
64		-135	-20	20	0	0	-20	40	-80	-300	-720	-880	-970	-860	-360	
		25	12	17	22	26	16	12		60	84	37	26	66		
		-134	-20	18	-18	0	-13	41		-305	-739	-878	-962	-888		
65			5	-30	-80	-100	-50	25		-220	-710	-910	-1025	-870	-280	
			12	18	19	27	19	8		80	96	43	31	63		
			7	-33	-91	-90	-49	25		-204	-733	-899	-1016	-871		
66			-30	-95	-130	-160	-120	-5		-220	-770	-990	-1040	-820	-180	
			14	12	18	22	15	13			69	38	30	70		
			-30	-97	-145	-157	-113	-4			-797	-998	-1034	-834		
67			-150	-250	-210	-220	-140	10	-330	-980	-1070	-1070	-700	-140		
			31	15	13	15	15	24		54	43	36	84			
			-138	-251	-217	-218	-138	9		-971	-1065	-1115	-736			
68				-280	-295	-250	-100				-950	-1130	-1070	-520		
				15		15					54	44	54	82		
				-283		-247					-885	-1143	-1096	-500		
69					-310							-1150				
												100				
												-1276				

Flight interval 16 (July 30 to August 26, 1978)

	<i>u</i> -component								<i>v</i> -component							
	19	20	21	22	23	24	25	26	19	20	21	22	23	24	25	26
49		50	-80	-180						-250	-430	-470				
										66	49	29				
										-285	-444	-469				
50	170	95	-80	-240	-300				-150	-320	-520	-510	-430			
	18	35	55	49	22					60	37	38				
	172	100	-119	-263	-300					-342	-530	-526				
51	130	60	-50	-210	-300				-140	-400	-620	-610	-490			
	11	14	52	35	35					69	59	63				
	131	61	-60	-220	-311					-379	-605	-640				
52	75	70	70	10	-100				-100	-480	-800	-900	-680			
	7	15	29	58	42					92	79	85				
	75	70	69	-2	-109					-500	-795	-898				
53	40	125	160	200	110				-60	-540	-870	-955	-630			
	7	17	27	26	31					85	81	73	71			
	40	126	155	196	103					-514	-862	-945	-596			
54		-10	-40	70	135	60				-590	-840	-910	-600	-60		
		29	41	47	16	26				86	45	50	76			
		-10	-35	48	134	63				-552	-826	-905	-612			
55	-50	-90	-150	-30	90	90			-110	-630	-860	-890	-700	-200		
	36	27	33	41	27	23				91	53	46	73			
	-51	-91	-142	-23	86	89				-655	-804	-874	-634			
56	-50	-70	-40	70	70	55			-140	-670	-875	-1005	-780	-290		
	29	33	54	45	27	29				89	50	54	61	114		
	-48	-81	-64	71	73	70				-632	-856	-912	-708	-264		
57	0	30	130	220	190	90	40		-120	-650	-850	-850	-700	-360	-60	
	13	32	56	50	29	34	26			89	43	40	62	99		
	-1	23	86	199	211	110	42			-693	-848	-844	-688	-350		
58	10	130	270	320	280	170	75		-90	-580	-760	-770	-670	-440	-160	
	24	43	46	53	39	31	20			110	46	33	45	94	73	
	14	114	235	316	291	192	76			-622	-798	-787	-691	-407	-122	
59	30	160	310	350	300	210	110	30	-40	-490	-660	-725	-700	-610	-300	-60
	39	39	37	35	40	31	25	44		117	56	44	40	75	100	
	28	169	302	325	310	213	113	37		-493	-713	-740	-721	-552	-252	
60	20	120	260	300	280	230	125	30	-20	-320	-610	-660	-720	-670	-430	-60
	55	44	31	36	29	31	24	20		145	77	45	48	53	120	
	27	123	252	281	268	174	131	31		-334	-590	-689	-720	-673	-380	
61		60	180	230	235	220	125	40	-150	-480	-640	-730	-735	-560	-100	
		33	38	30	29	21	30	23		92	87	48	49	67	140	
		63	183	218	227	220	128	43		-99	-457	-661	-750	-776	-541	
62			110	190	200	180	120	40			-380	-620	-760	-810	-660	-210
			47	29	31	38	31	21			102	49	50	50	142	
			125	189	186	173	122	42			-364	-637	-772	-828	-656	
63		-65	35	115	120	115	115	60	-80	-300	-630	-770	-850	-760	-270	
		29	16	20	32	42	24	15			81	71	53	49	105	
		-64	37	113	109	106	114	62			-277	-646	-793	-865	-778	
64		-40	30	45	40	45	60	70	-40	-220	-620	-780	-880	-810	-300	
		36	14	18	32	41	18	11			71	91	53	41	73	
		-44	32	48	28	27	59	70			-208	-625	-809	-874	-804	
65			25	10	-50	-55	0	20			-170	-630	-850	-930	-820	-250
			13	19	25	41	21	15			87	101	59	46	70	
			26	11	-59	-81	0	22			-202	-635	-845	-953	-834	
66			-30	-60	-155	-165	-110	35	-200	-730	-960	-1000	-800	-180		
			17	13	27	35	19	15			73	58	47	84		
			-28	-60	-156	-170	-114	35			-717	-985	-1006	-825		
67			-130	-225	-210	-210	-130	40	-420	-1000	-1150	-1090	-700	-120		
			31	16	20	23	17	27			58	64	56	96		
			-127	-223	-213	-218	-130	42			-966	-1140	-1053	-701		
68				-250	-260	-260	-80				-1060	-1300	-1180	-530		
				19		20					67	61	72	105		
				-250		-261					-1031	-1263	-1173	-578		
69					-250							-1550				
												53				
												-1547				

Flight interval 17 (August 26 to November 8, 1978)

	<i>u</i> -component								<i>v</i> -component							
	19	20	21	22	23	24	25	26	19	20	21	22	23	24	25	26
49		10	-160	-250						-230	-420	-430				
										43	27	14				
										-245	-414	-431				
50	85	45	-140	-280	-330				-135	-305	-500	-485	-410			
	11	22	35	26	10					38	23	20				
	86	43	-148	-271	-330					-303	-489	-480				
51	50	10	-60	-250	-290				-140	-390	-600	-600	-425			
	7	10	38	25	21					48	44	45				
	50	8	-73	-235	-285					-364	-597	-599				
52	0	40	50	0	-110				-120	-440	-760	-800	-520			
	5	11	23	49	30					71	62	73				
	0	39	53	28	-114					-453	-749	-825				
53	10	80	150	160	90				-100	-510	-840	-895	-600			
	5	13	20	18	22					65	60	50	50			
	10	78	147	167	93					-512	-816	-882	-580			
54		-40	-50	40	115	35				-560	-800	-830	-610	-110		
		24	25	28	13	18				71	27	30	61			
		-43	-50	48	115	37				-590	-811	-863	-613			
55	-60	-150	-160	-50	90	70			-90	-550	-790	-820	-630	-240		
	16	11	19	23	16	15				36	31	26	45			
	-59	-150	-158	-48	83	70				-541	-777	-817	-638			
56	-40	-60	-50	50	135	90			-90	-570	-810	-820	-710	-400		
	15	26	36	29	18	25				71	33	34	42	95		
	-41	-71	-41	72	136	92				-619	-824	-831	-714	-406		
57	15	35	115	205	180	120	40		-90	-560	-800	-780	-670	-440	-90	
	9	23	40	28	19	29	20			65	31	23	41	84		
	16	38	111	200	168	118	40			-597	-808	-782	-675	-454		
58	10	100	230	290	250	170	75		-90	-530	-760	-760	-680	-460	-160	
	17	36	27	21	22	27	15			91	27	13	25	80	53	
	10	88	229	299	251	171	74			-580	-761	-759	-695	-518	-142	
59	0	130	280	300	275	210	135	20	-60	-460	-690	-750	-720	-600	-270	-30
	25	29	27	16	19	23	22	31		87	41	20	19	57	89	
	16	135	269	303	268	194	131	23		-423	-712	-745	-720	-620	-276	
60	-10	95	240	275	245	230	165	40	-20	-240	-620	-725	-745	-720	-440	-70
	32	24	25	18	13	19	21	13		80	63	23	21	33	104	
	-11	95	238	275	249	231	162	40		-168	-574	-706	-735	-723	-419	
61		30	160	220	235	225	160	40	-100	-510	-700	-775	-815	-620	-150	
		25	32	13	12	11	8	19		69	75	21	20	37	38	
		28	154	222	239	224	159	42		-117	-512	-705	-770	-823	-594	
62			70	175	185	160	100	35			-380	-680	-815	-900	-700	-270
			37	17	20	23	28	20			81	28	32	31	131	
			69	172	192	156	91	41			-370	-671	-816	-888	-746	
63		-75	0	85	100	80	65	35	-50	-300	-700	-850	-950	-800	-360	
		14	12	16	19	29	21	15			59	56	32	34	93	
		-76	-2	88	110	72	65	36			-283	-658	-854	-962	-862	
64		-50	5	15	-10	-10	10	10	-50	-220	-710	-890	-1000	-890	-400	
		18	8	16	20	24	13	11			41	81	33	24	53	
		-51	4	15	9	-12	7	11			-230	-692	-898	-1013	-901	
65			0	-25	-100	-115	-80	-10			-190	-710	-1000	-1110	-940	-320
			8	16	17	28	16	16			55	86	40	32	52	
			-1	-23	-86	-123	-84	-10			-208	-752	-976	-1129	-964	
66			-60	-80	-170	-220	-160	-10			-240	-850	-1170	-1240	-940	-200
			12	13	22	21	21	14				69	47	28	93	
			-61	-83	-144	-210	-173	-10				-861	-1152	-1241	-945	
67			-80	-185	-250	-280	-215	-25				-300	-1100	-1410	-1420	-920
			19	26	18	16	11	27					93	57	39	65
			-83	-184	-237	-280	-217	-26					-1165	-1412	-1367	-919
68				-225	-270	-310	-240						-1340	-1720	-1650	-800
				18		19							64	48	67	145
				-230		-304							-1409	-1714	-1577	-775
69					-200								-1900			
													100			
													-2061			

Flight interval 19 (January 6 to April 12, 1979)

	u-component								v-component							
	19	20	21	22	23	24	25	26	19	20	21	22	23	24	25	26
49		40	-210	-340						-330	-560	-590				
										60	35	14				
										-314	-564	-589				
50	130	80	-160	-320	-320				-180	-430	-700	-640	-560			
	13	18	45	25	16					30	30	20				
	130	81	-152	-323	-319					-435	-712	-645				
51	90	40	-50	-220	-245				-200	-530	-825	-810	-600			
	7	13	41	41	37					67	47	74				
	90	42	-51	-247	-259					-524	-816	-805				
52	50	70	90	20	-60				-140	-620	-1050	-1050	-710			
	8	13	28	57	49					83	74	84				
	50	70	94	18	-52					-630	-1040	-1048				
53	20	50	200	230	120				-90	-700	-1170	-1170	-880			
	8	25	14	20	43					127	42	58	98			
	20	54	199	225	105					-769	-1151	-1136	-845			
54		0	-30	60	90	60				-700	-1080	-1120	-850	-220		
		36	43	41	20	25				109	47	44	92			
		-5	-51	74	95	62				-711	-1089	-1124	-870			
55	-70	-170	-170	-50	130	110			-80	-720	-1040	-1110	-860	-340		
	20	15	26	32	23	15				50	42	35	63			
	-69	-168	-173	-63	125	110				-704	-1053	-1102	-896			
56	-40	-80	-40	70	190	140			-120	-770	-1100	-1110	-900	-420		
	16	32	43	36	31	33				86	40	43	70	126		
	-41	-82	-52	81	206	135				-755	-1107	-1110	-945	-420		
57	-15	35	150	270	240	180	50		-110	-760	-1100	-980	-905	-560	-70	
	11	23	51	33	27	37	23			64	40	27	58	106		
	-15	41	149	263	233	165	50			-776	-1092	-985	-892	-503		
58	20	115	330	365	310	220	90		-70	-650	-1030	-975	-890	-640	-190	
	28	49	36	35	32	38	17			125	36	22	37	115	60	
	18	106	324	378	315	218	92			-664	-1006	-975	-889	-570	-159	
59	20	140	370	400	355	260	130	30	-20	-480	-930	-950	-925	-770	-370	-10
	42	49	38	14	20	20	28	33		146	57	18	20	49	110	
	30	135	368	403	349	253	133	35		-529	-930	-954	-934	-721	-306	
60	10	120	300	340	320	300	135	25	-10	-320	-800	-925	-960	-890	-480	-50
	36	25	32	15	12	29	20	13		83	81	19	21	50	101	
	10	119	301	347	315	275	144	26		-302	-779	-912	-952	-858	-506	
61		50	220	290	280	290	90	15	-190	-630	-890	-995	-1020	-590	-100	
		26	41	18	12	12	22	20		73	95	29	21	40	102	
		47	195	292	282	290	97	16		-189	-670	-882	-989	-1006	-703	
62			110	230	250	220	70	20			-490	-850	-1020	-1095	-790	-200
			44	21	16	17	26	20			95	36	25	23	119	
			100	234	243	219	89	18			-489	-856	-1018	-1094	-910	
63		-60	40	90	130	90	70	25	-50	-370	-810	-1040	-1125	-940	-280	
		13	13	16	21	25	17	14		64	59	35	29	73		
		-60	38	90	132	99	74	24		-366	-827	-1051	-1138	-977		
64		-50	40	60	20	20	25	10	-10	-300	-800	-1060	-1180	-1020	-280	
		26	11	21	20	26	16	11		56	107	33	26	62		
		-51	40	66	13	18	29	9		-319	-863	-1058	-1186	-1036		
65			20	-20	-90	-105	-70	5			-190	-720	-1130	-1260	-1080	-180
			10	17	22	23	21	9			67	89	51	26	70	
			19	-22	-88	-95	-67	5			-195	-806	-1165	-1261	-1082	
66			-10	-80	-150	-185	-130	15			-170	-950	-1230	-1310	-1040	-90
			11	18	19	28	22	15			97	42	37	100		
			-9	-73	-161	-196	-124	13				-923	-1221	-1315	-1032	
67			-60	-160	-215	-250	-160	-10			-190	-1080	-1360	-1360	-980	-70
			16	17	15	17	15	27			60	47	41	84		
			-62	-163	-213	-245	-159	-14				-1047	-1411	-1383	-906	
68				-150	-140	-180	-130					-1100	-1470	-1430	-820	
				16		18						56	52	65	145	
				-140		-194						-1134	-1500	-1447	-677	
69					0								-1700			
													34			
													-1653			

STUDIES OF COLUMBIA GLACIER, ALASKA

Flight interval 20 (April 12 to August 18, 1979)

	<i>u</i> -component								<i>v</i> -component							
	19	20	21	22	23	24	25	26	19	20	21	22	23	24	25	26
49		-10	-220	-350						-330	-530	-580				
										61	46	15				
										-323	-560	-579				
50	130	40	-160	-290	-320				-190	-430	-665	-620	-550			
	13	37	35	28	16					63	23	22				
	130	53	-160	-308	-319					-439	-676	-632				
51	70	40	-60	-190	-260				-190	-500	-780	-800	-600			
	5	16	40	43	39					79	45	77				
	70	45	-33	-234	-291					-499	-754	-775				
52	30	60	100	35	-70				-160	-580	-960	-1100	-730			
	8	11	36	29	46					66	95	43				
	30	60	96	29	-57					-538	-984	-1070				
53	25	60	160	250	170				-110	-660	-1100	-1160	-820			
	8	28	23	27	36					142	70	78	82			
	25	69	167	234	166					-693	-1045	-1104	-778			
54		-35	-50	50	95	60				-700	-1110	-1120	-830	-140		
		37	39	42	14	17				110	43	45	66			
		-38	-69	49	98	61				-722	-1036	-1085	-766			
55	-50	-180	-190	-60	75	50			-80	-710	-1020	-1070	-870	-250		
	24	18	22	28	33	39				61	35	31	90			
	-51	-184	-193	-52	88	61				-713	-1008	-1074	-809			
56	-50	-100	-55	75	160	70			-150	-710	-1040	-1110	-910	-380		
	19	36	40	30	22	35				95	37	36	50	136		
	-50	-111	-70	77	164	85				-769	-1064	-1098	-900	-468		
57	-5	30	160	260	220	120	30		-150	-700	-1000	-980	-860	-490	-50	
	18	28	39	40	26	35	26			78	30	32	56	101		
	-4	29	124	238	238	138	27			-755	-1007	-995	-863	-523		
58	30	140	300	360	320	210	90		-140	-620	-925	-925	-830	-590	-190	
	26	46	40	26	18	31	17			118	40	16	21	93	60	
	36	134	288	356	319	222	89			-674	-944	-930	-837	-612	-201	
59	30	180	360	405	330	250	150	20	-80	-520	-830	-910	-865	-700	-360	-20
	29	32	24	14	18	23	31	41		97	36	17	18	57	123	
	36	186	353	402	334	253	144	17		-511	-843	-908	-868	-721	-353	
60	10	130	300	340	290	260	180	50	-30	-400	-710	-840	-860	-830	-510	-70
	43	42	33	14	10	27	34	17		141	82	17	17	47	169	
	14	133	291	338	291	263	170	50		-333	-717	-840	-867	-841	-534	
61	40	200	260	260	270	215	70		-180	-570	-790	-885	-920	-700	-160	
	28	41	15	10	10	26	23			78	94	24	17	31	122	
	45	197	261	262	269	209	69			-144	-531	-798	-889	-922	-673	
62			80	185	205	200	140	30			-440	-760	-905	-955	-810	-250
			43	16	15	15	22	25			95	26	24	19	102	
			97	186	204	198	136	31			-424	-753	-886	-938	-824	
63	-110	-15	90	110	85	40	20		-105	-350	-720	-910	-980	-890	-300	
	12	12	12	19	20	26	24			61	42	31	23	115		
	-110	-16	88	104	93	58	18			-381	-743	-897	-958	-877		
64	-70	-10	80	10	30	20	20		-90	-250	-680	-910	-990	-910	-330	
	25	10	17	16	12	22	14			50	87	27	12	89		
	-66	-8	75	-7	30	31	21			-234	-711	-900	-990	-913		
65			10	0	-90	-80	-35	10			-190	-690	-940	-1020	-930	-300
			9	19	16	21	21	20			63	100	38	25	71	
			10	-6	-95	-67	-25	9			-151	-678	-958	-1022	-944	
66			25	-120	-130	-125	-110	-10	-200	-600	-1000	-1035	-920	-210		
			11	15	14	18	14	16			84	30	24	63		
			27	-119	-141	-127	-107	-10			-764	-1016	-1044	-903		
67			-110	-200	-170	-140	-110	20	-280	-955	-1060	-1075	-830	-180		
			17	12	15	14	22	27			41	48	33	127		
			-112	-201	-169	-139	-106	20			-922	-1073	-1096	-830		
68				-170	-130	-110	-110				-860	-1110	-1080	-630		
				14		16					51	33	58	92		
				-168		-112					-889	-1116	-1113	-634		
69					-40							-1170				
												14				
												-1168				

Flight interval 21 (August 18 to October 20, 1979)

	<i>u</i> -component								<i>v</i> -component							
	19	20	21	22	23	24	25	26	19	20	21	22	23	24	25	26
49		40	-100	-205						-210	-340	-370				
										49	37	15				
										-249	-363	-378				
50	95	50	-80	-190	-180				-145	-280	-430	-410	-345			
	11	29	24	25	13					50	16	20				
	96	60	-79	-208	-184					-277	-430	-418				
51	55	50	-35	-155	-170				-150	-320	-490	-480	-370			
	5	10	30	30	27					52	35	54				
	55	50	-18	-153	-181					-283	-474	-479				
52	25	55	40	0	-60				-120	-340	-610	-690	-430			
	6	5	23	40	34					34	62	59				
	25	55	49	-18	-89					-310	-619	-674				
53	10	20	90	135	70				-95	-410	-670	-730	-480			
	6	18	16	17	20					91	49	49	45			
	10	20	103	135	67					-374	-688	-706	-491			
54		-15	-35	50	90	25				-490	-670	-710	-480	-90		
		19	25	24	7	10				58	27	26	34			
		-13	-27	42	89	25				-506	-659	-686	-457			
55	-55	-130	-120	-20	50	25			-70	-460	-630	-650	-510	-150		
	14	15	19	22	22	22				52	30	25	60			
	-56	-132	-118	-21	60	30				-446	-634	-653	-511			
56	-40	-75	-40	50	80	50			-90	-450	-640	-665	-540	-210		
	11	20	29	23	14	21				53	27	27	31	79		
	-40	-71	-20	42	77	48				-484	-641	-675	-547	-260		
57	5	20	95	145	130	90	30		-100	-430	-635	-640	-520	-270	-50	
	12	21	33	28	18	21	15			57	26	22	38	60		
	5	16	93	149	135	94	28			-442	-627	-628	-527	-290		
58	20	85	170	225	200	140	60		-90	-410	-600	-590	-500	-320	-110	
	17	26	30	23	18	19	11			67	30	14	20	58	38	
	20	87	167	227	205	136	59			-410	-574	-590	-502	-338	-113	
59	15	110	205	250	205	155	90	15	-40	-340	-530	-580	-530	-400	-200	-20
	20	23	19	16	19	17	18	26		68	29	21	19	41	70	
	14	97	204	261	214	157	86	14		-286	-512	-570	-529	-411	-225	
60	10	90	190	215	185	160	95	25	-10	-170	-410	-540	-555	-500	-290	-60
	31	26	23	16	13	18	20	12		88	56	20	22	31	100	
	6	86	189	223	194	160	91	25		-176	-382	-543	-550	-504	-316	
61	40	85	160	165	160	85	30		-20	-260	-515	-570	-580	-410	-110	
	19	29	15	13	10	18	15			54	67	24	22	34	84	
	30	84	170	169	162	81	29			-52	-315	-516	-577	-584	-432	
62		70	125	135	125	85	20			-150	-490	-600	-635	-520	-200	
		32	15	16	16	12	16			70	25	25	21	57		
		53	128	148	123	83	18			-235	-484	-598	-634	-515		
63	-60	15	75	80	70	50	15		-60	-100	-480	-615	-665	-630	-270	
	14	12	11	16	18	17	16			58	41	27	21	76		
	-62	14	76	87	76	47	15			-140	-477	-619	-660	-607		
64	-35	25	25	5	-5	0	15		-30	-100	-490	-630	-725	-650	-320	
	19	8	12	16	22	18	11			38	59	26	22	73		
	-31	24	25	14	-15	-1	15			-129	-488	-648	-721	-648		
65		25	5	-45	-60	-45	0			-120	-510	-700	-770	-670	-320	
		7	16	15	23	17	16			45	83	35	26	57		
		25	7	-41	-65	-46	0			-91	-549	-711	-783	-672		
66		5	-50	-100	-130	-115	-5			-110	-600	-840	-870	-660	-310	
		12	12	18	20	11	14				65	39	27	48		
		4	-47	-86	-140	-117	-6				-603	-828	-873	-685		
67		-50	-115	-125	-165	-125	5			-220	-820	-1020	-1000	-650	-290	
		16	16	14	17	15	24				57	45	40	84		
		-51	-115	-121	-161	-126	-1				-865	-1028	-969	-626		
68			-210	-115	-210	-100					-930	-1220	-1180	-620		
			14		16						51	37	57	76		
			-205		-217						-953	-1217	-1156	-548		
69					-90								-1600			
													75			
													-1455			

Flight interval 22 (October 20, 1979, to February 29, 1980)

	<i>u</i> -component								<i>v</i> -component							
	19	20	21	22	23	24	25	26	19	20	21	22	23	24	25	26
49		10	-180	-300						-270	-450	-520				
										56	33	12				
										-258	-459	-523				
50	100	50	-150	-290	-270				-140	-370	-590	-550	-420			
	10	28	24	21	13					48	16	16				
	100	54	-138	-296	-272					-352	-595	-552				
51	60	35	-70	-160	-220				-165	-440	-740	-680	-490			
	5	12	52	47	32					59	60	84				
	60	38	-9	-213	-225					-432	-690	-708				
52	30	40	40	10	-50				-120	-500	-900	-900	-550			
	7	14	38	74	44					85	101	108				
	30	40	79	19	-85					-431	-882	-945				
53	15	35	120	205	100				-90	-590	-950	-1030	-640			
	7	25	25	19	26					126	74	53	60			
	15	41	141	198	95					-658	-983	-1032	-691			
54		-40	-70	50	125	25				-640	-940	-1010	-700	-100		
		24	20	40	11	11				73	22	43	51			
		-39	-64	67	123	24				-625	-936	-977	-701			
55	-50	-170	-170	-50	105	60			-80	-690	-910	-960	-770	-180		
	17	22	27	31	31	29				74	44	34	85			
	-52	-168	-150	-56	112	60				-657	-917	-963	-777			
56	-50	-90	-50	80	155	110			-110	-720	-1020	-1000	-810	-270		
	12	23	39	32	19	29				62	36	38	44	112		
	-51	-88	-11	86	149	98				-712	-985	-980	-816	-361		
57	20	50	160	250	220	150	30		-120	-700	-940	-940	-830	-400	-50	
	15	29	39	31	24	29	18			79	30	25	51	83		
	16	38	183	276	237	147	28			-694	-940	-939	-817	-466		
58	20	130	270	340	310	200	70		-100	-600	-900	-920	-840	-550	-140	
	19	35	42	27	23	29	13			88	42	17	27	87	46	
	18	135	308	341	307	192	68			-652	-912	-923	-840	-544	-131	
59	15	180	330	390	325	260	100	10	-80	-500	-850	-915	-870	-710	-270	-20
	22	34	36	13	19	24	23	26		103	55	16	19	58	92	
	9	172	340	393	333	256	97	12		-482	-839	-909	-875	-716	-289	
60	10	130	300	350	315	285	140	20	-20	-320	-700	-880	-910	-850	-500	-50
	33	35	34	12	11	16	20	11		117	85	15	19	27	98	
	7	131	305	352	318	280	136	20		-389	-694	-878	-920	-862	-479	
61		50	200	280	285	280	160	30	-150	-590	-860	-965	-1015	-700	-110	
		25	47	16	12	14	26	19		71	107	26	19	46	122	
		46	178	289	292	274	148	31		-182	-571	-852	-965	-1010	-682	
62			120	220	240	220	150	30			-480	-860	-1020	-1100	-850	-160
			52	20	15	20	17	20			114	33	23	27	80	
			85	226	248	212	148	30			-456	-852	-1024	-1088	-876	
63		-75	30	120	135	130	85	25	-80	-380	-860	-1080	-1170	-1000	-220	
		14	18	19	12	19	23	19		89	67	20	23	101		
		-76	26	132	140	118	82	25		-328	-857	-1080	-1170	-1009		
64		-40	20	60	10	5	20	5	-40	-290	-890	-1140	-1260	-1100	-270	
		19	10	20	22	33	21	12		51	98	37	33	82		
		-42	19	68	26	-14	17	5		-321	-924	-1120	-1249	-1118		
65			30	-20	-100	-120	-100	-10			-200	-940	-1300	-1400	-1160	-260
			9	21	23	37	20	9			58	113	53	42	68	
			29	-15	-90	-139	-99	-10			-226	-924	-1297	-1395	-1171	
66			-5	-60	-190	-210	-205	-45			-190	-1050	-1470	-1510	-1200	-200
			17	15	26	26	25	22				80	56	34	113	
			-8	-57	-170	-217	-208	-47				-1112	-1427	-1519	-1205	
67			-25	-100	-230	-305	-250	-15			-280	-1220	-1740	-1720	-1250	-200
			21	29	10	22	26	35				105	33	53	149	
			-26	-99	-229	-305	-252	-17				-1382	-1742	-1706	-1178	
68				-220	-225	-330	-260					-1550	-2050	-1980	-1000	
				22		33						80	82	116	153	
				-214		-346						-1585	-2041	-1928	-958	
69					-130								-2550			
													100			
													-2419			

Flight interval 23 (February 29 to May 12, 1980)

	u-component								v-component							
	19	20	21	22	23	24	25	26	19	20	21	22	23	24	25	26
49		30	-220	-330						-370	-610	-610				
										62	36	15				
										-319	-604	-606				
50	125	65	-170	-390	-370				-160	-450	-710	-675	-450			
	13	42	47	27	16					72	32	21				
	123	60	-156	-385	-367					-423	-712	-673				
51	60	70	-30	-240	-300				-190	-510	-900	-800	-540			
	8	15	61	51	39					77	69	92				
	60	70	-3	-245	-294					-536	-907	-877				
52	45	65	100	30	-100				-150	-550	-1060	-1080	-640			
	9	16	27	87	59					97	71	128				
	45	64	107	63	-82					-522	-1082	-1181				
53	30	50	100	250	120				-100	-640	-1150	-1220	-770			
	9	30	35	21	37					151	104	61	84			
	30	53	118	248	117					-812	-1258	-1261	-823			
54		-25	-50	100	150	50				-730	-1130	-1220	-850	-200		
		39	43	57	16	15				118	47	61	74			
		-22	-41	103	149	49				-798	-1135	-1187	-863			
55	-70	-200	-180	-50	110	90			-100	-820	-1150	-1200	-920	-370		
	24	24	36	42	32	14				83	58	46	88			
	-70	-198	-190	-59	116	90				-823	-1150	-1211	-939			
56	-50	-150	-50	70	160	100			-180	-920	-1180	-1220	-1000	-500		
	16	22	45	40	27	28				59	42	47	61	108		
	-50	-148	-34	75	154	93				-895	-1182	-1211	-984	-505		
57	0	50	200	310	280	165	50		-200	-850	-1150	-1150	-950	-560	-50	
	21	35	47	38	30	42	26			95	38	30	64	122		
	-2	56	203	295	289	169	50			-873	-1162	-1140	-963	-592		
58	20	125	380	415	360	240	90		-160	-720	-1100	-1110	-970	-650	-200	
	26	46	46	39	28	37	20			117	46	24	32	111	72	
	22	141	369	408	364	222	89			-790	-1110	-1116	-986	-685	-197	
59	10	200	415	460	400	280	150	20	-80	-560	-1010	-1075	-1025	-830	-330	-40
	29	44	51	18	24	23	28	39		132	76	22	24	55	114	
	10	213	415	459	402	274	148	21		-582	-957	-1071	-1027	-846	-348	
60	-5	160	360	390	340	325	170	30	-30	-400	-850	-1025	-1045	-1010	-500	-50
	44	39	37	20	14	22	26	17		129	92	25	23	37	132	
	-3	161	345	394	344	318	166	30		-398	-863	-1016	-1059	-1000	-559	
61		50	250	325	315	350	170	25	-200	-630	-990	-1080	-1110	-740	-90	
		29	55	17	13	18	33	25		81	127	28	22	60	153	
		56	227	329	317	341	174	24		-179	-602	-987	-1066	-1092	-765	
62			140	250	260	230	150	40		-500	-940	-1110	-1180	-950	-280	
			59	21	19	25	24	22		129	34	30	33	114		
			111	246	267	239	149	39		-507	-943	-1106	-1179	-984		
63	-80	40	130	140	130	100	30		-80	-400	-910	-1125	-1225	-1050	-370	
	15	16	17	24	20	25	20			82	60	40	24	108		
	-79	39	132	144	121	102	28			-397	-945	-1123	-1208	-1028		
64	-60	25	40	10	5	20	10		-65	-300	-900	-1160	-1255	-1110	-390	
	22	11	16	24	29	20	13			55	82	41	29	79		
	-60	25	38	-5	16	28	10			-269	-867	-1126	-1248	-1116		
65		10	-30	-110	-115	-70	0		-220	-920	-1210	-1285	-1140	-300		
		12	12	21	39	28	9			77	66	49	44	94		
		9	-29	-107	-115	-63	0			-223	-901	-1200	-1309	-1129		
66		-25	-100	-155	-175	-145	-5		-190	-1000	-1275	-1325	-1110	-350		
		16	21	20	27	21	22			115	42	36	93			
		-26	-105	-157	-165	-142	-5			-927	-1270	-1347	-1107			
67		-60	-150	-230	-200	-150	-30		-220	-1050	-1350	-1400	-1000	-330		
		17	23	20	23	16	32			81	64	55	92			
		-62	-149	-219	-199	-151	-34			-1072	-1337	-1428	-1007			
68			-150	-150	-210	-180				-1030	-1460	-1480	-820			
			14		33					52	54	117	82			
			-152		-194					-1074	-1449	-1416	-789			
69					-120							-1520				
												49				
												-1552				

Flight interval 24 (May 12 to July 22, 1980)

	<i>u</i> -component								<i>v</i> -component							
	19	20	21	22	23	24	25	26	19	20	21	22	23	24	25	26
49		30	-210	-360						-430	-630	-620				
										73	36	16				
										-364	-613	-611				
50	125	60	-170	-360	-380				-220	-470	-630	-660	-530			
	13	37	49	31	18					64	32	24				
	124	48	-189	-339	-373					-460	-634	-661				
51	70	55	-60	-320	-370				-240	-530	-770	-740	-600			
	10	14	55	46	37					72	62	83				
	70	56	-39	-331	-372					-562	-809	-823				
52	55	75	90	-80	-250				-200	-600	-1060	-1090	-720			
	11	17	32	70	49					103	85	103				
	55	74	85	-41	-213					-569	-1039	-1175				
53	50	60	100	190	90				-170	-700	-1140	-1200	-800			
	10	29	33	29	40					146	98	82	91			
	50	61	117	189	77					-822	-1201	-1278	-839			
54		-35	-65	60	180	100				-750	-1090	-1180	-800	-180		
		47	45	51	14	20				141	49	55	64			
		-35	-72	75	181	99				-839	-1129	-1185	-820			
55	-110	-220	-200	-60	130	100			-100	-820	-1100	-1150	-870	-350		
	28	20	29	30	26	20				68	47	33	73			
	-109	-216	-197	-73	124	99				-860	-1096	-1143	-847			
56	-60	-90	0	90	170	110			-190	-870	-1160	-1160	-930	-520		
	16	27	51	43	24	25				72	48	51	55	97		
	-59	-91	-57	94	175	110				-879	-1142	-1153	-903	-510		
57	0	50	160	300	250	160	80		-200	-900	-1090	-1015	-900	-520	-50	
	25	34	45	36	28	44	29			94	35	29	59	126		
	3	57	155	281	244	170	81			-887	-1099	-1045	-885	-552		
58	40	180	365	430	365	235	125		-150	-780	-1030	-975	-880	-600	-180	
	56	53	32	35	23	33	23			134	32	22	26	98	83	
	61	187	377	418	351	240	124			-770	-1031	-984	-877	-600	-208	
59	40	240	390	450	375	260	170	50	-50	-600	-930	-975	-930	-780	-380	-10
	60	47	44	19	21	19	27	44		141	67	24	21	47	109	
	53	251	411	444	363	265	171	46		-600	-904	-970	-925	-747	-362	
60	-10	185	320	390	335	310	180	90	-20	-400	-750	-915	-925	-900	-520	-100
	55	35	35	18	13	25	28	20		118	86	23	22	42	140	
	-4	184	324	387	329	318	189	91		-378	-775	-911	-937	-856	-548	
61		50	220	270	325	300	165	110	-200	-530	-850	-950	-1000	-700	-220	
		29	52	15	13	17	30	36		80	120	24	22	54	142	
		56	240	269	318	208	183	106		-167	-548	-848	-940	-980	-740	
62			120	220	250	190	140	115			-400	-810	-960	-1040	-860	-320
			39	16	19	22	26	28			84	27	31	30	123	
			131	214	237	207	150	115			-463	-794	-948	-1043	-863	
63	-60	40	145	125	100	100	95		-210	-350	-780	-965	-1060	-940	-400	
	17	16	13	22	21	21	20			78	48	37	24	90		
	-58	39	142	121	102	107	94			-354	-784	-980	-1067	-916		
64	-50	20	40	0	20	55	50		-110	-260	-770	-980	-1085	-960	-380	
	25	10	14	19	23	20	16			52	69	32	23	78		
	-50	21	37	-8	30	57	51			-210	-783	-979	-1094	-949		
65			20	-50	-125	-85	-30	-10	-240	-800	-1010	-1110	-970	-320		
			11	17	17	28	27	11		73	92	40	32	89		
			19	-50	-124	-82	-28	-10		-236	-790	-1012	-1113	-987		
66			0	-100	-110	-135	-80	-10	-280	-910	-1090	-1140	-940	-280		
			16	20	14	21	14	22			111	31	28	64		
			2	-105	-113	-127	-80	-10			-910	-1091	-1138	-949		
67			-100	-170	-125	-150	-85	25	-410	-1000	-1150	-1160	-880	-300		
			21	15	16	17	14	30			54	52	40	81		
			-101	-170	-125	-149	-84	22			-977	-1106	-1165	-880		
68				-165	-125	-120	-85					-930	-1210	-1180	-720	
				16		20						56	36	73	104	
				-171		-109						-947	-1211	-1207	-676	
69					-10								-1200			
													37			
													-1235			

Flight interval 25 (July 22 to September 2, 1980)

	<i>u</i> -component								<i>v</i> -component							
	19	20	21	22	23	24	25	26	19	20	21	22	23	24	25	26
49		50	-130	-220							-290	-420	-420			
											65	35	20			
											-278	-432	-426			
50	120	45	-150	-270	-280				-150	-350	-530	-470	-400			
	13	33	44	35	17					56	29	27				
	120	52	-121	-290	-283					-352	-528	-482				
51	20	50	-70	-180	-250				-170	-380	-650	-590	-420			
	10	11	40	37	31					56	46	67				
	20	50	-50	-177	-263					-379	-596	-563				
52	20	70	75	10	-90				-150	-400	-790	-820	-500			
	8	13	28	52	39					84	75	77				
	20	69	83	36	-99					-402	-734	-796				
53	20	40	80	150	50				-100	-420	-800	-830	-540			
	7	20	23	24	40					102	70	68	91			
	20	38	83	157	38					-444	-796	-841	-525			
54		-30	-50	30	110	30				-470	-750	-790	-550	-110		
		36	39	39	9	14				108	43	42	43			
		-34	-40	43	109	30				-572	-763	-805	-547			
55	-80	-120	-145	-50	90	50			-210	-500	-730	-770	-560	-220		
	20	16	23	31	17	15				54	37	34	46			
	-78	-120	-153	-49	86	50				-499	-713	-743	-515			
56	-100	-105	-60	40	85	40			-150	-600	-750	-750	-600	-280		
	11	24	37	35	20	16				64	35	42	47	63		
	-100	-112	-78	39	91	45				-555	-738	-729	-608	-272		
57	-30	0	70	130	100	60	10		-120	-570	-690	-680	-560	-320	-50	
	17	24	39	36	24	30	20			65	30	28	51	86		
	-29	-5	61	150	98	58	11			-525	-695	-663	-553	-253		
58	20	75	205	230	180	100	35		-80	-500	-650	-610	-530	-360	-60	
	37	37	32	34	26	28	27			93	32	21	30	85	98	
	6	67	190	218	199	120	43			-478	-663	-617	-532	-318	-83	
59	30	120	220	255	235	160	70	20	-50	-360	-570	-585	-550	-420	-120	-20
	40	31	30	24	26	18	27	34		94	45	30	26	45	108	
	32	121	229	256	216	159	75	19		-401	-585	-603	-558	-395	-147	
60	15	90	190	230	200	190	100	40	-20	-230	-460	-540	-545	-480	-220	-45
	40	22	25	23	19	24	18	14		72	63	29	31	40	90	
	13	90	187	225	197	200	106	40		-227	-529	-551	-552	-486	-266	
61		20	120	165	180	165	110	50	-100	-340	-505	-540	-535	-340	-70	
		21	34	20	19	14	19	20		58	79	32	31	44	87	
		26	138	159	166	165	111	48		-112	-349	-518	-556	-558	-395	
62			60	125	145	130	100	60			-270	-460	-555	-585	-450	-120
			28	20	21	23	17	16			61	33	33	30	78	
			61	126	140	136	102	58			-318	-462	-561	-579	-445	
63		-90	20	75	90	90	75	50	-85	-230	-460	-560	-595	-530	-180	
		18	12	12	21	25	13	11		58	43	34	29	55		
		-86	22	72	71	88	76	49		-228	-429	-549	-591	-514		
64		-60	25	40	10	10	30	20	-60	-190	-440	-570	-610	-550	-200	
		25	9	11	19	29	14	9		45	53	32	29	58		
		-60	24	40	14	21	32	20		-125	-411	-539	-599	-534		
65			-5	-10	-40	-60	-30	10	-130	-440	-580	-625	-550	-200		
			8	12	17	27	17	7		51	65	39	31	56		
			-5	-11	-50	-49	-25	10		-132	-449	-567	-639	-550		
66			-45	-70	-110	-110	-75	5	-90	-500	-625	-640	-510	-190		
			13	14	17	23	10	13		76	37	30	43			
			-47	-72	-104	-100	-75	5		-467	-636	-663	-513			
67			-90	-150	-110	-95	-50	10	-150	-600	-700	-660	-470	-200		
			13	12	13	16	15	19		42	43	39	87			
			-90	-151	-110	-93	-51	9		-622	-707	-658	-447			
68				-190	-110	-75	-25				-600	-740	-700	-400		
				15							53	40	45	71		
				-192		-74					-588	-749	-690	-388		
69					-75							-700				
												100				
												-778				

Flight interval 26 (September 2 to October 30, 1980)

	<i>u</i> -component								<i>v</i> -component							
	19	20	21	22	23	24	25	26	19	20	21	22	23	24	25	26
49		25	-125	-200						-270	-415	-420				
										58	31	25				
										-262	-417	-419				
50	100	60	-100	-240	-230				-120	-320	-500	-470	-380			
	11	28	34	28	30					48	23	40				
	100	61	-98	-243	-229					-345	-505	-486				
51	60	60	-25	-160	-200				-130	-380	-600	-580	-415			
	9	9	31	35	30					45	36	63				
	61	61	-39	-173	-207					-385	-600	-579				
52	30	80	110	30	-70				-130	-480	-750	-840	-520			
	8	14	28	52	38					88	74	77				
	30	80	109	21	-68					-463	-755	-794				
53	0	40	125	150	70				-110	-470	-810	-910	-600			
	8	23	20	22	40					115	60	64	91			
	0	43	120	145	70					-473	-840	-863	-577			
54		-10	-20	80	125	70				-500	-760	-800	-560	-90		
		36	37	35	8	14				108	41	37	38			
		-6	-34	59	126	70				-533	-788	-815	-602			
55	-50	-170	-130	-40	90	105			-90	-530	-750	-760	-585	-240		
	19	15	19	29	13	16				51	31	32	35			
	-49	-167	-135	-41	88	101				-559	-744	-782	-583			
56	-50	-80	-30	80	130	110			-150	-600	-770	-800	-660	-340		
	10	24	35	33	19	15				65	32	39	44	59		
	-49	-79	-41	71	127	111				-558	-772	-781	-633	-302		
57	-20	0	110	200	180	120	40		-130	-620	-725	-720	-600	-370	-50	
	16	22	33	30	18	25	19			59	26	24	38	73		
	-20	8	103	185	178	115	44			-561	-731	-700	-573	-253		
58	0	80	250	280	235	140	50		-90	-500	-680	-665	-580	-400	-100	
	36	36	28	26	21	28	28			91	28	16	24	85	100	
	-7	88	239	254	236	159	71			-475	-657	-662	-561	-368	-61	
59	10	130	260	280	225	170	80	0	-40	-280	-620	-640	-590	-460	-180	-20
	40	31	25	19	20	18	28	33		94	38	24	20	43	113	
	8	126	254	276	226	175	90	2		-370	-590	-635	-587	-431	-151	
60	0	110	225	250	210	185	90	5	-10	-160	-440	-600	-610	-570	-300	-65
	37	19	25	17	15	21	19	13		64	63	22	24	36	94	
	3	109	206	247	209	197	102	5		-162	-496	-599	-590	-542	-295	
61		40	150	180	180	165	90	20		-90	-300	-540	-590	-590	-400	-100
		20	34	16	14	12	19	20		55	79	26	24	39	88	
		42	139	167	177	171	100	21		-74	-348	-559	-592	-597	-422	
62		70	145	150	125	80	35			-280	-520	-590	-650	-500	-180	
		28	17	16	23	18	17			62	28	26	30	86		
		69	140	141	140	89	35			-277	-533	-607	-641	-516		
63		-50	10	90	90	85	65	35	-60	-230	-480	-585	-650	-560	-200	
		20	11	11	17	20	12	11		55	38	28	24	51		
		-49	10	87	77	94	70	35		-207	-503	-598	-637	-572		
64		-10	25	55	15	20	30	35	-25	-140	-430	-575	-630	-590	-220	
		21	8	10	14	23	14	8		41	51	23	23	57		
		-13	26	56	0	28	38	35		-129	-511	-603	-659	-627		
65			20	-15	-50	-40	-15	25		-90	-420	-620	-655	-600	-200	
			7	13	15	23	16	6		47	71	34	27	54		
			21	-12	-59	-48	-17	25		-109	-453	-649	-684	-620		
66			-15	-60	-80	-75	-55	5		-90	-500	-650	-680	-560	-200	
			12	17	15	17	9	13			93	33	23	42		
			-13	-56	-89	-76	-54	3			-537	-664	-666	-577		
67			-20	-125	-100	-85	-45	25		-150	-610	-710	-700	-540	-200	
			12	10	12	14	10	18			37	37	33	58		
			-17	-123	-110	-87	-44	20			-584	-708	-710	-506		
68				-250	-100	-80	-15				-725	-760	-720	-490		
				16	9	9					56	37	32	78		
				-247		-81					-608	-716	-736	-375		
69					-100								-760			
													100			
													-646			

Flight interval 27 (October 30, 1980, to March 7, 1981)

	<i>u</i> -component								<i>v</i> -component							
	19	20	21	22	23	24	25	26	19	20	21	22	23	24	25	26
49		-20	-190	-320						-320	-550	-550				
										69	33	19				
										-299	-544	-549				
50	120	10	-180	-370	-370				-160	-400	-670	-625	-500			
	11	32	25	20	17					54	17	15				
	120	6	-178	-366	-369					-387	-670	-625				
51	50	25	-120	-260	-350				-200	-510	-800	-740	-560			
	10	8	23	39	38					41	26	71				
	50	25	-115	-257	-349					-509	-802	-753				
52	25	70	90	20	-100				-200	-580	-1000	-1000	-640			
	9	17	39	76	45					109	103	112				
	25	69	101	50	-99					-631	-982	-1033				
53	25	70	160	220	120				-150	-600	-1050	-1100	-700			
	10	28	22	26	41					141	67	75	93			
	25	69	161	222	117					-676	-1082	-1115	-748			
54		-20	-35	60	140	50				-620	-1000	-1060	-730	-100		
		50	48	41	14	17				150	53	44	64			
		-18	-31	65	140	49				-709	-1000	-1047	-749			
55	-90	-170	-180	-50	100	90			-70	-680	-965	-1015	-790	-220		
	24	20	25	37	21	28				70	41	41	58			
	-89	-171	-189	-40	102	88				-730	-981	-1047	-780			
56	-100	-140	-70	90	175	100			-160	-760	-975	-995	-920	-320		
	11	31	49	36	25	32				84	45	43	85	122		
	-99	-134	-64	77	164	98				-739	-984	-1009	-829	-359		
57	-30	10	120	230	210	130	20		-180	-790	-955	-920	-840	-420	-50	
	19	25	35	31	20	31	25			68	27	25	60	89		
	-29	11	118	219	210	138	18			-733	-948	-923	-806	-406		
58	20	120	270	320	305	180	60		-120	-680	-885	-870	-770	-480	-140	
	47	47	27	19	17	35	36			119	27	12	20	106	128	
	17	121	285	317	297	189	63			-634	-876	-874	-773	-492	-124	
59	35	170	310	350	310	230	110	20	-40	-500	-800	-835	-810	-610	-220	-10
	53	43	20	17	15	24	38	42		130	30	21	15	58	151	
	33	159	318	352	304	232	105	21		-480	-799	-838	-809	-625	-226	
60	25	150	250	295	285	265	150	40	-20	-320	-690	-775	-810	-740	-400	-50
	47	18	33	13	11	22	25	16		59	81	16	19	38	124	
	23	150	274	293	281	271	149	40		-321	-689	-771	-800	-722	-406	
61		40	170	250	240	260	150	60	-130	-560	-755	-805	-830	-590	-110	
		24	44	16	9	9	20	26		68	102	25	16	28	92	
		37	183	247	238	262	153	60		-141	-561	-738	-802	-616	-560	
62			70	175	195	180	120	60		-440	-715	-815	-840	-680	-190	
			39	17	14	25	26	23		85	28	22	33	122		
			67	170	192	192	128	61		-408	-711	-822	-860	-710		
63	-70	20	100	100	105	90	40		-65	-330	-690	-825	-880	-750	-280	
	11	14	13	14	19	13	15			68	46	24	23	59		
	-71	21	101	101	111	89	40			-331	-678	-816	-880	-765		
64	-60	15	60	10	20	25	20		-30	-240	-660	-830	-910	-810	-310	
	20	9	13	15	17	18	11			47	67	24	17	72		
	-60	14	56	9	32	29	20			-267	-712	-840	-908	-837		
65			20	-10	-60	-50	-20	15		-190	-650	-870	-950	-820	-300	
			8	17	16	21	18	9		56	91	38	24	60		
			21	-9	-65	-48	-20	15		-190	-668	-902	-953	-848		
66			-15	-60	-115	-120	-70	10		-180	-710	-920	-960	-800	-280	
			15	16	17	15	17	18			87	36	20	75		
			-16	-62	-115	-115	-68	8			-749	-921	-956	-834		
67			-50	-130	-145	-135	-95	35		-240	-800	-990	-1000	-760	-320	
			16	15	12	14	15	24			53	37	33	86		
			-47	-129	-150	-133	-94	30			-814	-997	-1009	-704		
68				-220	-150	-110	-15			-1000	-1060	-1020	-700			
				22		15					77	45	55	111		
				-222		-109					-881	-1052	-1041	-551		
69					-50								-1060			
													35			
													-1066			

Flight interval 28 (March 7 to June 16, 1981)

	<i>u</i> -component								<i>v</i> -component							
	19	20	21	22	23	24	25	26	19	20	21	22	23	24	25	26
49		10	-270	-360						-340	-650	-630				
										74	36	18				
										-285	-633	-628				
50	100	50	-240	-380	-350				-150	-460	-730	-670	-620			
	13	34	50	28	80					58	33	22				
	99	40	-215	-362	-325					-448	-730	-674				
51	30	25	-130	-220	-250				-200	-550	-840	-800	-650			
	12	12	50	43	70					61	57	77				
	30	25	-89	-220	-287					-539	-883	-809				
52	0	25	50	0	-100				-160	-610	-1020	-1050	-700			
	9	17	47	94	54					107	127	139				
	-1	24	83	52	-90					-663	-1023	-1084				
53	-30	70	190	220	150				-70	-680	-1230	-1210	-790			
	9	22	25	30	42					108	74	85	95			
	-30	70	194	220	136					-793	-1184	-1184	-806			
54		-60	-10	50	160	50				-740	-1150	-1160	-800	-160		
		55	49	54	20	19				164	53	59	91			
		-73	-24	104	163	50				-790	-1083	-1131	-813			
55	-80	-190	-200	-90	100	50			-80	-800	-1050	-1140	-900	-300		
	27	27	29	41	26	25				91	48	45	73			
	-79	-201	-205	-43	100	50				-733	-1048	-1124	-880			
56	0	-150	-100	50	170	100			-90	-810	-1030	-1120	-910	-440		
	19	26	53	31	27	24				70	49	37	61	93		
	-2	-155	-100	62	179	101				-804	-1086	-1120	-951	-469		
57	30	65	140	260	250	200	40		-90	-800	-1050	-985	-860	-500	-40	
	22	23	40	36	23	34	28			65	31	29	50	90		
	31	65	135	275	251	186	37			-825	-1065	-1008	-890	-563		
58	50	100	305	380	350	240	100		-60	-700	-970	-960	-865	-620	-80	
	48	49	30	21	24	30	34			124	30	13	27	89	123	
	45	104	318	383	346	230	91			-694	-976	-959	-875	-596	-208	
59	50	160	410	390	375	280	150	20	-30	-500	-860	-890	-890	-750	-260	-20
	62	52	26	17	16	29	40	48		156	40	21	16	70	159	
	56	173	406	394	377	265	149	10		-571	-859	-900	-892	-759	-388	
60	35	135	310	330	300	285	190	45	-20	-330	-780	-835	-895	-835	-480	-50
	59	49	34	17	12	19	29	19		165	84	22	19	33	143	
	36	137	337	334	295	280	184	44		-312	-774	-850	-889	-847	-531	
61		50	190	255	260	275	180	60	-160	-610	-820	-890	-925	-640	-160	
		28	49	16	10	11	21	28		77	112	26	17	34	100	
		53	223	256	258	275	176	55		-155	-588	-809	-892	-916	-687	
62			60	170	200	190	120	60			-500	-780	-910	-945	-760	-280
			47	17	16	23	29	27			102	28	26	30	137	
			84	175	195	184	119	54			-483	-763	-898	-954	-818	
63		-75	-5	100	90	100	90	60	-105	-400	-770	-910	-975	-870	-340	
		14	15	12	18	19	16	17			76	44	31	22	71	
		-75	-5	99	97	107	86	57			-410	-729	-891	-961	-854	
64		-35	20	15	0	15	30	40	-75	-300	-750	-900	-980	-900	-320	
		23	10	12	19	19	20	13			51	61	32	19	78	
		-34	19	15	-5	17	39	39			-291	-721	-884	-965	-884	
65			0	-60	-100	-100	-45	15	-230	-710	-915	-1010	-900	-300		
			9	14	17	18	18	11			59	76	40	21	60	
			-1	-63	-101	-91	-41	14			-223	-670	-897	-992	-881	
66			-50	-115	-150	-135	-80	0	-220	-730	-970	-1020	-820	-300		
			17	7	16	21	23	20			40	34	28	102		
			-53	-115	-161	-131	-55	0			-742	-952	-1013	-859		
67		-110	-165	-165	-175	-100	20		-260	-800	-1025	-970	-790	-370		
		17	20	8	13	15	25				73	27	31	87		
		-110	-174	-166	-168	-96	15				-877	-1022	-1023	-789		
68			-250	-180	-120	-70					-870	-1100	-1020	-700		
			18		19						58	42	68	102		
			-252		-116						-874	-1151	-1117	-585		
69					-90								-1075			
													28			
													-1083			

Flight interval 29 (June 16 to September 1, 1981)

	<i>u</i> -component								<i>v</i> -component							
	19	20	21	22	23	24	25	26	19	20	21	22	23	24	25	26
49		70	-120	-220						-280	-415	-420				
										66	34	15				
										-373	-429	-437				
50	125	60	-100	-260	-150				-120	-300	-475	-460	-400			
	13	29	42	29	15					50	28	23				
	128	67	-57	-277	-160					-332	-472	-475				
51	65	50	-50	-130	-100				-130	-400	-610	-560	-440			
	10	11	37	31	31					57	42	56				
	66	50	-56	-126	-122					-364	-582	-536				
52	25	25	20	20	-25				-120	-490	-750	-710	-510			
	7	12	33	66	39					74	89	98				
	25	25	54	12	-97					-416	-612	-647				
53	-60	-80	70	-85	-100				-90	-550	-815	-800	-600			
	9	17	22	23	27					84	66	65	62			
	-60	-83	76	-74	-110					-480	-792	-803	-569			
54		0	-10	50	170	65				-600	-820	-790	-560	-80		
		38	32	37	14	12				114	34	40	63			
		-2	31	44	161	66				-679	-821	-795	-523			
55	-80	-150	-120	0	100	130			-60	-600	-810	-770	-590	-210		
	20	21	24	27	15	15				73	40	30	40			
	-79	-154	-123	7	96	131				-519	-741	-726	-543			
56	-95	-105	-55	70	110	75			-120	-580	-775	-785	-630	-340		
	8	20	35	30	16	14				37	32	35	36	55		
	-96	-115	-33	81	111	82				-556	-764	-776	-623	-276		
57	-30	-15	50	155	155	110	30		-100	-550	-725	-750	-560	-350	-40	
	20	25	33	27	17	21	16			48	26	30	37	60		
	-32	-26	69	166	147	115	36			-505	-725	-722	-592	-307		
58	-20	20	125	235	240	170	75		-50	-520	-640	-650	-540	-380	-30	
	40	40	50	22	16	19	20			82	22	27	18	56	85	
	-68	-13	163	253	246	175	81			-470	-648	-625	-541	-357	-66	
59	-15	25	200	290	255	210	120	40	-40	-360	-600	-585	-560	-460	-130	-10
	56	48	52	20	16	18	23	29		108	32	29	16	44	94	
	-60	18	206	289	255	215	133	38		-360	-610	-606	-566	-442	-188	
60	-20	20	80	220	220	205	150	60	-20	-200	-415	-520	-555	-515	-250	-50
	42	40	56	22	13	14	18	13		114	52	26	17	24	88	
	-36	9	170	238	217	205	156	59		-277	-443	-566	-555	-522	-299	
61		5	45	180	190	190	150	60		-80	-350	-515	-575	-580	-410	-90
		20	34	24	12	12	15	17		56	79	22	19	34	68	
		7	72	171	180	193	153	58		-154	-452	-531	-584	-611	-415	
62			20	115	150	155	100	60			-300	-500	-590	-625	-520	-200
			35	20	14	18	18	18			77	25	23	24	82	
			43	124	144	148	99	58			-268	-488	-590	-625	-521	
63	-80	-25	80	110	80	80	65		-75	-250	-515	-600	-660	-600	-250	
	12	15	10	14	14	13	12			52	30	24	17	58		
	-80	-23	79	103	84	82	64			-219	-473	-610	-689	-592		
64	-50	10	30	0	25	70	60		-60	-190	-505	-620	-685	-635	-270	
	19	12	11	16	20	14	9			43	42	27	20	55		
	-53	6	36	37	8	55	60			-189	-463	-633	-713	-624		
65		15	0	-30	-40	50	55			-100	-500	-700	-775	-680	-260	
		11	14	12	19	16	10			52	57	27	21	53		
		14	1	-21	-41	41	55			-136	-509	-658	-770	-635		
66		-10	-30	-90	-80	10	50			-120	-590	-795	-850	-670	-200	
		15	18	15	20	20	17				59	32	27	88		
		-14	-33	-63	-81	-14	53				-544	-802	-852	-661		
67		-35	-80	-90	-50	-10	60			-180	-660	-950	-980	-600	-240	
		20	25	13	13	11	22				79	42	31	72		
		-40	-74	-77	-52	-14	59				-794	-984	-912	-655		
68			-80	20	0	-25					-800	-1170	-1200	-700		
			20		19						47	44	69	101		
			-78		-2						-854	-1145	-1019	-663		
69				80								-1400				
												120				
												-1314				

APPENDIX B: TERMINUS POSITION AS A FUNCTION OF TIME

The y -coordinate of the terminus position is given in meters for the date of each flight (table 1), for selected equally spaced x -coordinates, also in meters. The numbers in parentheses are the j -numbers of five columns of the square grid to which the indicated x -coordinates correspond. Row $i=69$ is at $y=13,036$ meters. The terminus positions were measured from the vertical aerial photographs, printed at a scale of about 1:20,000. The terminus did not separate from Heather Island (fig. 3) until late 1978, between the dates of flights 18 and 19, as

shown by the values for $x=8,224$ m. Because the y -coordinate increases upglacier, terminus retreat is indicated where the value in the table increases down the page.

For an analysis of the changes in terminus position, see Meier and others (1985a), in which the changes are described in a different coordinate system. They are given here only to supplement the velocity-geometry data set. Therefore, they are given here in the x,y coordinate system (eq. 3), which is compatible with the square grid on which the other variables of the data set are given.

Flight Number	x=5,555	5,936	6,317	6,698	7,080	7,461	7,842	8,224	8,605
	(21)		(22)		(23)		(24)		(25)
9	12,660	12,420	12,360	12,330	12,210	11,990	11,810	11,600	11,790
10	12,660	12,410	12,300	12,300	12,340	11,960	11,770	11,600	11,780
11	12,660	12,450	12,500	12,890	13,070	13,060	11,900	11,600	11,790
12	12,710	12,690	12,940	12,990	12,900	12,520	11,920	11,600	12,110
13	12,880	12,660	12,760	12,620	12,490	12,310	11,970	11,600	12,110
14	12,840	12,640	12,640	12,500	12,310	12,170	11,940	11,600	12,090
15	12,840	12,600	12,460	12,300	12,330	12,070	11,930	11,600	12,400
16	12,940	12,510	12,470	12,370	12,610	12,590	11,950	11,600	12,400
17	12,890	12,490	12,520	12,410	12,620	12,780	12,630	11,600	12,410
18	12,640	12,490	12,510	12,760	12,860	12,960	12,790	11,600	12,470
19	12,660	12,460	12,440	12,610	12,730	12,780	12,700	12,570	12,380
20	12,610	12,390	12,310	12,300	12,310	12,480	12,460	12,460	12,360
21	12,670	12,480	12,590	12,680	12,430	12,250	12,260	12,420	12,380
22	12,670	12,680	12,620	12,590	12,690	13,030	13,040	12,540	12,430
23	12,610	12,530	12,530	12,580	12,570	12,660	12,670	12,530	12,470
24	12,590	12,370	12,330	12,340	12,380	12,390	12,480	12,470	12,440
25	12,670	12,410	12,390	12,250	12,210	12,230	12,460	12,670	12,470
26	12,650	12,430	12,420	12,220	12,250	12,260	12,540	12,730	12,780
27	12,660	12,440	12,460	12,280	12,330	12,500	12,490	12,700	12,810
28	12,590	12,360	12,400	12,220	12,090	12,350	12,480	12,480	12,660
29	12,630	12,400	12,270	12,100	12,150	12,280	12,460	12,630	12,560
30	12,700	12,450	12,460	12,440	12,440	12,750	13,430	13,250	12,840